UiT
THE ARCTIC
UNIVERSITY
OF NORWAY

Faculty of Science and Technology – Department of Geoscience

Metamorphic evolution in external zones of the Dom Feliciano-Kaoko orogenic system

Examples from the Brusque Metamorphic Complex, Dom Feliciano Belt (Brazil) and the Central Kaoko Zone, Kaoko Belt (Namibia)

—

Caroline Asvald

Master's thesis in Geology – GEO-3900

May 2018

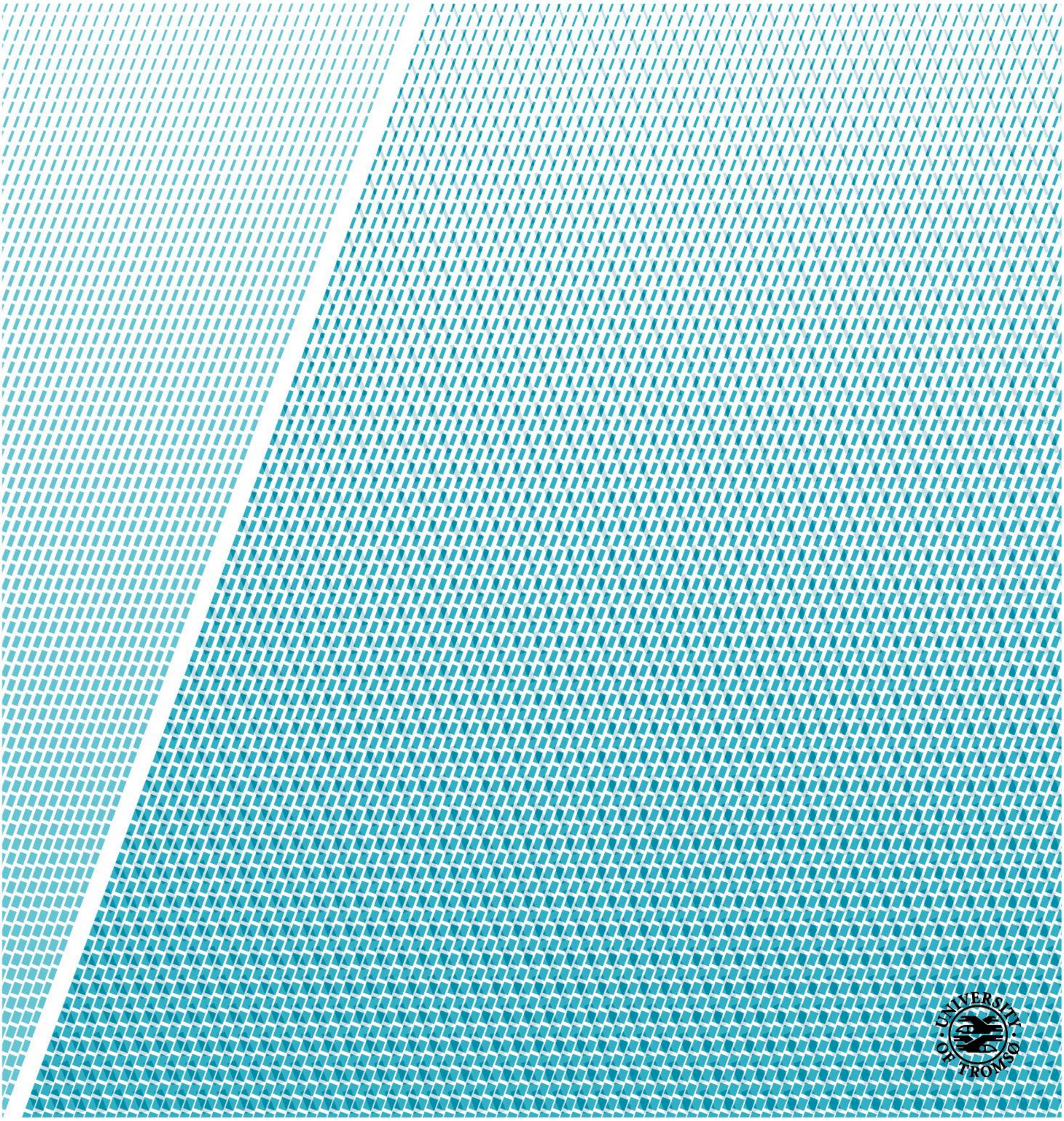

UiT The Arctic University of Norway

Faculty of Science and Technology

Department of Geosciences

GEO-3900

Master thesis in Hard Rock Geology

Metamorphic evolution in external zones of the Dom Feliciano-Kaoko orogenic system

Submitted by : Caroline Asvald

First supervisor : Prof. Jiří Konopásek

Co-supervisors : Prof. Maria de Fatima Bitencourt

Abstract

The Brusque Metamorphic Complex in the Dom Feliciano Belt (Brazil) and the Central Kaoko Zone in the Kaoko Belt (Namibia) represent foreland fold- and thrust belts in external parts of the northern Dom Feliciano-Kaoko orogenic system. P-T phase equilibrium modelling of metamorphosed sedimentary rocks from both units was performed with an aim to compare thermal conditions during orogenesis on both sides of the orogen.

Petrographic and field observations of metapelitic samples from the Brusque Metamorphic Complex suggest that the western part of the complex can be subdivided into three different metamorphic zones: two zones corresponding to greenschist facies conditions, and a central zone corresponding to lower amphibolite facies conditions. These zones are now separated by discrete transcurrent shear zones and large-scale, elongated granitoid intrusions. Phase equilibrium modelling of one sample form the central (garnet-bearing) zone suggests that garnet started to crystallize at ca. 510°C and 4.8 kbar. Estimated peak metamorphic conditions of this sample suggest temperatures of ca. 560-570°C and pressures of ca. 6-7 kbar. Assuming an average crustal density of 2.8 g/cm^3, these conditions suggest an apparent thermal gradient of ca. 22-26°C/km for the central zone of the Brusque Metamorphic Complex. Phase equilibrium modelling of one phyllite sample from the northwestern zone suggests lower metamorphic temperatures (ca. 375-475 °C), although accurate P-T constrain was not possible for this sample.

The Central Kaoko Zone consists of an inverted barrowian sequence of metapelitic rocks ranging from lower greenschist to higher amphibolite facies conditions, and the unit has been subdivided from east to west into chlorite, biotite, garnet, staurolite, kyanite and kyanite-sillimanite-muscovite metamorphic zones. Modelling of one sample from the garnet zone suggests that garnet started to grow at ca. 523 °C and 4.5 kbar and the rock reached peak metamorphic conditions of ca. 540-560°C and 6.5-9.0 kbar. P-T modelling of one sample from the staurolite zone suggest that the garnet started to crystallize at ca. 564°C and 6.6 kbar and the rock reached peak metamorphic conditions of ca. 595-630°C and 7.4-8.1 kbar. P-T modelling of one sample from the kyanite zone suggests that the garnet equilibrated at temperatures at ca. 630-660°C and 9.6-10.4 kbar.

The modelling suggests apparent thermal gradient between 16 and 23°C/km for the Central Kaoko Zone, which overlaps with thermal gradient from the Brusque Metamorphic Complex. These results imply that despite a large difference in timing of metamorphism, the thermal state of the crust was similar during underthrusting of the western and eastern margin of the northern Dom Feliciano-Kaoko orogenic system.

Acknowledgements

This work was supported by the Norwegian Centre for International Cooperation in Education (SIU) and the Coordenação de Aperfeicoamento de Pessoal de Nível Superior (CAPES) in Brazil through the grant project no. UTF-2016-CAPES-SIU10024.

First of all, I would like to thank my supervisor Jiří Konopásek. Your way of teaching and enthusiasm during these years has inspired me to learn more about metamorphic petrology, and I am very grateful that I had the chance to learn from your geological expertise. Thank you for all your help, feedback, time and patience during the last year. Jack James Percival, thank you for all feedback and for always taking the time to listen and answer questions, you will make an excellent professor one day, I am sure.

To Maria de Fatima Bitencourt, Luana Moreira Florisbal, Roberto Sacks de Campos, Giuseppe Betino De Toni and Matheus Battisti for all the help and assistance during our fieldwork. The two weeks we spent together in the field were incredible. A special thanks to Giuseppe who spent one semester here in Tromsø, thank you for always being so helpful and positive.

I want to thank Radek Skoda and Petr Gadas at the Masary University in Brno for their help and expertise during the SEM analysis of mineral chemistry, and the lab staff here in Tromsø for help with thin section preparation and for creating such a positive and good atmosphere at the lab. Kai Naufeld, thank you for all your help with at the SEM with garnet element maps.

Thank you Ragnhild, for all the laughs, talks, frustration and good times we have shared together during the year, I am so glad that you moved to Tromsø and that I got to know you.

I tillegg, takk til jentene på brakka for 5 fantastiske år! Vi klarte det! Til min fantastiske familie i Harstad, Mamma, Pappa, «lille» bror Håkon og Benedikte for all støtte og for at dere er dere. Sist men ikke minst: Marcus, uten deg vet jeg ikke hva jeg ville ha gjort, takk for at du holdt ut og for at du alltid støtter og oppmuntrer meg.

Table of Contents

List of Tables

List of Figures

Abbreviations

Minerals

Ab Albite
Amp amphibole
Ap apatite
And andalusite
Bt biotite
Cal calcite
Cld chloritoid
Cpx clinopyroxene
Chl chlorite
Grt garnet
Hem hematite
Ilm ilmenite
Kfs K-feldspar
Ky kyanite
Pa paragonite
Pl plagioclase
Mag magnetite
Mc Microcline
Ms muscovite
Opq opaque
Qz quartz
Rt rutile
Sil sillimantite
St staurolite
Ttn titanite

Others

a.p.f.u. atoms per formula unit.

X_{Mg}	$Mg^{2+} / (Mg^{2+} + Fe^{2+})$
X_{An}	$Ca^{2+} / (Ca^{2+} + Na^{+} + K^{+})$
X_{Alm}	$Fe^{2+} / (Fe^{2+} + Mg^{2+} + Mn^{2+} + Ca^{2+})$
X_{Prp}	$Mg^{2+} / (Fe^{2+} + Mg^{2+} + Mn^{2+} + Ca^{2+})$
X_{Sps}	$Mn^{2+} / (Fe^{2+} + Mg^{2+} + Mn^{2+} + Ca^{2+})$
X_{Grs}	$Ca^{2+} / (Fe^{2+} + Mg^{2+} + Mn^{2+} + Ca^{2+})$

PPl	Plane polarized light
XPL	Crossed polarized light

“There are many reasons for studying metamorphism but all ultimately relate to a single goal: understanding the evolution of the Earth’s crust” –Frank S. Spears

1 Research objectives and background

Understanding the thermal conditions and depth levels of events that have affected rocks during orogenesis can give important insight into controls and processes that facilitate crustal thickening.

During the formation of the Dom Feliciano-Kaoko orogenic system (Figure 1.1.1) in the Neoproterozoic times, the metamorphism in its marginal zones took place in substantially different periods of the orogenic history. The Brusque Metamorphic Complex of the Dom Feliciano Belt in Brazil represents the western (in the present day coordinates) marginal zone of the orogen and its collisional evolution is indirectly dated at ca. 650-630 Ma (Oyhantçabal et al., 2009; Lenz et al., 2011; Florisbal et al., 2012). The Central Kaoko Zone in the Kaoko Belt of Namibia can be considered as equivalent to the Brusque Metamorphic Complex in terms of the pre-collisional history (sedimentary basins developed on top of an extended crust) and also the position during the collision at the eastern margin of the orogenic system. The major difference between them is the timing of peak metamorphism, which has been dated in the Kaoko Belt at ca. 575-550 Ma (Goscombe et al., 2003; Goscombe et al., 2005a).

This thesis represents a metamorphic study of six samples of metasedimentary rocks, three from the Brusque Metamorphic Complex in Brazil and three from the Central Kaoko Zone in Namibia. The aim is to provide information on the P-T conditions during the metamorphic evolution at the western and eastern margin of the Dom Feliciano-Kaoko orogenic system, respectively.

This study involved field and laboratory work, petrographic studies, analyses of mineral composition and equilibrium modelling of observed mineral assemblages. Perple_X software (Connolly, 2005) was used for construction of P-T pseudosections constrained by whole rock chemistry of individual samples.

Interpretations of the results were made with focus on tectonic interpretation of position of the samples in the crust during metamorphism and comparison of thermal gradients that existed during metamorphic peak in each of the studied units.

1.1 Geological setting

The Dom Feliciano Belt in south Brazil and Uruguay, and the Kaoko Belt along the SW coast of Africa represent adjacent parts of one branch of a large orogenic system that developed during the Neoproterozoic Era (Figure 1.1.1).

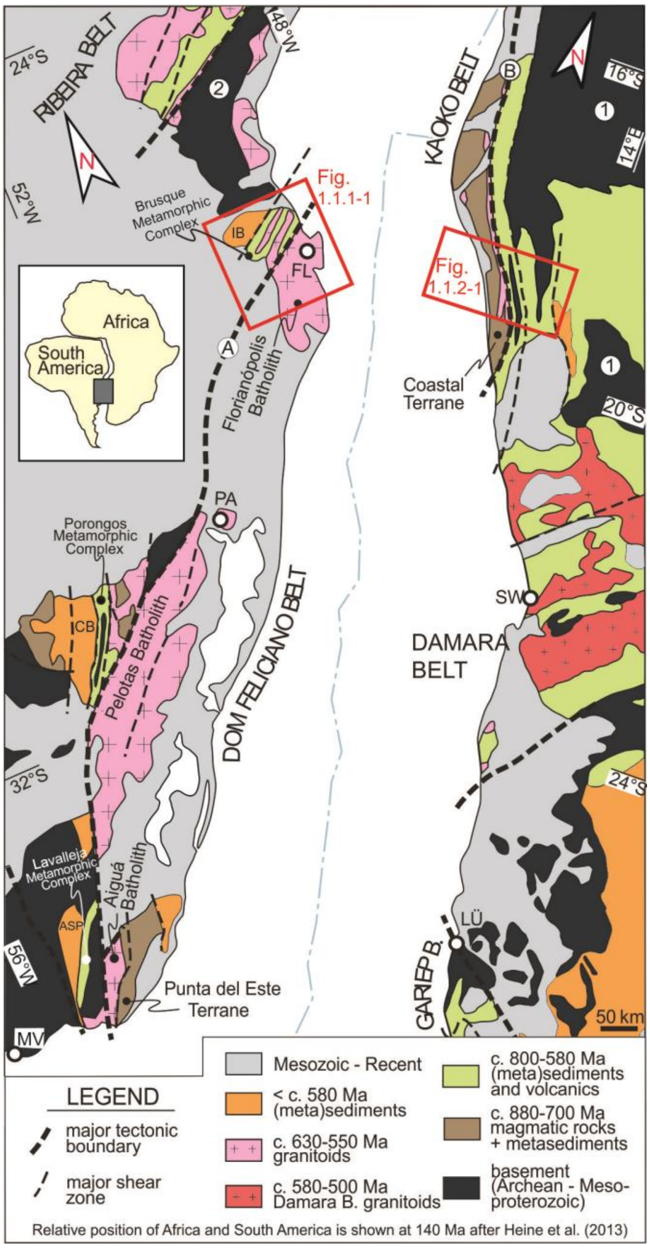

Figure 1.1.1 Simplified geological map of the Dom Feliciano and Kaoko belts modified after Konopásek et al. (2014). The red rectangles show the position of Figure 1.1.1-2 and 1.1.1-3. Pre-Neoproterozoic domains: 1- Congo Craton; 2-Luís Alves Terrane. A – Sierra Ballena-Dorsal Canguçu-Major Gercino shear zone; B – Village-Three Palm shear zone system. IB:Itajaí Basin, CB: Camaquã Basin, ASP: Arroyo del Solado-Piriápolis Basin. MV Montevideo, PA Porto Alegre, FL Florianópolis, Lü Lüderitz, SW Swakopmund.

The Dom Feliciano-Kaoko orogenic system formed as a result of the break-up of Rodinia and the subsequent amalgamation of West Gondwana, referred to as the Brasiliano Cycle in South America, and the Pan-African Cycle in Africa (Porada, 1979; Pisarevsky et al., 2003; Li et al., 2008; Gray et al., 2008).

In early Neoproterozoic, crustal stretching of Rodinia led to the formation of several rift basins bounded by Archean - Mesoproterozoic cratonic masses. During this event of crustal stretching, detrital material that formed by erosion of surrounding cratons and products of syn-sedimentary volcanism were continuously filling newly formed rift basins. Based on dating of syn-rift volcanic rock, sedimentological observations and provenance studies of detrital zircons, the rift phase started at ca. 820 Ma and continued up to ca. 680-660 Ma (Konopásek et al. (2017) and references therein). With the change of tectonic forces from extensional to compressional in late Neoproterozoic, the volcano-sedimentary rocks were metamorphosed and deformed between ca 650-550 Ma during the assembly of West Gondwana (Goscombe et al., 2003; Goscombe et al., 2005a; Lenz et al., 2011; Oyhantçabal et al., 2009; Florisbal et al., 2012).

The Mesozoic opening of the Atlantic Ocean divided the Dom Feliciano-Kaoko orogenic system, and moved the adjacent parts to their present location. Porada (1979) provided the first correlation among the pre-Mesozoic geological units on both sides of the Atlantic. So far, the link among geological units in the individual orogenic belts is solely based on similar timing of tectonic processes, and their spatial connection before opening of the Atlantic Ocean is still poorly understood (Konopásek et al., 2016).

In this chapter, the regional geology of the northern branch of the Dom-Feliciano-Kaoko-Gariep orogenic system will be presented with focus on the study areas; the northernmost part of the Dom Feliciano Belt located in SE Brazil, and the Kaoko Belt in NW Namibia.

1.1.1 The Dom Feliciano Belt

The 150 km wide, NE-SW trending Dom Feliciano Belt (Figure 1.1.1) extends approximately 1200 km along the Atlantic coast of southern Brazil and Uruguay (Basei et al., 2000; Basei et al., 2011). The northwestern margin of the Dom Feliciano Belt is represented by Archean to Paleoproterozoic basement rocks. On a large scale, the Dom Feliciano belt can be described as four main crustal segments, The Foreland Basins, The Schist Belt, The Granite Belt and the Punta del Este Terrain (Preciozzi et al., 1999; Basei et al., 2000).

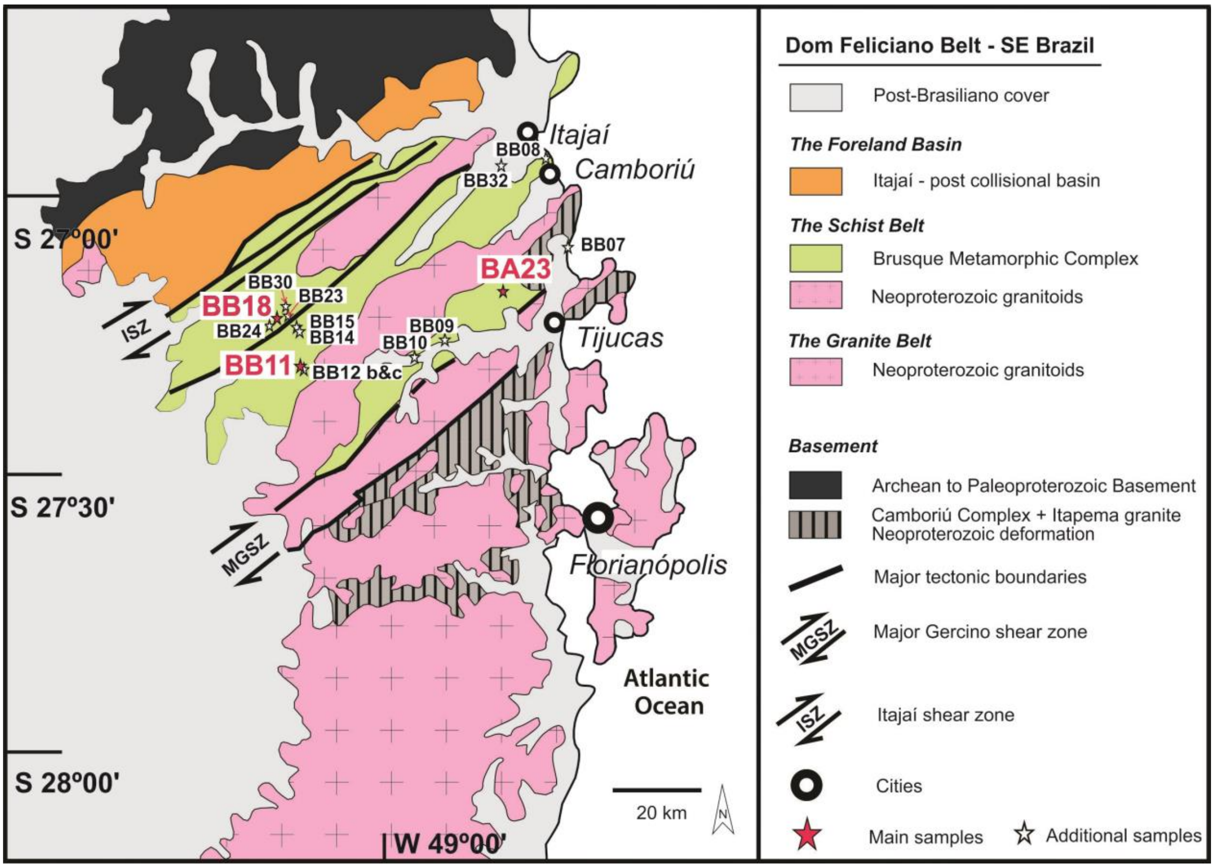

Figure 1.1.1-1 Geological map showing main geological features of the northernmost part of the Dom Feliciano Belt, Santa Catarina, Brazil (Modified after Hartmann et al. (2003) and Florisbal et al. (2012)). The location of samples are indicated with stars. Sample BB18, BB11 and BA23 was used for thermodynamic modelling.

1.1.1.1 The Foreland basins

The westernmost part of the Dom Feliciano Belt consists of late Neoproterozoic to Cambrian anchimetamorphic sedimentary and volcanic rocks (Basei et al., 2011). In the Santa Catarina state (S Brazil) these appear in the post collisional Itajaí Basin (Figure 1.1.1-1), deposited between ca. 650-545 Ma (Guadagnin et al., 2010; de Campos et al., 2012a). In the Rio Grande do Sul state (S Brazil) and in Uruguay, the equivalent basins are called the Camaquã- and Arroyo del Solado-Piriápolis basin, respectively (Basei et al., 2000). The Itajaí Shear Zone in the Santa Catarina state represents the boundary between the Itajaí basin sedimentary rocks and the adjacent low to medium grade meta-volcano-sedimentary rocks of the Brusque Metamorphic Complex (Figure 1.1.1-1).

1.1.1.2 The Schist Belt

The NE-SW trending schist belt is located between the Foreland Basins and the Granite Belt (Figure 1.1.1-1). It consists of a variety of supracrustal rocks metamorphosed at greenschist- to lower amphibolite facies conditions during the collision in the Neoproterozoic (Oyhantçabal et al., 2009). In the Santa Catarina state, these metamorphosed-volcano-sedimentary rocks are called the Brusque Metamorphic Complex (BMC). The schist belt continues into the Rio Grande do Sul state and Uruguay, where the equivalents to the Brusque Metamorphic Complex are called the Porongos- and Lavalleja metamorphic complexes, respectively (Basei et al., 2000; de Campos et al., 2012a). The supracrustal rocks in the Brusque Metamorphic Complex were intruded by several post-collisional granitoid bodies at between ca. 620-590 Ma, which gives an upper age limit of the collisional event of ca. 620 Ma (Florisbal et al., 2012).

1.1.1.3 The Granite Belt

The Granite Belt is located east of the Schist Belt and consists of voluminous post collisional granitoids, together with basement remnants (Figure 1.1.1-1). In the Santa Catarina state, the granitoids are all considered as parts of a large igneous complex called the Florianópolis Batholith (Basei et al., 2000). The 630-590 Ma sub-alkaline to alkaline granitoids in the Florianópolis Batholith were originally interpreted as roots of a magmatic arc (Porada, 1979; Basei et al., 2000). However, recent studies of chemical composition, trace elements and isotopic signatures have shown large variability of mantle/crustal contribution and different mantle sources, which can suggest an intra-continental, post-collisional setting of the granitoid magmatism related to the development, and activity of the Major Gercino Shear Zone (de Campos et al., 2012a; Florisbal et al., 2012).

The Granite Belt continues south as the Pelotas Batholith in Rio Grande do Sul state and the Aiguá Batholith in Uruguay (Figure 1.1.1). The individual batholiths are separated in the field by a younger post-Brasiliano cover (Basei et al., 2000).

1.1.1.4 Punta del Este Terrane

The Punta del Este Terrane is located east of the Sierra Ballena Shear Zone in Uruguay (Figure 1.1.1) and represents the easternmost tectonic unit of the Dom Feliciano Belt. The Punta del Este Terrane consists of amphibolites, gneisses and migmatites that show evidence of a high-grade metamorphic event at ca. 650 Ma (Oyhantçabal et al., 2009; Lenz et al., 2011).

1.1.2 The Kaoko Belt

The ca. 700 km long, NNW trending Kaoko Belt crops out along the Atlantic coast of Namibia and southernmost Angola (Figure 1.1.1). The Kaoko Belt was described by Goscombe et al. (2003) as a classic example of a sinistral transpressional orogen. It shows an overall transport of units east, towards autochthonous Archean-Paleoproterozoic autochthonous basement (i.e. the Congo Craton). The Kaoko Belt was originally divided by Miller (1983) into three tectonic zones; the Eastern Kaoko Zone (EKZ), the Central Kaoko Zone (CKZ), and the Western Kaoko zone (WKZ), where the limits of these zones represent major tectonic boundaries. The Western Kaoko Zone was later subdivided by Goscombe et al. (2005b), into two different segments based on the age of metamorphism; the Orogen Core in the west and the exotic Coastal Terrane in the east (Figure 1.1.2-1). The metamorphic grade increases from sub-greenschist facies in the foreland (EKZ), to granulite facies conditions in the Orogen Core (Goscombe et al., 2003; Goscombe et al., 2005a).

1.1.2.1 The Eastern Kaoko Zone

The Eastern Kaoko Zone (EKZ) can be described as the foreland of the orogen, which consists of a thick sequence of basal clastic sedimentary rocks, shelf carbonates and overlying molasse, all deposited on top of the autochthonous Congo Craton basement. The shelf carbonates are folded into large-scale open folds and metamorphosed at sub-greenschist facies conditions (Goscombe et al., 2003; Goscombe et al., 2005b; Ulrich et al., 2011). The Sesfontein thrust marks the boundary between the Eastern- and Central Kaoko zones, where the low- to high grade rocks west of the Sesfontein thrust are transported over the very low grade rocks of the foreland (Goscombe et al., 2003; Jung et al., 2014).

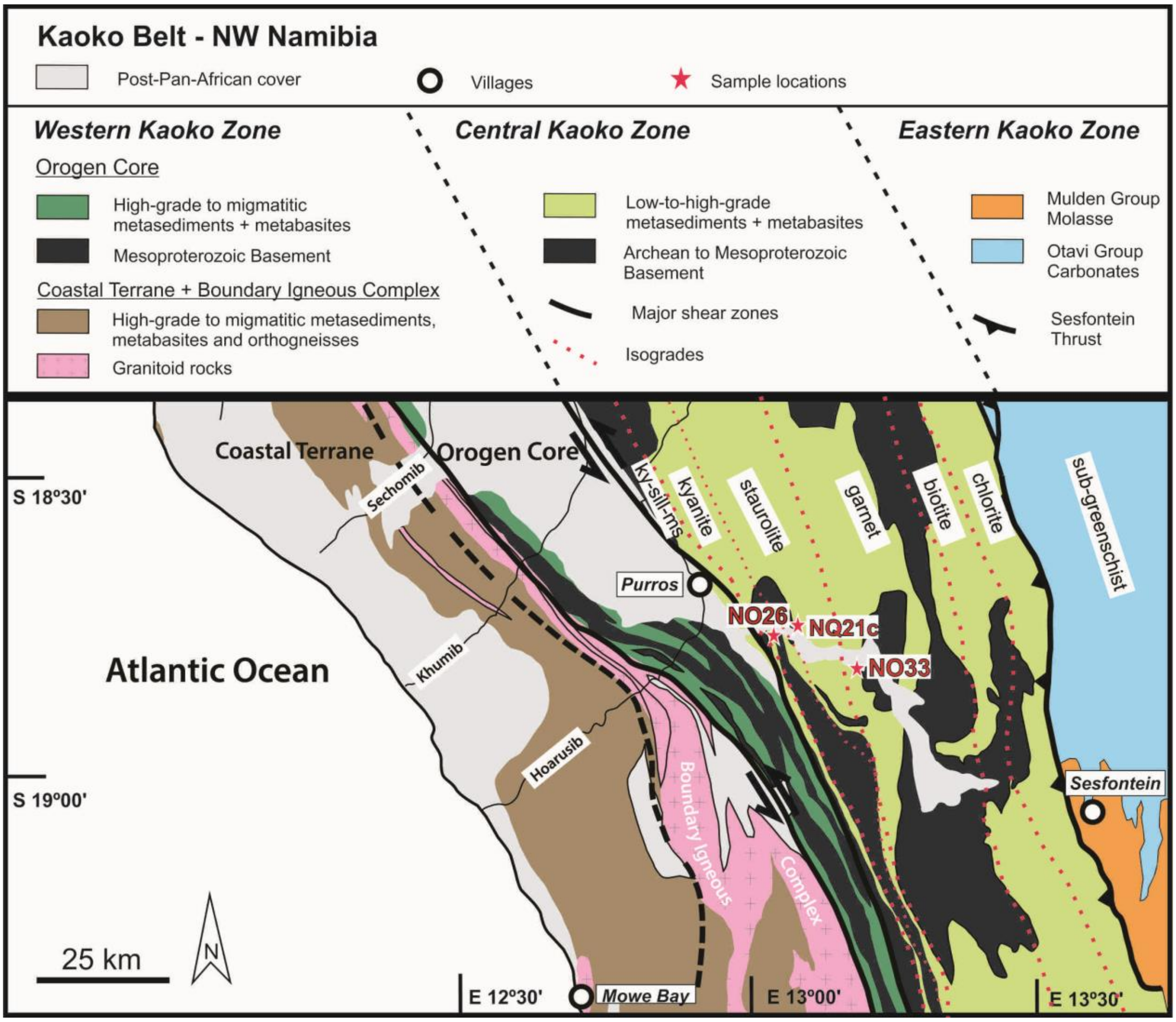

Figure 1.1.2-1 Simplified geological map of the Kaoko Belt in SW Namibia, modified after Ulrich et al.(2010) and Goscombe et al.(2003). Sample locations are marked with red stars.

1.1.2.2 The Central Kaoko Zone

The Central Kaoko Zone, also referred to as the Escape Zone, consists of a deformed and metamorphosed sequence of meta-volcano-sedimentary rocks with conditions ranging from lower greenschist to higher amphibolite facies. Basement rocks of the Congo Craton appears in the Central Kaoko Zone as basement windows in anticlines. The metapelitic rocks found in the Central Kaoko Zone were described by Goscombe et al. (2003) as an inverted barrowian sequence, with metamorphic grade increasing from east to west. The boundary between the Central- and Western Kaoko Zone is marked by a major mylonite to ultramylonite zone, called the Purros Mylonite Zone. The Purros Mylonite Zone extends throughout the entire length of the Kaoko Belt, and shows an overall sinistral movement, with an oblique reverse component (Goscombe et al., 2003; Ulrich et al., 2011).

1.1.2.3 The Orogen Core

The Orogen Core consists of strongly deformed meta-volcano-sedimentary rocks (mostly deep-water facies), metamorphosed at upper amphibolite to granulite facies conditions at ca 580-550 Ma. Deformed basement rocks that show clear affinity to the Congo Craton are interleaved with the metasedimentary rocks of the Orogen Core unit (Seth et al., 1998; Goscombe et al., 2005a; Goscombe et al., 2005b; Ulrich et al., 2011). The Orogen Core is separated from the adjacent Coastal Terrane by granitoid intrusions belonging to the 580-550 Ma Boundary Igneous Complex, which presumably masks the suture between the Orogenic Core and the exotic Coastal Terrane (Seth et al., 1998; Konopásek et al., 2008).

1.1.2.4 The Coastal Terrane

The Coastal Terrane mostly consists of migmatitic metasedimentary rocks, occasionally intercalated with orthogneisses and amphibolites. The metamorphosed sedimentary and volcanic rocks of the Coastal Terrane shows evidence of a metamorphic event that took place at ca. 650-630 Ma (Franz et al., 1999; Goscombe et al., 2005a; Konopásek et al., 2008). In contrast to the rest of the Kaoko Belt, no basement rocks has been recognized in the Coastal Terrain, which together with its metamorphic history lead to the discussion about its pre-collisional position and origin (Seth et al., 1998; Goscombe et al., 2003; Goscombe et al., 2005a). Based on the age of syn-sedimentary igneous rocks and the age of metamorphism, the Coastal Terrane has been correlated to the Punta del Este Terrane in the southernmost part of the Dom-Feliciano belt in Uruguay (Oyhantçabal et al., 2009; Lenz et al., 2011). Konopásek et al. (2017) interpreted the Punta del Este-Coastal Terrane as the axial part of an Neoproterozoic rift.

1.2 Study areas and previous work

This chapter introduces the two study areas incorporated in this thesis, the Brusque Metamorphic Complex and the Central Kaoko Zone. Previous studies focusing on metamorphic conditions of the study areas will be presented.

1.2.1 Brusque Metamorphic Complex

The Brusque Metamorphic Complex (Figure 1.1.1-1) represents the northernmost unit of the Schist Belt in the Dom-Feliciano Belt. It includes a variety of clastic- and carbonate sedimentary rocks, as well as syn-sedimentary volcanic rocks. The metasedimentary rocks in the BMC consist of metarhytmites, metapelites, quartzites, marbles, calc-silicates and marls, which are locally interlayered with metabasalts and meta-ultramafic rocks (de Campos et al., 2012b; de Campos et al., 2012a). Post-collisional 620-590 Ma granitic bodies and dykes are abundant within the Brusque Complex (de Campos et al., 2012a; Florisbal et al., 2012).

Basei et al. (2011) published first, and so far the only estimation of the metamorphic conditions in the Brusque Metamorphic Complex. Their results were obtained from schematic AFM-projections (compatibility diagrams) and the intersection of assumed mineral reactions. Basei et al. (2011) used model petrogenetic diagrams for the KFMASH, and KMnFMASH systems, assuming an average pelitic bulk composition of the rocks. A quantitative estimate of metamorphic conditions for some parts of the BMC was then made based on mineral associations found in petrographic thin sections. In other words; the metamorphic conditions that these rocks experienced during the Neoproterozoic collision have only been estimated through petrographic investigations and they still await quantification, e.g. through thermodynamic modelling.

1.2.2 The Central Kaoko Zone

The low-to-high grade metasedimentary rocks that are found in the Central Kaoko Zone are dominated by metaturbidite and metagreywacke schists with minor amounts of carbonate, metaquartzite, metaarkose and two metamorphosed diamictite units. Metavolcanic rocks such as mafic schists and amphibolites are found in minor amounts within the metasedimentary rocks (Goscombe et al., 2003).

Goscombe et al. (2003) distinguished estimated peak metamorphic conditions from 15 samples from the Central Kaoko Zone. By the use of petrographic observations, bulk rock analysis and mineral chemistry, they estimated metamorphic peak conditions across the Central Kaoko Zone by conventional thermobarometry modelling. Their studies suggests that the Central Kaoko Zone reached P-T conditions ranging from 530 to 690 °C and 8.5 to 9.0 kbar, corresponding to a metamorphic field gradient ranging from 17- to 23 °C/km.
Based on petrographic observations and dating of metamorphic garnet, they stated that the peak metamorphic conditions in the Central Kaoko Zone were reached at ca. 575 Ma, during what Goscombe et al. (2003) defined as the transpressional phase of the collision.

Will et al. (2004) studied samples from a cross-section through the Central Kaoko Zone. Using different mineral-pair thermometers- and barometers, in addition to pseudosection modelling, they estimated peak metamorphic conditions and P-T paths from four mineral zones in the Central Kaoko Zone; the garnet zone, the staurolite zone, the kyanite zone and the kyanite-sillimanite-muscovite zone. Their thermodynamic modelling resulted in metamorphic field gradient of 20 °C/km, similar to those found by Goscombe et al. (2003).

The studies of Goscombe et al. (2003), and Will et al. (2004) have provided good knowledge about metamorphic isograds across the Central Kaoko Zone (see Figure 1.1.2-1).

2 Methods of work

Various methods of data collection and analysis were used during this research; fieldwork, preparation of petrographic thin sections, analysis of mineral composition and estimation of metamorphic conditions. The methodology will be presented in this chapter.

2.1 Fieldwork

The main purpose of the fieldwork was to collect samples from the Brusque Metamorphic Complex, which were later used for estimation of metamorphic conditions. The fieldwork took place in the Santa Catarina state, Brazil, in the area between Florianopolis and Itajai cities (Figure 1.1.1-1) from 13th to 22nd June 2017). 13 samples of metasedimentary rocks across the Brusque Metamorphic Complex were collected in the field and structural measurements of various planar fabrics such as foliation and crenulation cleavage were made. The software Orient 3.6.3 was used for construction of stereographic plots (http://www.frederickvollmer.com/orient/).

2.2 Thin section preparation

Petrographic thin sections were made from 16 samples, 13 from the Brusque Metamorphic Complex and 3 from the Central Kaoko Zone of the Kaoko Belt. The samples were first cut into two pieces using a diamond saw. The cuts were made perpendicular to a foliation, and if present, parallel with to the lineation. Selected sample areas were cut into small blocks (1 cm x 2 cm x 3 cm) and labeled. Further preparation of thin sections; gluing, cutting and polishing, was made by the laboratory staff at the Institute of Geoscience of the University of Tromsø.

2.3 Optical microscopy

Petrographic study of mineral assemblages, crystallization relationships and mineral textural positions was performed by using Leica Laborlux 11 Pol S polarization microscope at the Institute of Geoscience of the University of Tromsø. Based on stable mineral assemblages and degree of preservation of minerals, six out of the 16 samples were selected for estimation of metamorphic conditions. In those thin sections, minerals of specific interest were marked for further quantitative chemical analysis. Photomicrographs presenting petrographic observations were taken using a Leica DFC450 camera connected to the polarization microscope.

2.4 Scanning electron microprobe (SEM) imaging

Finding stable mineral assemblages in samples, and quantifying minerals chemical composition is a crucial part of understanding previous metamorphic conditions. In order to do analysis with high vacuum scanning electron microscope/microprobe, the petrographic thinsections were coated with carbon.

2.4.1 Qualitative analysis

All qualitative analyses were performed at the University of Tromsø, the Arctic University of Norway. Identifications of opaque phases and mineral phases too small for recognition under petrographic microscope were performed using a Hitachi TM3030 tabletop electron microscope at the Department of Geosciences. High-resolution element maps of garnet were conducted at the Faculty of Health Sciences, using a Zeiss MERLIN VP compact SEM.

2.4.2 Quantitative analysis of mineral chemistry

Quantitative measurements of mineral compositions were made by wavelength dispersive X-ray spectroscopy at the Faculty of Science of Masaryk University in Brno, Czech Republic. A CAMECA SX100 electron microprobe equipped with five spectrometers was used to conduct point analysis for all mineral phases that are usually present as solid solutions in natural samples. The operating voltage and beam radius used are presented in Table 2.4.1.

Table 2.4-1 - Parameters used for quantitative analysis of mineral phases

Minerals	**Acceleration voltage**	**Beam size**
Garnet, ilmenite, rutile, spinel	15keV 20 nA	2 μm
Plagioclase, K-feldspar	15keV 10 nA	5 μm
Biotite, white mica, chlorite, staurolite	15keV 10 nA	3 – 5 μm

Recalculations from weight percentages of oxides to atoms per formula units were made in Excel spreadsheets.

2.5 Preparation of samples for bulk chemical analysis

Analysis of bulk chemical composition of six samples were performed at Bureau Veritas Laboratory in Vancouver, Canada. The analyses were conducted by inductively coupled plasma emission spectroscopy (ICP-ES) in combination with lithium borate fusion. The amount of FeO was determined for one sample containing magnetite.

Preparation of samples selected for chemical analysis was done at the Department of Geosciences, UiT, the Arctic University of Norway and involved crushing and milling to an analytical grain size.

2.5.1 Crushing

The samples were crushed down to approximately 5 mm size using a Retsch jaw crusher. Prior to the crushing, weathered surfaces were cut away from the samples. The samples were washed and air-dried overnight prior to the actual crushing process in order to avoid contamination from other samples or soil. The jaw crusher was washed and blow-dried thoroughly before introduction of each new sample.

2.5.2 Milling

Crushed rock material was milled using a Retsch Planetary ball mill PM 100. All samples were milled in a 250 ml Agate bowl, with 15 agate balls of 3 cm in diameter. The samples were milled to achieve analytical grainsize (less than 20 microns), using a speed of 450 rpm and 10 minutes intervals of milling. Depending on the physical properties of the samples, varying milling time was needed, and varied form 20 minutes and 2 hours. Between each sample, the bowl, balls, and measuring cup was washed using ethanol, and dried with an air gun. If particularly stained and hard to clean, the agate bowl and balls were cleaned for 10 minutes at 450 rpm, using some amount of the next sample that was later disposed.

2.6 Phase equilibrium modelling

Pseudosection, also called an equilibrium phase diagrams, are a mineral stability diagrams that are calculated for a specific bulk composition in a chosen P-T space. Composition isopleths are contours that graphically presents how the composition of minerals evolves through the P-T space. For the purpose of this research, construction of P-T pseudosections and compositional isopleths were made by the use of Perple_X software package, version 6.7.0 (Connolly, 2005).

Figure 2.6.1 shows a schematic overview of calculation steps related to problem solution using the Perple_X software package. Calculations of pseudosections were done through; BUILD (problem definition), VERTEX (calculations), PSSECT (graphical representation). Calculations of compositional isopleths were done through; WERAMI (digital interpretation) and PSTABLE (graphical representation). The effective bulk composition of sample NO33 and sample NQ21c were done through; BUILD (problem definition) and VERTEX (calculations). For visual reasons, the output from PSSECT was redrawn in CorelDRAW.

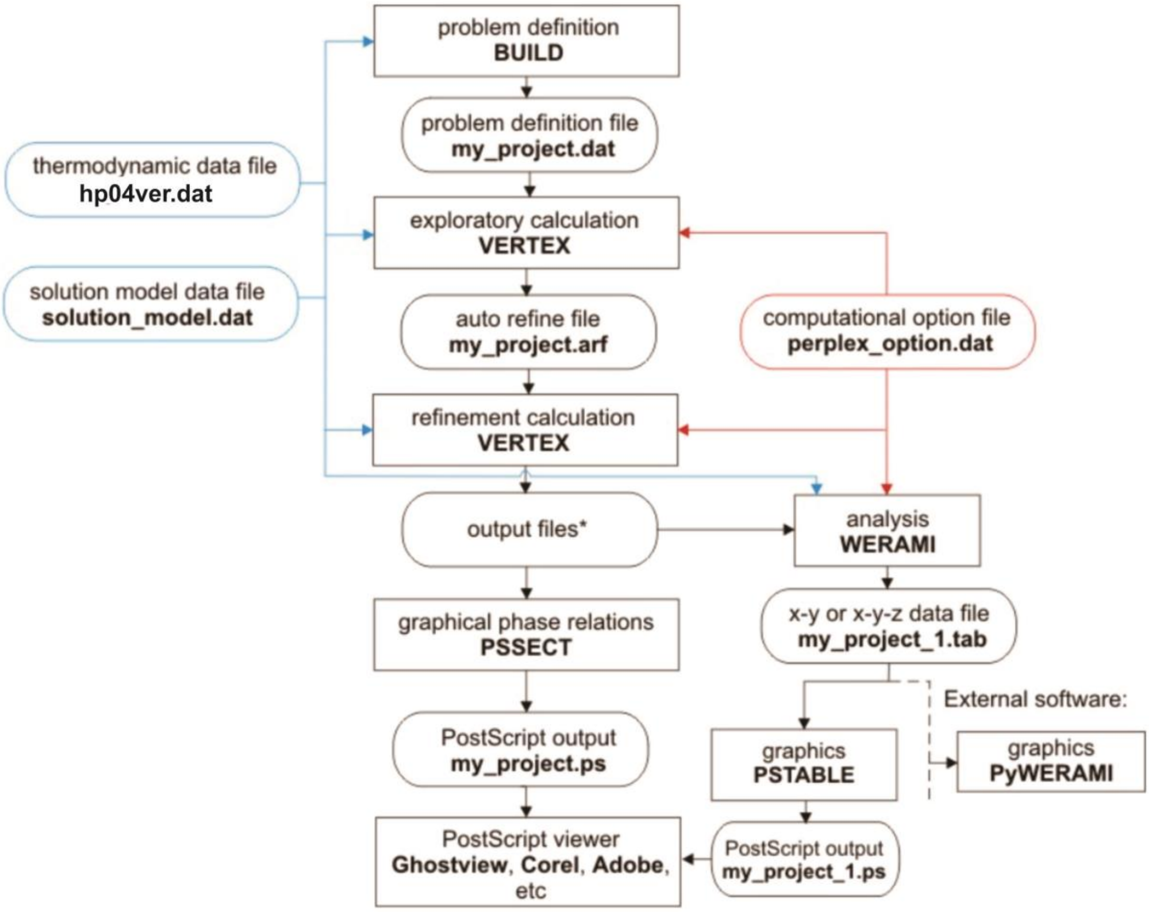

Figure 2.6.1 Perple_X program structure. Modified after Perple_X documentation; web-based tutorials (http://www.perplex.ethz.ch/perplex_66_seismic_velocity.html)

Methodology for the phase equilibrium modelling of individual samples and possible sources of error related to calculations will be described in further detail in section 3.5.

3 Results

3.1 Structural data (Fieldwork)

In order to relate metamorphic mineral assemblages to deformation, structural relationships observed in the field are important to consider. Dense vegetation and high degree of in situ weathering makes the outcrop situation in the Brusque Metamorphic Complex rather difficult with rare exposed tectonic boundaries and rare good outcrops. This chapter presents a brief summary of structural observations and data collected during the fieldwork in the Brusque Metamorphic Complex.

At least three different deformation phases were observed in the field – referred to throughout this chapter as D1, D2 and D3.

D1: The D1 deformation phase has produced recumbent (F1) folds and low-angle foliation (S1) as shown in Figure 3.1.1. F1 folds have axial planes parallel to the S1 fabric and they seem to affect compositional layering S0. S1 foliation is the dominant fabric in the Brusque Metamorphic complex (Figure 3.1.4). This flat lying fabric is associated with shearing is likely produced by low angle thrusting during early stages of collision (Basei et al., 2011).

.

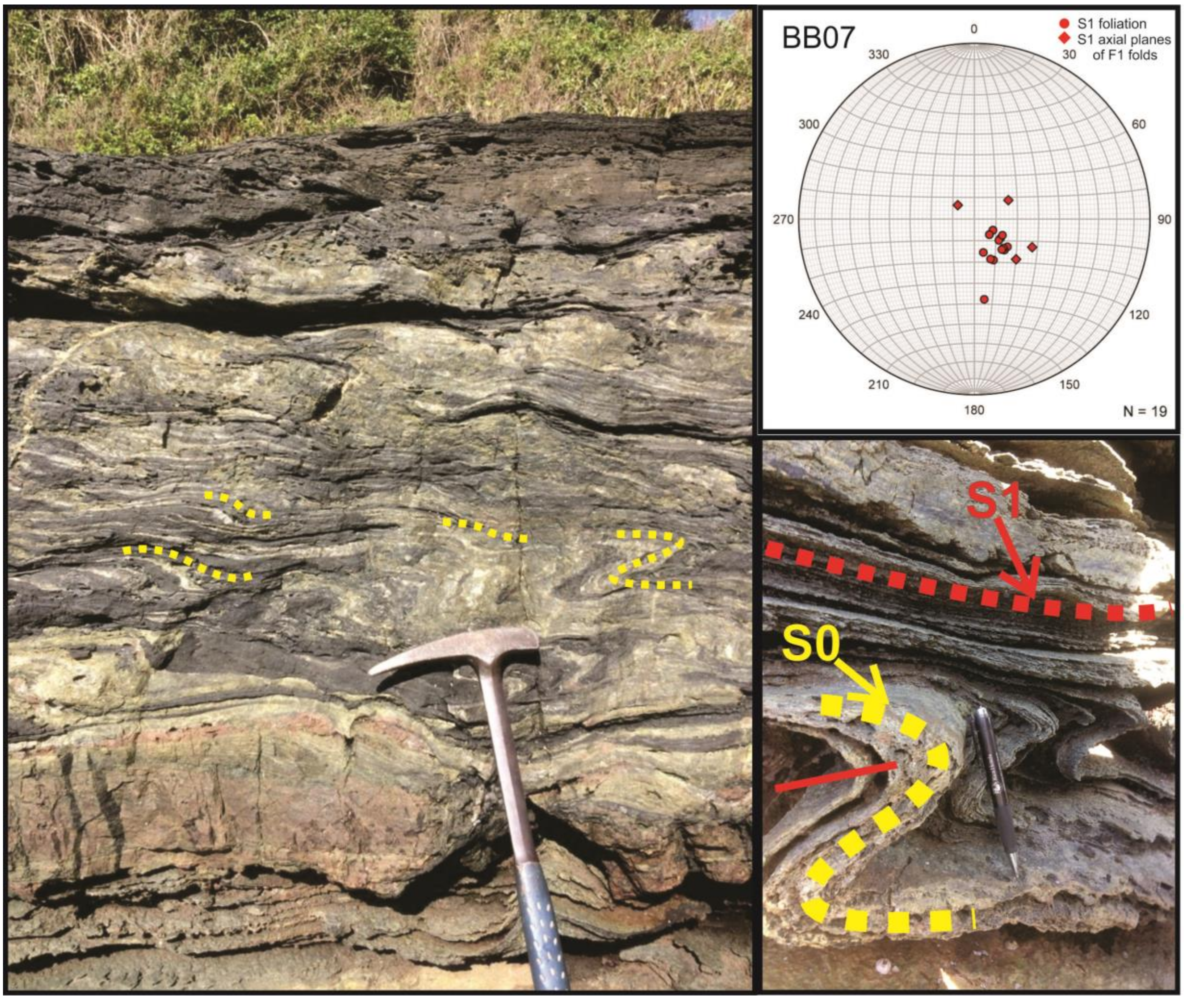

Figure 3.1.1-1 Field relationships at outcrop BB07 (picture facing west). S0 (yellow dotted lines) is folded into recumbent folds, producing low angle S1 foliation subparallel to F1 axial planes

D2: The low angle S1 foliation is at many locations overprinted by a later deformation event (D2) that resulting in upright folds and steeply dipping penetrative crenulation cleavage with NE-SW strike. At one locality (BB31) the D1 and D2 deformation events are observed together. Figure 3.1.2 shows F1 folds refolded by D2 in a quartzite at locality BB31. Figure 3.1.3 shows the relationship between the F2 folding and development of the S2 crenulation cleavage in a metasedimentary rock at locality BB08. The D2 event is expressed at some locations by sub-vertical crenulation cleavage planes at high angle to the S1 foliation, and at other locations as upright folds. The expression of this deformation event might be related differences in lithology as quartz rich lithologies show larger amplitude folding and more pelitic lithologies results in microfolding and development of crenulation cleavage.

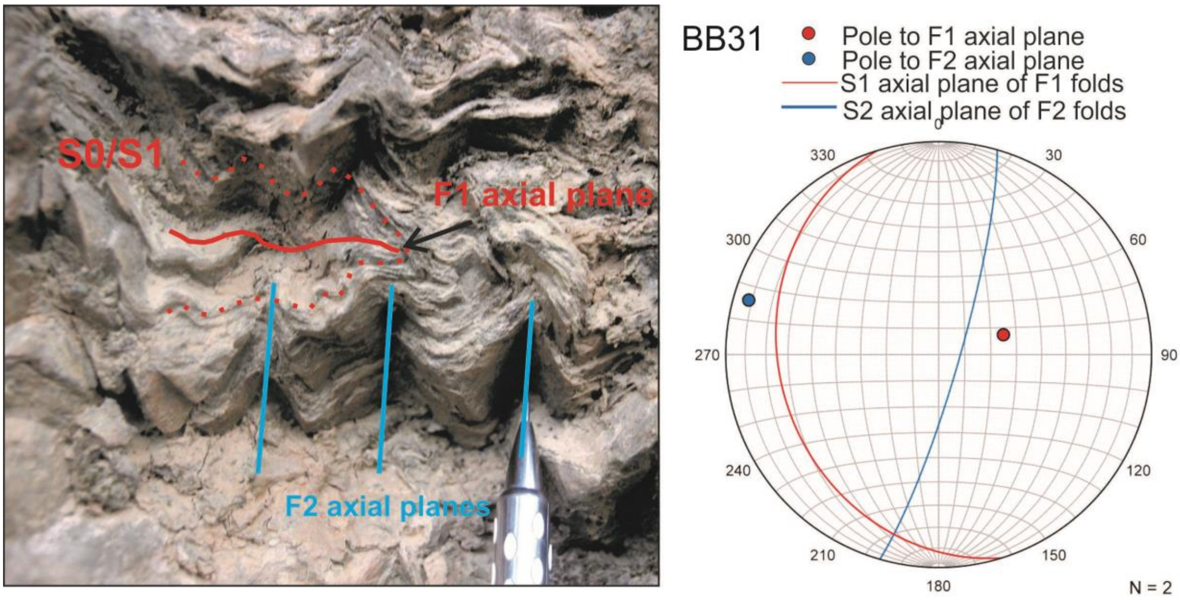

Figure 3.1.2 Quartzite at the locality BB31 (picture facing south). Sub-horizontal F1 folds are refolded by D2 at the locality BB31.

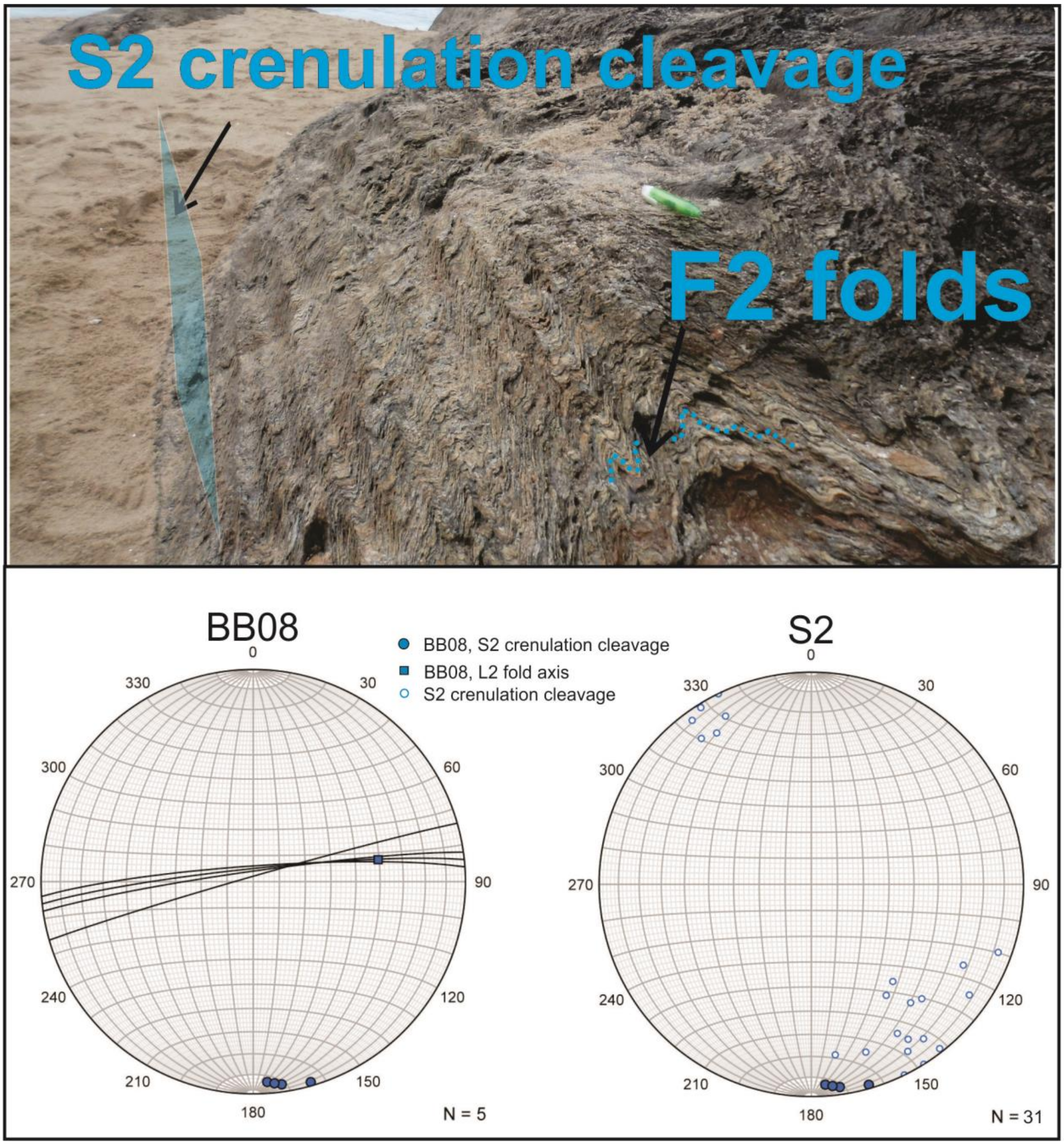

Figure 3.1.3 Highly penetrative crenulation cleavage (S2) in metasedimentary rock at outcrop BB08 (Picture facing west). The S0/S1 relics are folded into tight upright folds marked by blue dotted lines. The left stereoplot shows data collected from outcrop BB08 and the right stereoplot shows all measurments of the S2 crenulation cleavage collected across the Brusque Metamorphic Complex plotted as poles to planes.

D3: A steeply dipping crenulation cleavage with NW-SE trending strike has also been observed in the field (Figure 3.1.4). At one location the S2 and S3 crenulation cleavages were observed together, but the meaning of the D3 deformation event is still unclear.

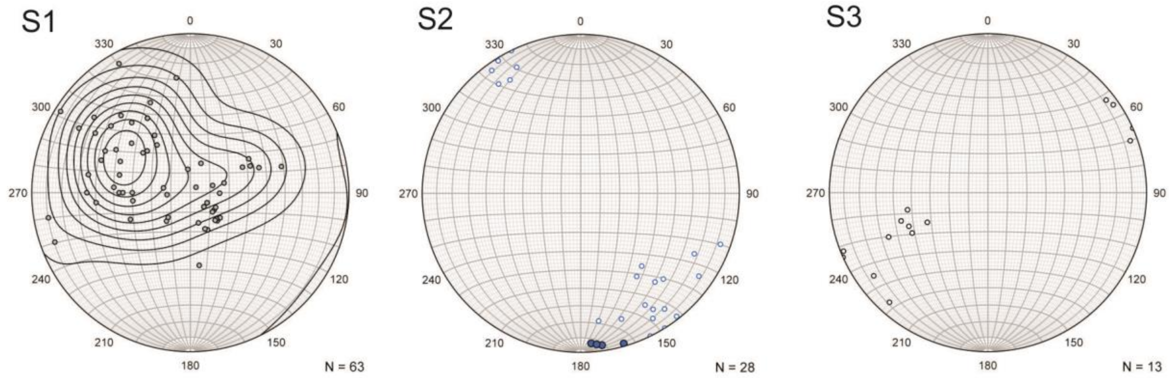

Figure 3.1.4 Summary of planar fabrics related to the three deformation phases that effected the Brusque Metamorphic Complex. Low angle (S1) foliation dipping SE is the dominant fabric of the Brusque Metamorphic Complex.

3.2 Sample introduction

Three samples from the Brusque Metamorphic Complex (Brazil) and three samples from the Central Kaoko Zone (Namibia) were studied in detail during this research.

Sample BB18 (S27.22928°, W49.17683°) is a low-grade phyllite from the northwestern part of the Brusque Metamorphic Complex (Figure 1.1.1-1). The hand specimen is very fine grained, it has a greyish-to-greyish-green color and a greasy luster. The sample has a well-developed flat lying foliation and some intercalated very thin quartz-rich layers (>1mm).

Sample BA23 (S27.17520°, W48.71758°) is a garnet-bearing quartzite from the southeastern part of the Brusque Metamorphic Complex (Figure 1.1.1-1). The hand specimen has a light gray color and a wavy foliation defined by alternating light gray and darker grey- to brownish layers. The matrix is fine grained, and contains scattered garnet porphyroblasts that are up to ~1mm large. The surface has a shiny luster due to the presence of fine-grained micas.

Sample BB11 (S27.31707°, W49.12555°) is a garnet-mica schist from the western part of the Brusque Metamorphic Complex (Figure 1.1.1-1). The hand specimen has a dark grey to greyish green color, with some light bands that define the wavy foliation. It has a fine grained texture, with up to ~2 mm large garnet porphyroblasts are visible by the naked eye.

Sample NO33 (S13.20402°, E18.85517°) is a garnet-mica schist from the garnet zone of the Central Kaoko Zone (Figure 1.1.2-1). It has a deep green color and a shiny luster. The sample has a wavy foliation which is defined by alternating layers of light grey and green color. The matrix is fine grained and contains large amount (~15%) of garnet porphyroblasts that are up to ~2 cm in diameter.

Sample NQ21c (S13.22722°, E18.91778°) is a staurolite-garnet-biotite schist from the staurolite zone in the Central Kaoko Zone (Figure 1.1.2-1). The rock is folded into asymmetric folds and a crenulation cleavage is visible in the hand specimen (Figure 3.2.1). It has a mixture of light grey and dark minerals, and some garnet porphyroblasts are visible by the naked eye (~1mm large).

Sample NO26 (S13.05970°, E18.79020°) is a quartzitic gneiss from the kyanite zone in the Central Kaoko zone (Figure 1.1.2-1). The hand specimen has a grey color, and a wavy foliation that is defined by light brown- and white layers. Some garnet porphyroblasts (<1 %) are visible by the naked eye and are up to ~2 mm in diameter.

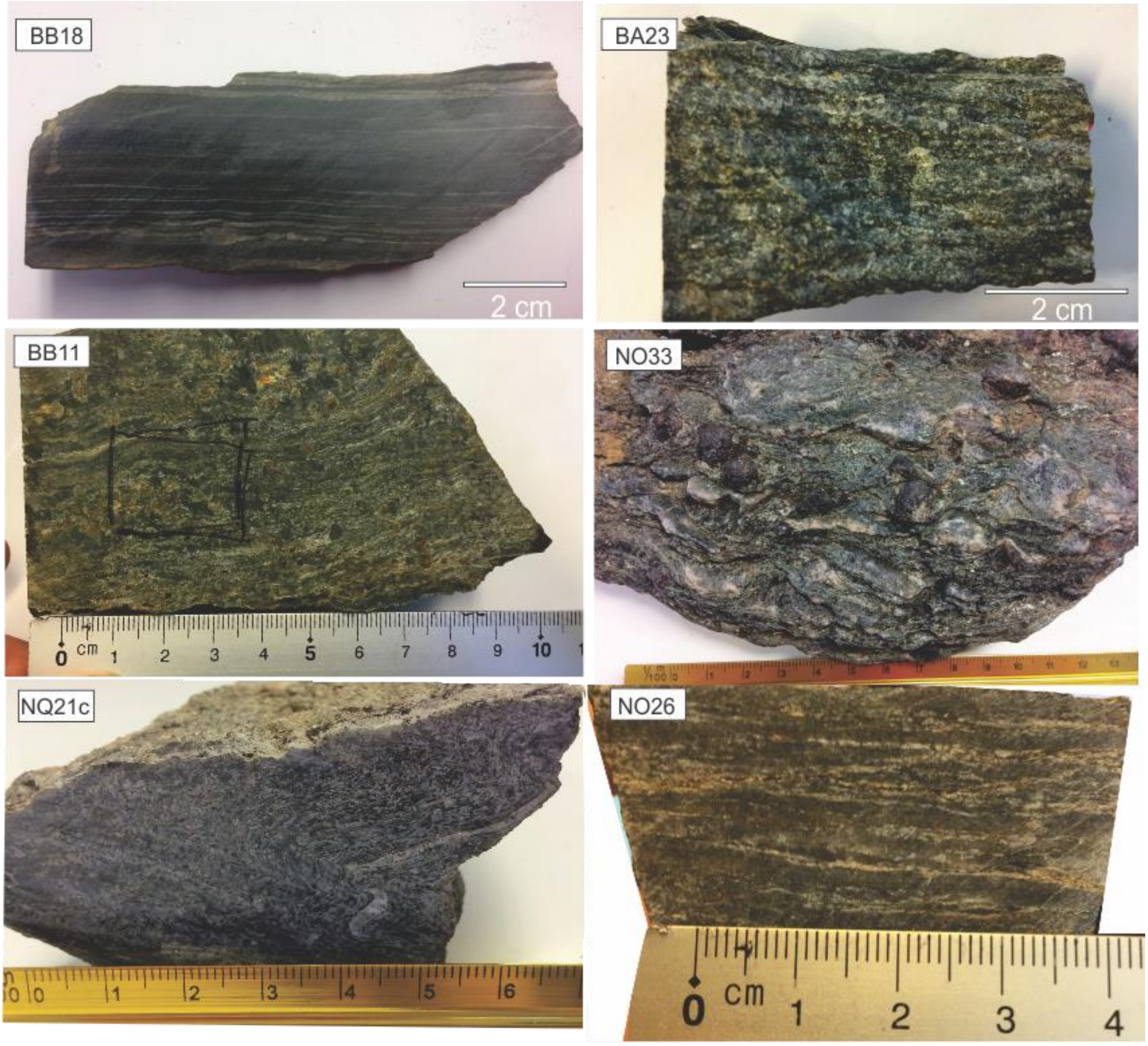

Figure 3.2.1 Photographs showing the macroscopic appearance of the studied samples.

3.3 Whole Rock Chemistry

Results of the whole rock chemical analysis of the studied sample are listed in Table 3.3.1.

Table 3.3.1- Representative whole rock chemistry of samples used for thermodynamic modelling

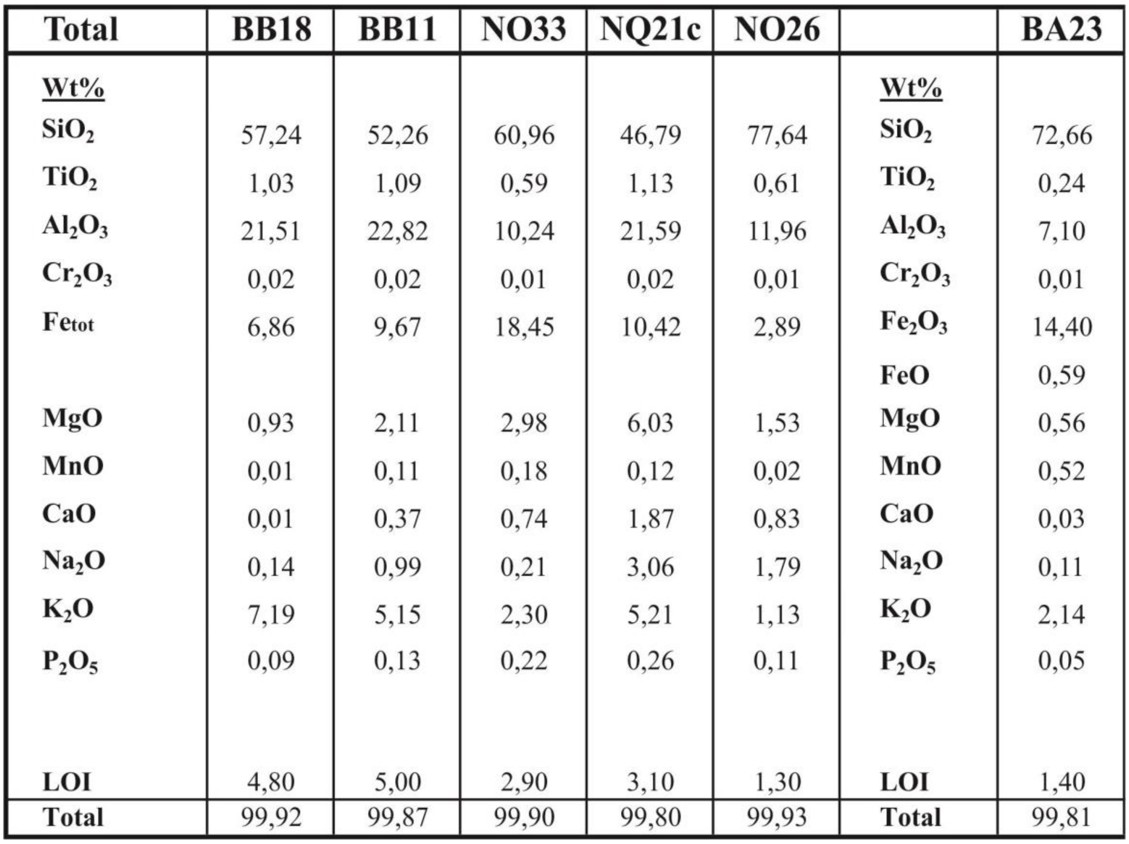

Total	BB18	BB11	NO33	NQ21c	NO26		BA23
Wt%						Wt%	
SiO_2	57,24	52,26	60,96	46,79	77,64	SiO_2	72,66
TiO_2	1,03	1,09	0,59	1,13	0,61	TiO_2	0,24
Al_2O_3	21,51	22,82	10,24	21,59	11,96	Al_2O_3	7,10
Cr_2O_3	0,02	0,02	0,01	0,02	0,01	Cr_2O_3	0,01
Fe_{tot}	6,86	9,67	18,45	10,42	2,89	Fe_2O_3	14,40
						FeO	0,59
MgO	0,93	2,11	2,98	6,03	1,53	MgO	0,56
MnO	0,01	0,11	0,18	0,12	0,02	MnO	0,52
CaO	0,01	0,37	0,74	1,87	0,83	CaO	0,03
Na_2O	0,14	0,99	0,21	3,06	1,79	Na_2O	0,11
K_2O	7,19	5,15	2,30	5,21	1,13	K_2O	2,14
P_2O_5	0,09	0,13	0,22	0,26	0,11	P_2O_5	0,05
LOI	4,80	5,00	2,90	3,10	1,30	LOI	1,40
Total	99,92	99,87	99,90	99,80	99,93	Total	99,81

3.4 Optical petrography and mineral chemistry

3.4.1 Samples from the Brusque Metamorphic Complex

Three samples from Brazil; BB18, BB11, BA23 were used for phase equilibrium. In this chapter, petrograpical observations of these samples will be presented together with representative mineral compositions. The representative mineral compositions are presented in Appendix A. Additional samples from the Brusque Metamorphic Complex are briefly described in order to later discuss regional changes of metamorphic grade in the Brusque Metamorphic Complex.

3.4.1.1 Sample BB18 - Phyllite

Sample BB18 is mainly composed of very fine-grained muscovite (~65%) and quartz (~25%) with minor amounts of chlorite (~5%) and ilmenite (~3%). Accessory zircon and monazite were found during SEM analysis. Figure 3.4.1-1 a) shows two ~0.2 mm thick chlorite-enriched zones that were identified during SEM analysis. Figure 3.4.1-1 b) shows the mineral assemblage inside another chlorite-enriched zone, where chlorite reaches the size of up to ~30 μm.

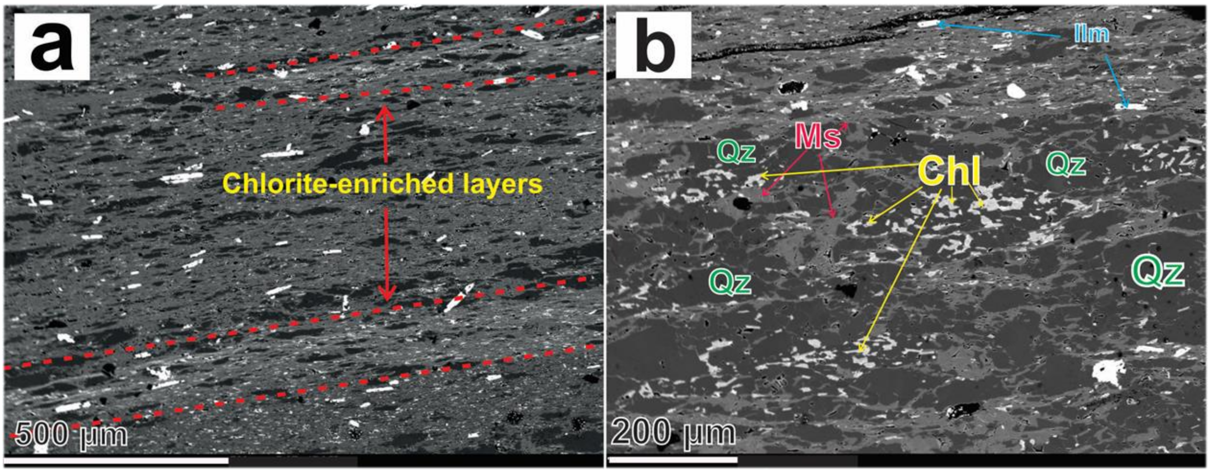

Figure 3.4.1-1 SEM images of sample BB18. a) The red dotted lines marks the two chlorite-enriched zones. White=ilmenite, light gray=chlorite, medium grey=muscovite, dark grey= quartz and back=holes. b) Stable mineral assemblage inside a chlorite-enriched zone in sample BB18, consisting of chl + ms + qz + ilm.

The chlorite is very fine grained (<30μm) and has X_{Mg} values between 0.20-0.22. Muscovite is present inside and outside the chlorite-enriched zones. It shows very little variation in chemical composition and has Si content of 3.09-3.16 a.p.f.u and $K^+/(K^++Na^+)$ ratio of 0.92-0.93.

Ilmenite crystals are homogeneously distributed throughout the sample. They are oriented in various directions with respect to the foliation and reach up to ~0.01 mm in length (see Figure 3.4.1-1). The ilmenite has a Ti^{3+} and Fe^{2+} content of 0.98-0.99 and 0.89-0.92 a.p.f.u respectively, corresponding to a pure ilmenite endmember. The representative microprobe analyses of chlorite, muscovite and ilmenite are listed in Appendix A.

3.4.1.2 Sample BA23 – Garnet-bearing quartzite

Sample BA23 consists of the mineral assemblage quartz (~85%), muscovite (~10%), magnetite (~3%) garnet (~2%) and accessory rutile, biotite and chlorite (<1%). Preferential alignment of muscovite defines the foliation (S1). Locally, crenulation cleavage is present within the muscovite layers (Figure 3.4.1-4).

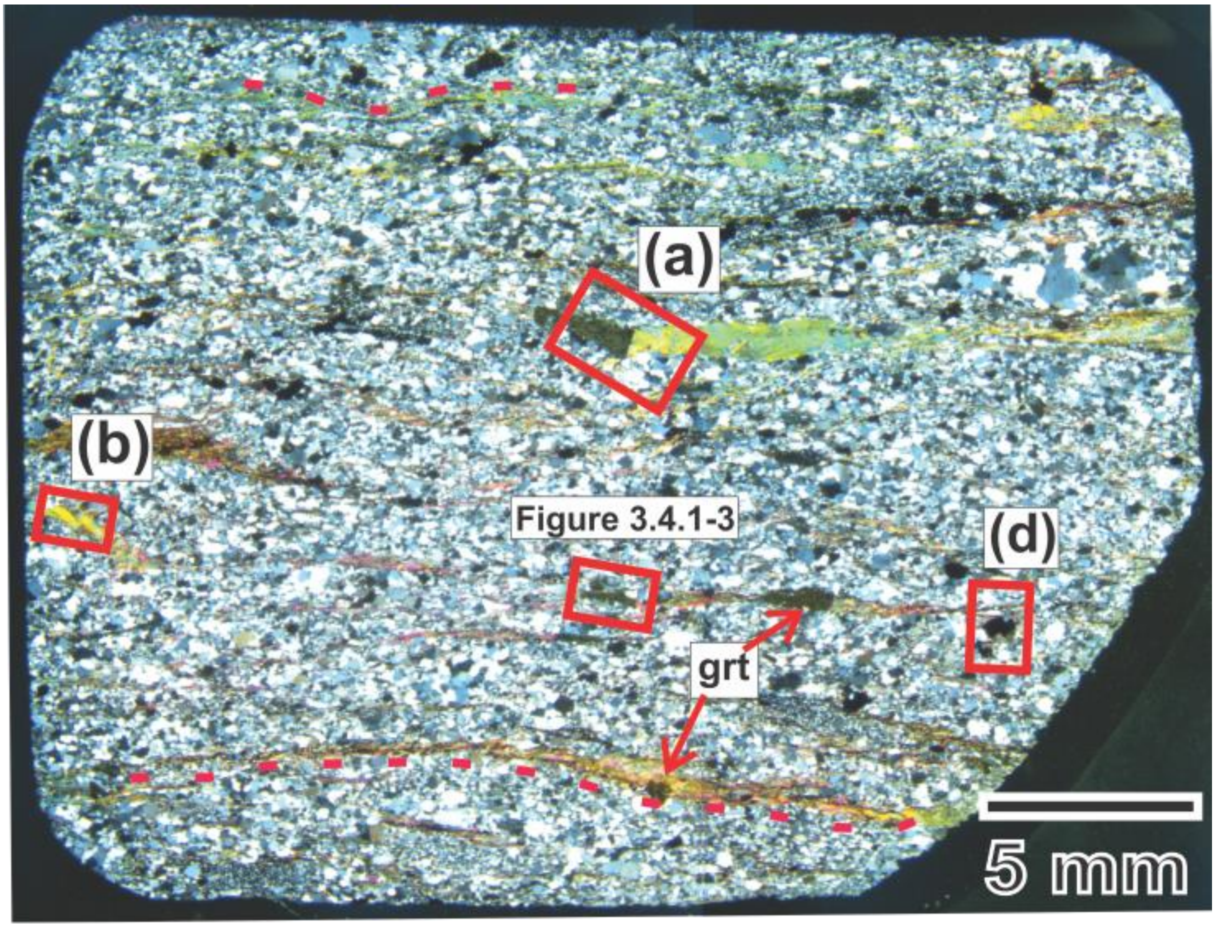

Figure 3.4.1-2 Overview photomicrograph of the sample BA23 (XPL). Red dashed line indicates the folded S1 fabric. Red boxes indicates the position of individual photomicrographs presented in Figure 3.4.1-3 and Figure 3.4.1-4.

Anhedral garnet porphyroblasts (~2 %) are restricted to mica-rich layers; they reach up to ~2.5 mm in length and are elongated sub-parallel to the foliation. Late fractures in garnets are frequent and occur perpendicular to the foliation. Garnet in sample BA23 is rich in spessartine component and has the following core-to-rim range in endmember proportions: $X_{Sps} = 0.71\text{-}0.61$, $X_{Alm} = 0.18\text{-}0.25$, $X_{Prp} = 0.04\text{-}0.12$ and $X_{Grs} = 0.06\text{-}0.03$. The core to rim range in X_{Mg} is 0.19-0.32 (Appendix A). Figure 3.4.1-3 shows the compositional change through the garnet in sample BA23.

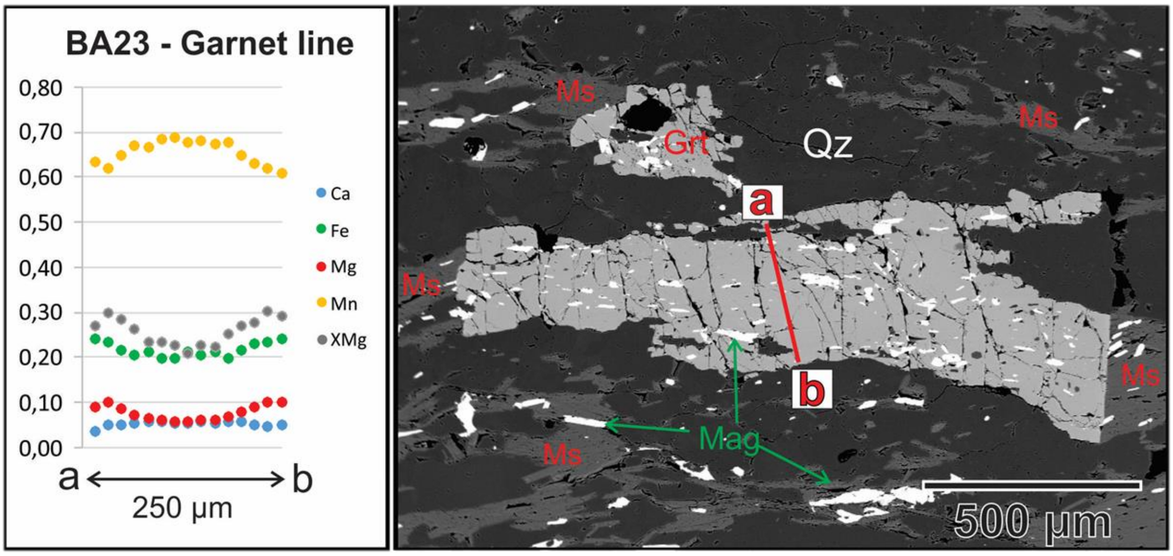

Figure 3.4.1-3 SEM image of garnet in sample BA23. The plot shows the mole fractions of divalent cations measured along the line a-b.

Garnet in sample BA23 displays numerous magnetite inclusions. The inclusions show a continuation of the matrix foliation in to the garnet grains, which together with the garnet elongation suggests a late syn-kinematic to post-kinematic growth with respect to the D1 deformation (Figure 3.4.1-3).

Fine-grained white mica locally reaches up to ~0.7 mm in length and has a $K^+/(K^++Na^+)$ ratio of 0.91-0.93. The Si and Al content ranges from 3.09-3.16 and 2.49-2.54 a.p.f.u., respectively. Some bands with muscovite are more brownish than other due to presence of fine Fe-oxide/hydroxide. The $Mg^{2+} + Fe^{2+} + Fe^{3+}$ from 0.36 to 0.38 a.p.f.u.

Magnetite is present as subhedral to anhedral porphyroblasts (up to ~1 mm large) and as fine-grained matrix magnetite. The magnetite is homogenously distributed throughout the sample and has a $Fe^{2+}/(Fe^{2+}+Fe^{3+})$ ratio of 0.49-0.57.

Biotite is rare. It reaches up to ~0.3 mm in length and has X_{Mg} of 0.74.

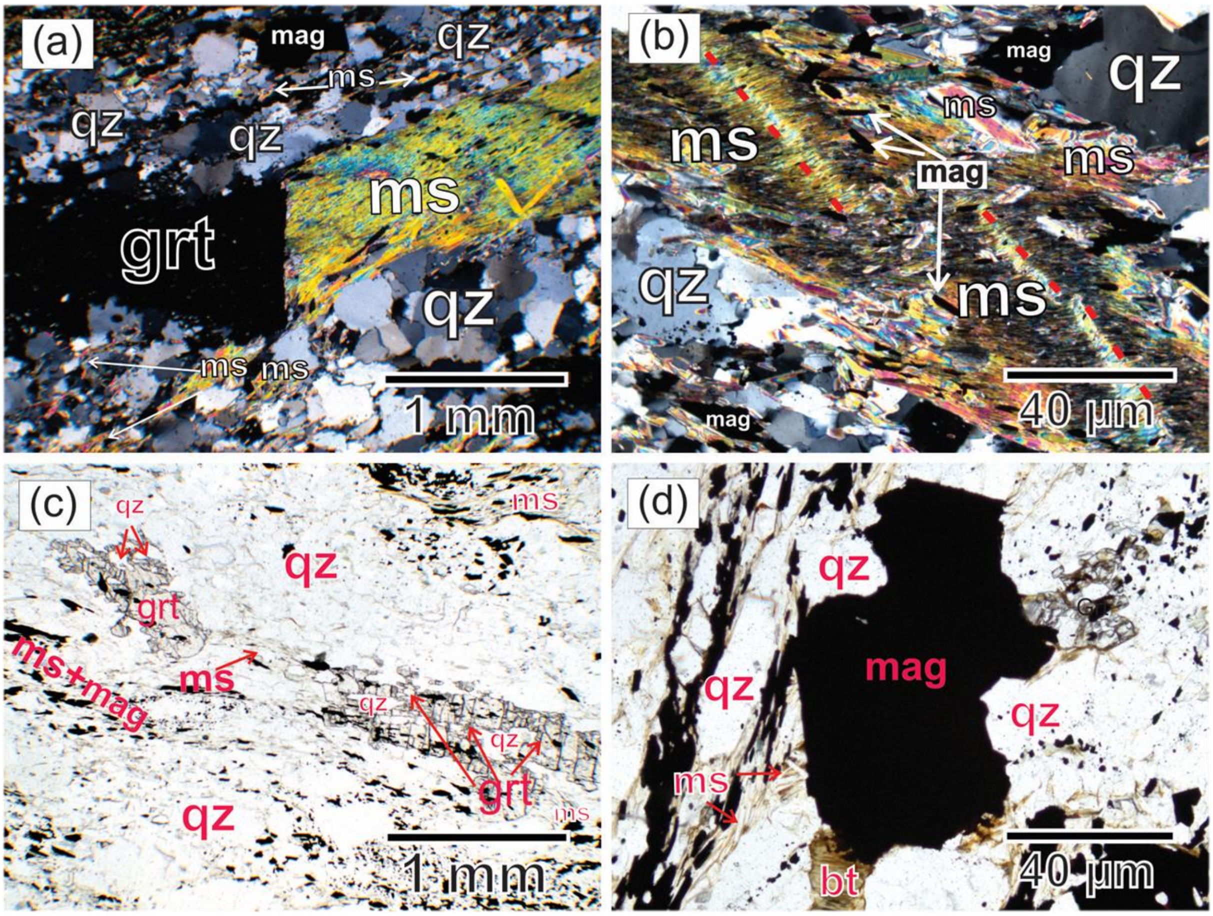

Figure 3.4.1-4 Textural relationships of the stable phases in sample BA23. (a) Photomicrograph (XPL) showing anhedral garnet growing in a muscovite layer (b) Photomicrograph (XPL) showing crenulation cleavage in a folded muscovite layer. The red dashed line marks the orientation of the crenulation cleavage. (c) Photomicrograph (PPL) showing skeletal garnet growing in a qz+ms+mag matrix. The garnet is oriented sub-parallel the S1 fabric. (d) Anhedral magnetite porphyroblasts.

3.4.1.3 Sample BB11 – Garnet-mica schist

Sample BB11 consists of porphyroblasts of garnet (~10%), chlorite (~6%), and biotite (~7%) growing in a fine-grained matrix of muscovite (~55%), quartz (~15%) and ilmenite (~1%). Accessory amounts of plagioclase, k-feldspar and apatite were found during SEM analysis.

Preferential alignment of muscovite and ilmenite defines the main foliation (S1) which has been folded into F2 folds. Development of a weak crenulation cleavage (S2) sub-parallel to axial planes of folds is visible in the thin section (Figure 3.4.1-6).

Euhedral to anhedral garnet porphyroblasts reach up to ~2.2 mm in diameter. Figure 3.4.1-5 shows a compositional profile through a garnet in sample BB11. Due to its anhedral shape, two points were measured at the position where the garnet rim shows a straight contact with the matrix. The two points are indicated with numbers in Figure 3.4.1-5, and the garnet composition are shown in Appendix A. The garnet in sample BB11 have the following core-to-rim range of endmember proportions: X_{Alm} 0.61-0.82, X_{Grs} 0.22-0.07, X_{Sps} 0.15-0.00 and X_{Prp} 0.03-0.10. The core-to-rim range in X_{Mg} is 0.05-0.11.

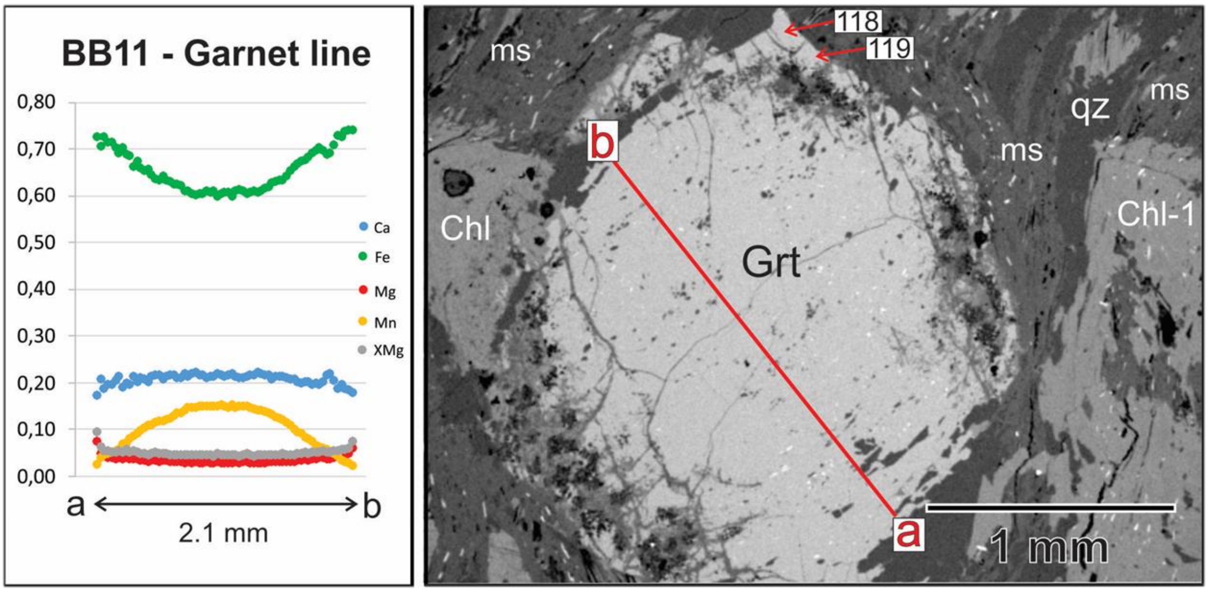

Figure 3.4.1-5 - SEM image of garnet from sample BB11. The plot shows the mole fractions of divalent cations measured along the line a-b. The red arrows show the position of two additional garnet-rim measurements that are presented in Appendix A.

Garnet in sample BB11 is mostly inclusion free, except for some very small quartz, ilmenite and apatite inclusions (Figure 3.4.1-5). The inclusions are oriented in various directions with respect to the S1 foliation (Figure 3.4.1-5), which suggests a syn-kinematic with respect to D1. Euhedral garnet relicts suggest a pre-kinematic growth with respect to D2, as it is cutting the S1 fabric and the F2 micro-folds bends around the crystal (Figure 3.4.1-6 (a)).

Subhedral, tabular chlorite porphyroblasts occur in two different textural positions; (1) with the c-axis parallel to the matrix foliation (Figure 3.4.1-6 (c) and (d) – chl 1) and (2) with the c-axis sub-parallel to the axial plane of F2 folds (Figure 3.4.1-6 (b) and (c) chl 2). The chlorite porphyroblasts range from ~0.5 mm to ~2.0 mm in length. Numerous ilmenite inclusions display a continuation of the matrix foliation in to the chlorite porphyroblasts (Figure 3.4.1-6 (d)). All metamorphic chlorite in sample BB11 has X_{Mg} values between 0.40-0.46. There is no significant difference in the chemical composition of chl-1 and chl-2. The textural relationships in sample BB11 suggests that chl-1 crystallized syn-kinematic to D1 and chl-2 crystallized syn-kinematic to D2.

Anhedral biotite porphyroblasts are up to ~0.5 mm long and occur both parallel- and at high angles to the matrix foliation (Figure 3.4.1-6 (a) and (b)). Biotite in sample BB11 has X_{Mg} between 0.38 and 0.43.

Anhedral plagioclase was identified during SEM analysis and shows no twinning, cleavage or zoning. The proportions of feldspar endmembers in the measured plagioclase grains are 6-14 % anorthite, 85-92% albite and less than 1% K-feldspar. The measured plagioclase grains therefore classify as albite and oligoclase. One single K-feldspar was found during SEM analysis. The K-feldspar has less than 3 % of albite component.

Bands of very fine-grained muscovite together with ilmenite have a brownish appearance in plane polarized light. Measured muscovite crystals contains various proportions of paragonite endmember and show $K^+/(K^++Na^+)$ ratio between 0.72 and 0.90. The Si and Al content of the measured grains is 3.09-3.20 and 2.63-2.79 a.p.f.u., respectively.

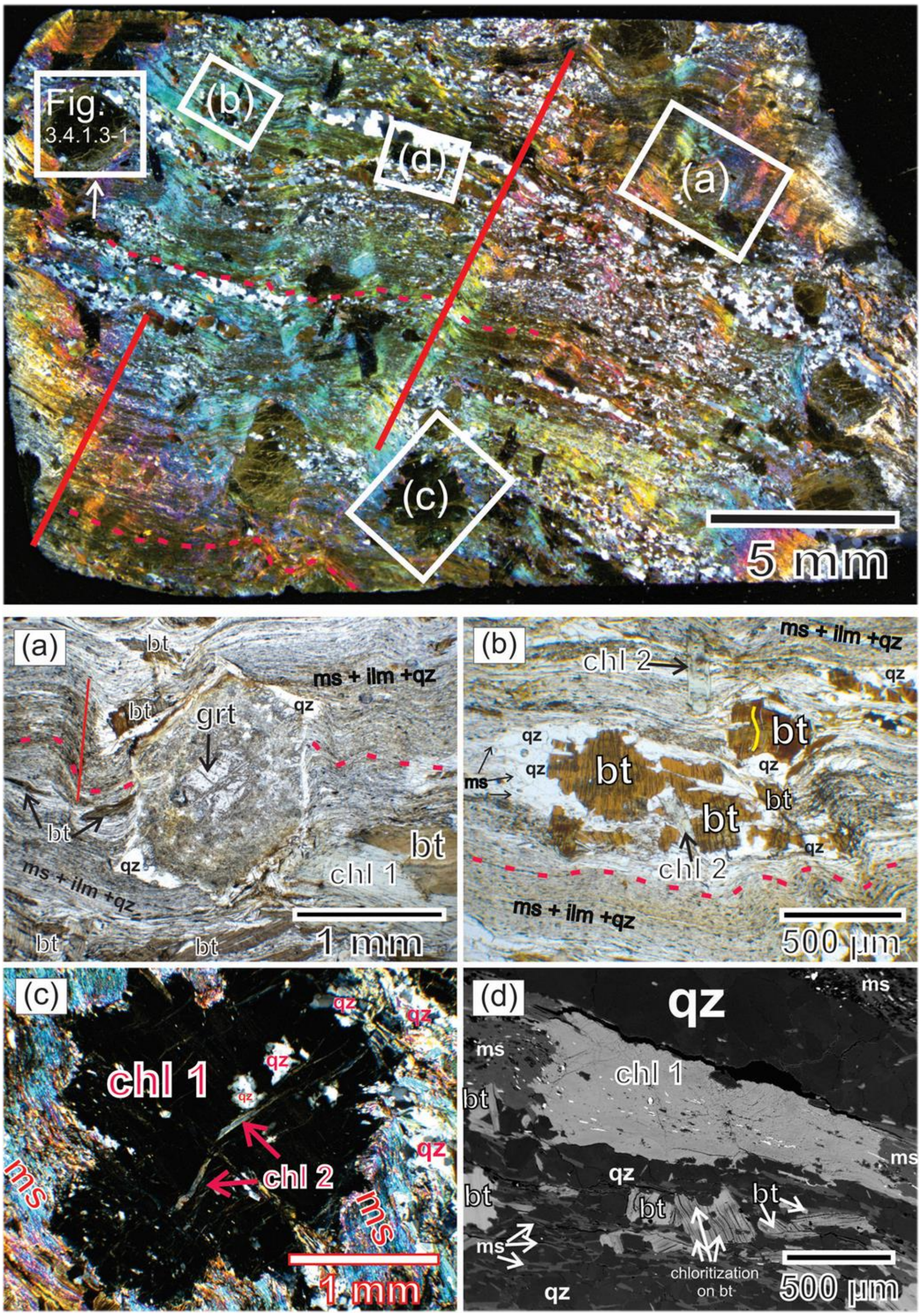

Figure 3.4.1-6 Textural relationships of stable mineral phases in sample BB11. The top picture show an overview microphotograph (XPL) of the thin section.The dashed red lines marks the S1 fabric and solid red lines indicates the orientation of the S2 crenulation cleavage (a) Photomicrograph (PPL) showing almost totally replaced euhedral garnet in a folded ms+ilm+qz matrix. In the lower right corner: biotite porphyroblasts consuming chlorite 1. (b) Photomicrograph (PPL) showing chl-2 crystals oriented sub-parallel to S2, and anhedral biotite porphyroblasts enveloped by quartz. (c) Photomicrograph (XPL) showing chl-2 growing inside of chl-1. Chl 1 is cut perpendicular to c-axis. (d) SEM image showing chl-1 growing in a fine-grained ms+ilm+qz layer, and chloritized biotite porphyroblasts. White= ilmenite.

3.4.1.4 Additional samples form the Brusque Metamorphic Complex

Additional samples from the Brusque Metamorphic Complex involves samples that were not chosen for thermobarometry, either due to the present mineral assemblage or due to strong alteration. The observed mineral assemblages of these samples are presented in Table 3.4.1 below.

Table 3.4.1 Mineral assemblages observed in additional samples from the Brusque Metamorphic Complex. The sample locations are presented in Figure 1.1.1-1.

Sample	**Mineral Assemblage**	**Coordinates**
BB09	Bt + Ms + Qz + Hem + Ilm	S 027°15.851' W 048°50.759'
BB10b	Bt + Ms + Qz + Opq + Chl	S 027°16.971' W 048°55.013'
BB23	Qz + Ms + Ilm + Chl	S 027°13.481' W 049°09.588'
BB24	Chl + Ms + Qz + Hem + Opq	S 027°14.414' W 049°10.550'
BB30	Ms + Qz + Ilm + Hem	S 027°12.450' W 049°09.496'
BB12b	Grt + Bt + Ms + Qz + Ilm	S 027°18.941 W 049°07.680'
BB12c	Grt + Chl + Bt + Qz + Pl + Ms + Ilm	S 027°18.941 W 049°07.680'
BB14	Grt + Bt + Ms + Chl + Qz + Opq	S 027°15.121' W 049°09.422'
BB15	Grt + Ms + Bt + Qz + Pl + Opq	S 027°14.103' W 049°09.517'
BB32	Grt + Ms + Bt + Chl + Qz + Ilm	S 026°56.649' W 048°42.954'
BB08	Cal + Chl + Bt + Qz + Ms + Pl	S 027°16.967' W 048°55.009'
BB07	Cal + Cpx + Qz + Pl + Amp + Ttn + Grt + Opq	S 027°05.347 W 048°35.731'

By the present mineral assemblages, the additional samples can be divided into 3 groups. Low-grade metapelitic samples (BB09, BB10b, BB23, BB24 and BB30), garnet-bearing metapelitic samples (BB12 (a and b), BB14, BB15 and BB32) and metamorphosed calc-silicates (BB08 and BB07). Garnet in additional samples are partially or totally replaced by fine grained micas and chlorite, but seem to have been developed during the D1 event by the presence of inclusion trails (Figure 3.4.1-7)

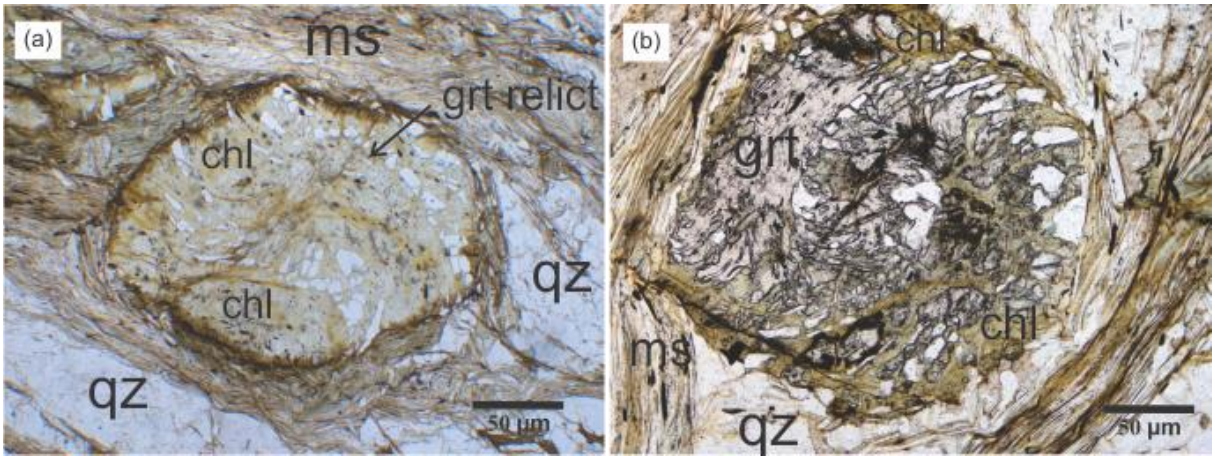

Figure 3.4.1-7 (a) Microphotograph (PPL) showing a garnet relict from the sample BB15. The garnet is totally replaced by fine grained chlorite, but quartz and ilmenite inclusion suggest a syn-kinematic, rotational growth. (b) Microphotograph (PPL) showing a garnet porphyroblast in sample BB12b, which has been partially replaced by chlorite. Inclusion trails of quartz reflects a syn-kinematic growth with respect to the D1 event.

3.4.2 Samples from the Central Kaoko Zone

Three samples from the Central Kaoko Zone in Namibia NO33, NQ21c and NO26 were used for thermodynamic modelling. In this chapter, petrograpical observations of these samples will be presented together with representative mineral compositions. The representative mineral compositions are presented in Appendix A.

3.4.2.1 Sample NO33 – Garnet-mica schist

Sample NO33 is a garnet-mica-schist from the garnet zone of the Central Kaoko Zone (Figure 1.1.2-1). The thin section consists of garnet (~5%) and biotite (~15%) porphyroblasts in a fine-grained matrix of quartz (~40 %) and chlorite (~20%). Minor amount of muscovite (<5%) and accessory amounts of ilmenite, magnetite and apatite were found during SEM analysis. The foliation (S1) is defined by alternating wavy layers of quartz and layers of aligned chlorite and biotite crystals. A weakly developed crenulation cleavage (S2) is present within one chlorite enriched layer (Figure 3.4.2-2 (a)).

Euhedral to anhedral garnet porphyroblasts are up to ~2.4 mm in diameter in the thin section. Figure 3.4.2-1 shows a compositional profile through a euhedral garnet in sample NO33. The garnets have the following core-to-rime range of endmember proportions: X_{Alm} 0.74-0.84, X_{Grs} 0.13-0.10, X_{Sps} 0.08-0.02 and X_{Prp} 0.04-0.04. The core-to-rim range in X_{Mg} is 0.04-0.05. The garnet contain numerous inclusions of ilmenite and apatite and inclusion trails reflects a syn-kinematic growth of garnet in sample NO33 with respect to the foliation (Figure 3.4.2-2 (c)).

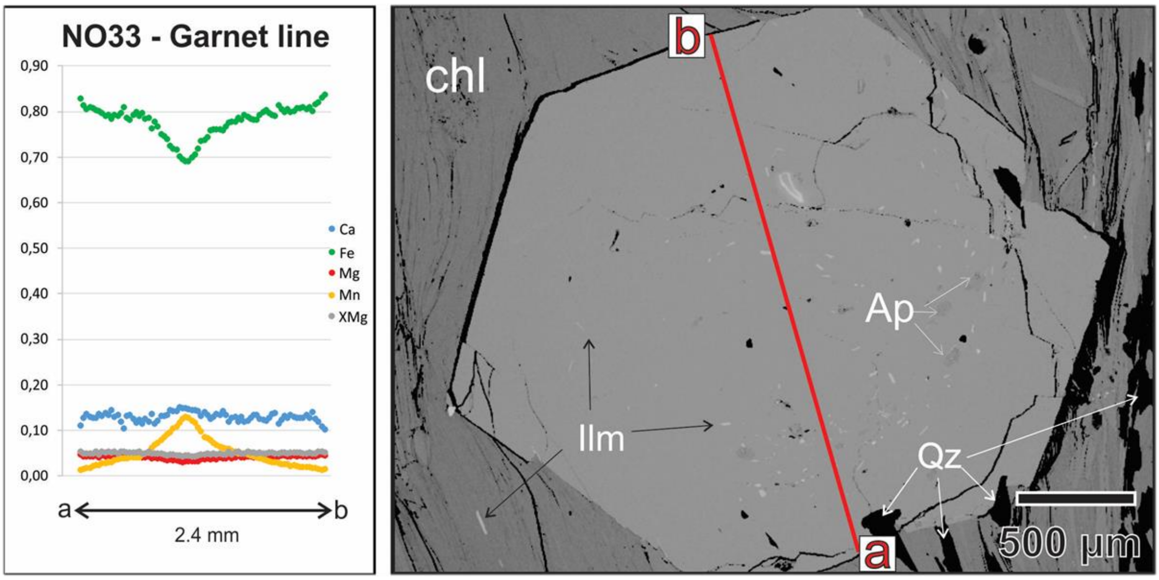

Figure 3.4.2-1 - SEM image of garnet in sample NO33. The plot shows the mole fractions of divalent cations measured along the line a-b.

Subhedral- to anhedral biotite porphyroblasts reach up to ~3.0 mm in length. The majority of biotite crystals are oriented parallel to the main foliation (S1), but locally biotite are oriented subparallel to crenulation cleavage (S2) (Figure 3.4.2-2 (a) and (b)). The chemical composition of the biotite in different textural positions shows no variation. The X_{Mg} of biotite porphyroblasts are between 0.28 and 0.30.

The chlorite is very fine grained, has a thin tabulate to needle-like shape and an X_{Mg} value of 0.32. White mica has a K^+/ (K^++Na^+) ratio between 0.83-0.85. The Si and Al content ranges between 3.09-3.11 and 2.69-2.74 a.p.f.u., respectively. The white mica has a Fe^{2+} and Mg^{2+} content up to 0.17 and 0.06 a.p.f.u., respectively.

Ilmenite occurs both in the matrix and as inclusions in garnet. The Fe^{2+}/ (Fe^{2+} + Ti^{4+}) is 0.5, corresponding to a pure ilmenite endmember composition.

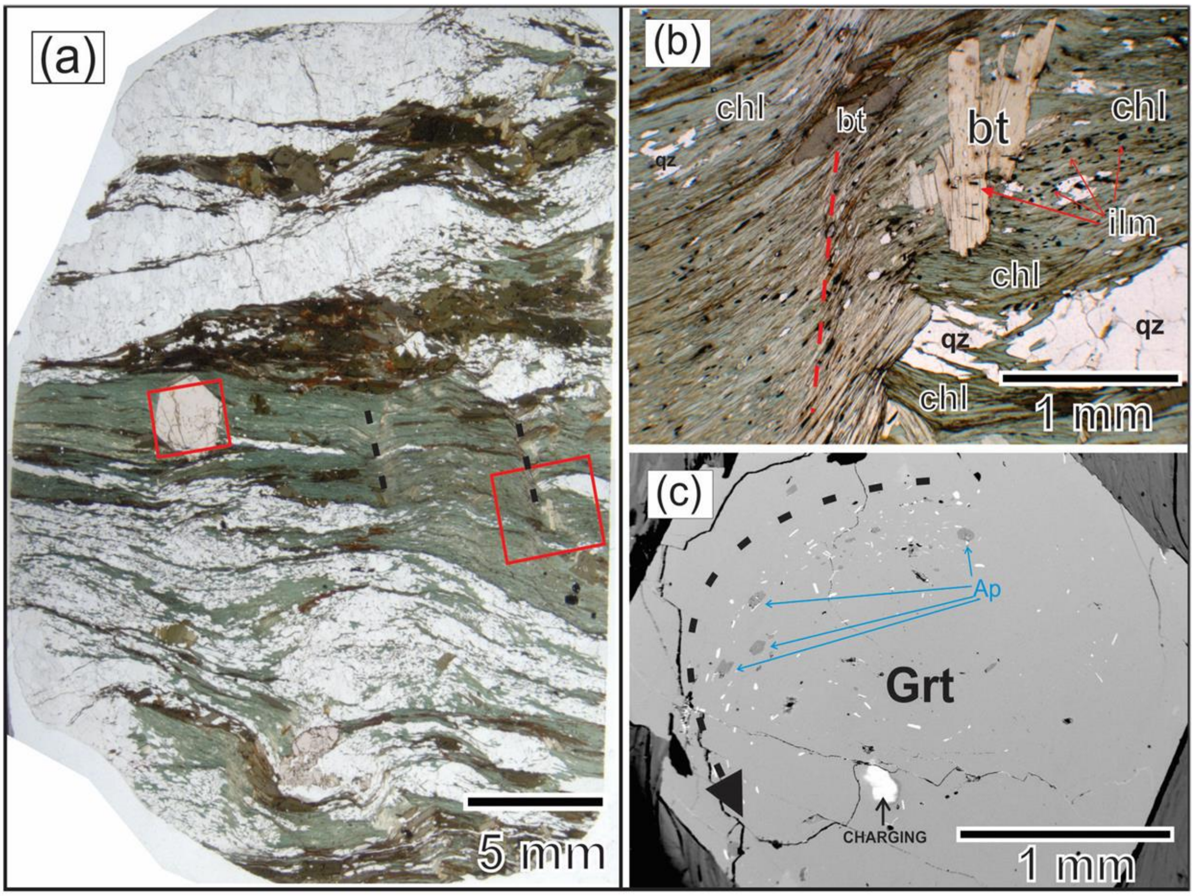

Figure 3.4.2-2 Textural relationships of minerals in sample NO33. (a) Overview microphotograph (PPL) of the sample (white=quartz, green=chlorite, brown=biotite oriented parallel to foliation, light brown=biotite oriented subparallel to crenulation cleavage, pink=garnet). The red boxes indicates the position of individual microphotographs (b) and (c), and the dotted black lines indicates crenulation cleavage in a chlorite layer. (b) Microphotograph (PPL) showing biotite porphyroblast oriented parallel to the crenulation cleavage. (c) SEM image showing inclusion trail of apatite and ilmenite (white needles) in garnet porphyroblast.

3.4.2.2 Sample NQ21c – Staurolite-garnet-mica schist

Sample NQ21c is from the staurolite zone in the Central Kaoko Zone (Figure 1.1.2-1). Porphyroblasts of garnet (~5%), biotite (~50%), chlorite (>1%), and staurolite (~2%) overgrow the folded matrix of plagioclase (~2%), quartz (~15%) and muscovite (~30%). Accessory amounts of ilmenite, rutile and apatite were found during SEM analysis. Two different fabrics were observed during petrographic investigation and can be seen in Figure 3.4.2-4. Alignment of muscovite, biotite and ilmenite defines the (S1) foliation. A later event has folded the S1 foliation into F2 folds, and development of crenulation cleavage (S2) sub-parallel to axial planes of F2 folds is visible in the thin section.

Rounded subhedral- to anhedral garnet porphyroblasts (~5%) reach up to 1.0 mm in diameter, and are partially consumed by biotite and muscovite. Garnet crystals contains inclusions of chlorite, quartz and ilmenite oriented at high angles with respect to the S2 fabric. Garnet in sample NQ21c has the following core-to-rim range of endmember proportions: X_{Alm} = 0.64-0.74, X_{Sps} = 0.18-0.05, X_{Grs} = 0.09-0.07 and X_{Prp} = 0.10-0.15. The core-to-rim range in X_{Mg} is 0.13-0.16.

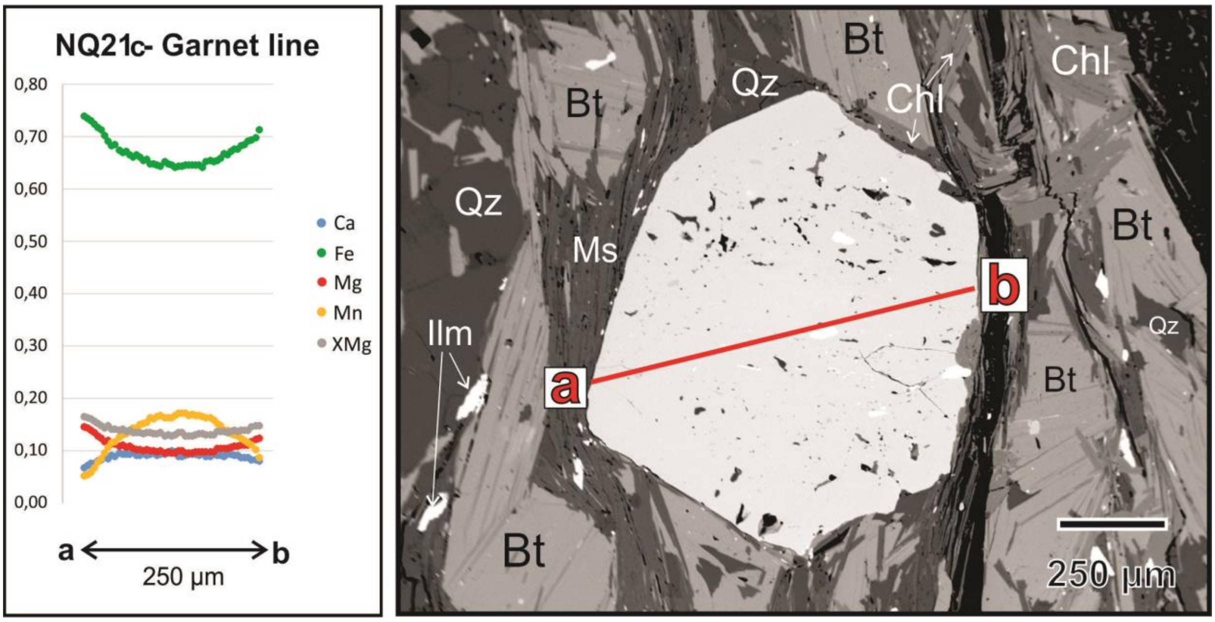

Figure 3.4.2-3 SEM image of garnet in sample NQ21c. The plot shows the mole fractions of divalent cations measured along the line a-b.

Euhedral to subhedral staurolite porphyroblasts (~2%) reach up to ~0.5 mm in length and are present in two textural positions. The majority of staurolite porphyroblasts are oriented sub-parallel to the crenulation cleavage (Figure 3.4.2-4(a)). One staurolite (Figure 3.4.2-4 (b)) is oriented perpendicular to the crenulation cleavage. These textural observations indicates a pre-to syn kinematic growth with respect to the development of the crenulation cleavage (S2). Alternatively, the staurolite may have been pre-kinematic and passively rotated during D2 deformation. Staurolite is chemically homogeneous and has X_{Mg} values between 0.20 and 0.22.

Biotite (~50%) occurs as thick- to thin tabulate porphyroblasts and reaches up to ~1.0 mm in length. Biotite porphyroblasts are oriented mainly sub-parallel to the S1 fabric and some are oriented parallel to axial planes of F2 folds, suggesting a pre- to syn- kinematic growth with respect to the D1 event. X_{Mg} values of the biotite are between 0.54-0.56. Some of the biotite is partially chloritized (Figure 3.4.2-4 (a)).

White mica (~30%) has a $K^+/(K^+ + Na^+)$ ratio between 0.74 – 0.79. The Si and Al content is 3.07-3.10 and 2.78-2.82 a.p.f.u., respectively.

Anhedral plagioclase reaches up to ~0.5 mm in diameter. The X_{An} of the plagioclase is between 0.19 and 0.25, corresponding to an oligoclase composition. Less than 1% K-feldspar component is present in plagioclase in sample NQ21c.

Euhedral to subhedral tabulate chlorite (>1%) is growing subparallel to the axial plane of D2 folds, which indicate syn-kinematic growth with respect to D2 (Figure 3.4.2-4 (d)). Chlorite porphyroblasts have X_{Mg} between 0.60 and 0.61.

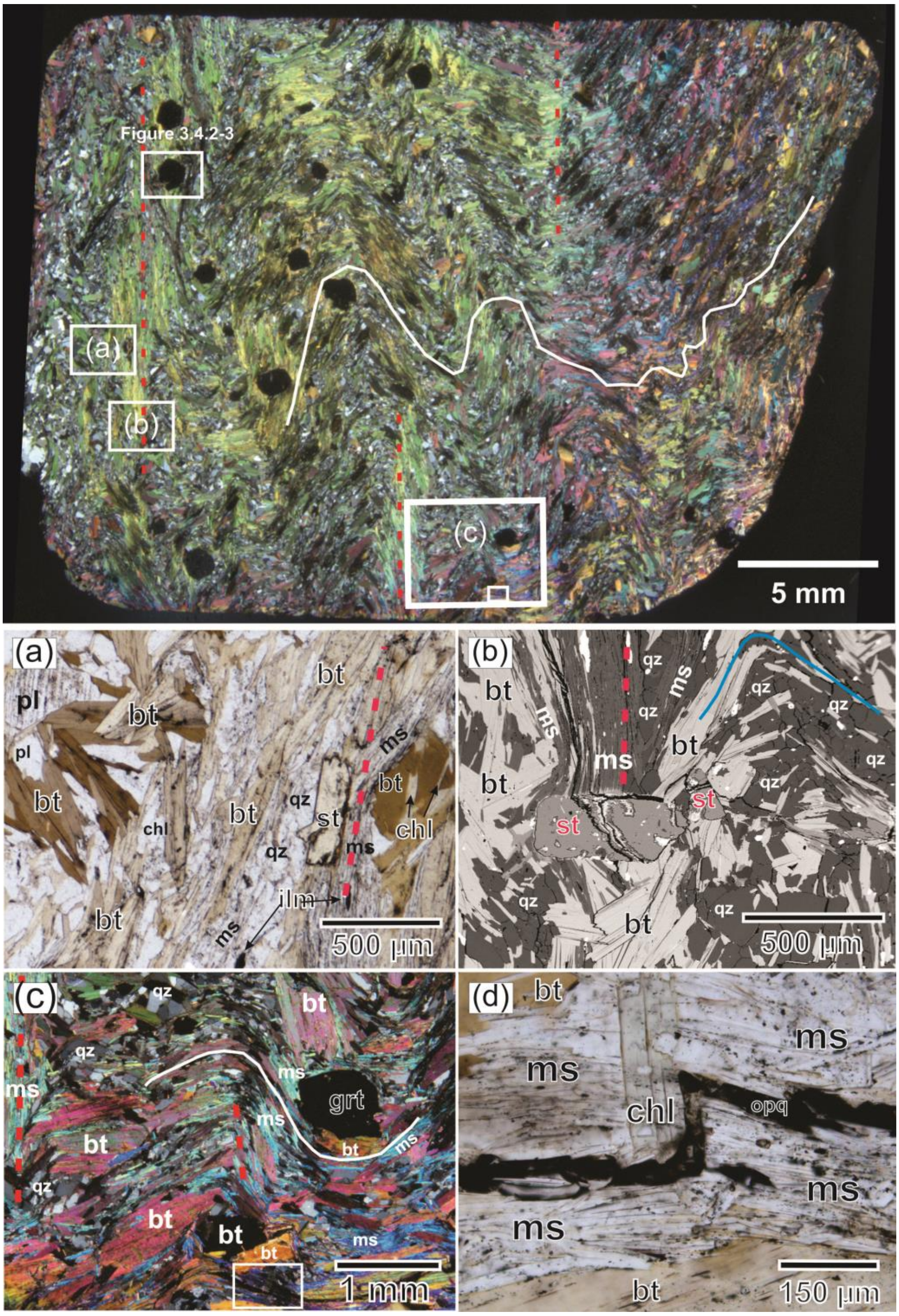

Figure 3.4.2-4 Textural relationships of the stable mineral phases in sample NQ21c. The picture in top shows an overview photomicrograph of the sample (XPL). Dashed red lines show the orientation of the crenulation cleavage (S2) and solid (blue and white) lines shows the folded S1 fabric. White boxes indicates the position of individual photomicrographs. (a) Photomicrograph (PPL) showing subhedral staurolite orientated parallel with the crenulation cleavage. (b) SEM Image showing staurolite oriented perpendicular to the crenulation cleavage. (c) Photomicrograph (XPL) showing biotite and muscovite consuming anhedral garnet. The rectangle indicates the position of (d). (d) Photomicrograph (PPL) showing metamorphic chlorite parallel to the crenulation cleavage (see (c)). Note the opaque spots in muscovite causing its brownish colour.

3.4.2.3 Sample NO26 – Kyanite-quartzite

Sample NO26 is a quartzite from the kyanite zone in the Central Kaoko zone (Figure 1.1.2-1). The sample consists of quartz (~85%), biotite (~10%), plagioclase (~5%), kyanite (~5%), garnet (~2%), and accessory rutile, staurolite, ilmenite, apatite, zircon and monazite. The matrix foliation (S1) is defined by alignment of thin-tabulate biotite crystals (Figure 3.4.2-5).

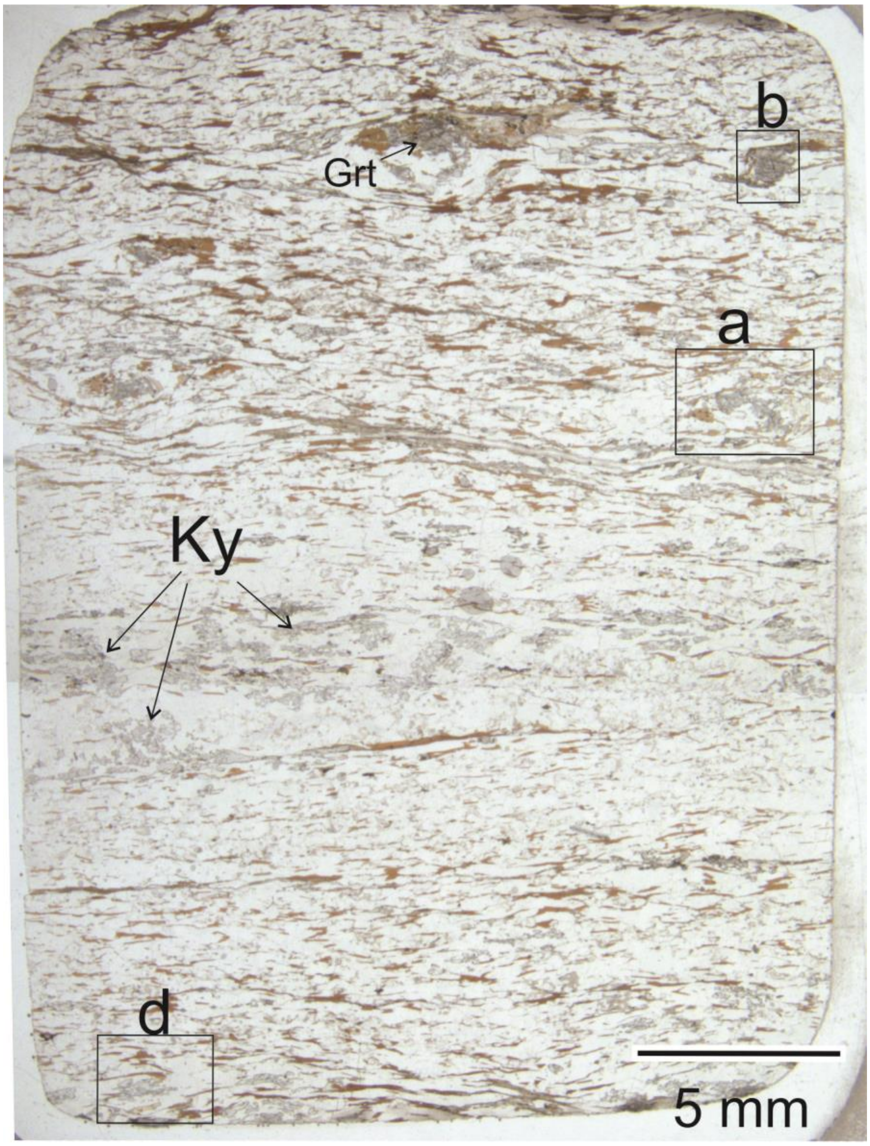

Figure 3.4.2-5 Overview photomicrograph of the sample NO26 (PPL). Black rectangles indicate the position of individual photomicrographs (a), (b) and (d) presented in figure 3.4.1-12. The preferred orientation of biotite (brown) defines the matrix foliation (S1).

Anhedral garnet (~2%) grows up to ~2 mm in length, and is partially replaced by fine-grained sericite, biotite and plagioclase (Figure 3.4.2-6). Except for some quartz inclusions, the garnets are mostly inclusion free. Garnet in sample NO26 has the following core-to-rim range in endmember proportions: X_{Alm} = 0.71-0.77, X_{Prp} = 0.22-0.14, X_{Grs} = 0.05-0.04 and X_{Sps} = 0.01-0.05. The core-to-rim range in X_{Mg} is 0.24-0.15. Figure 3.4.2-6 shows the compositional changes through the garnet in sample NO26.

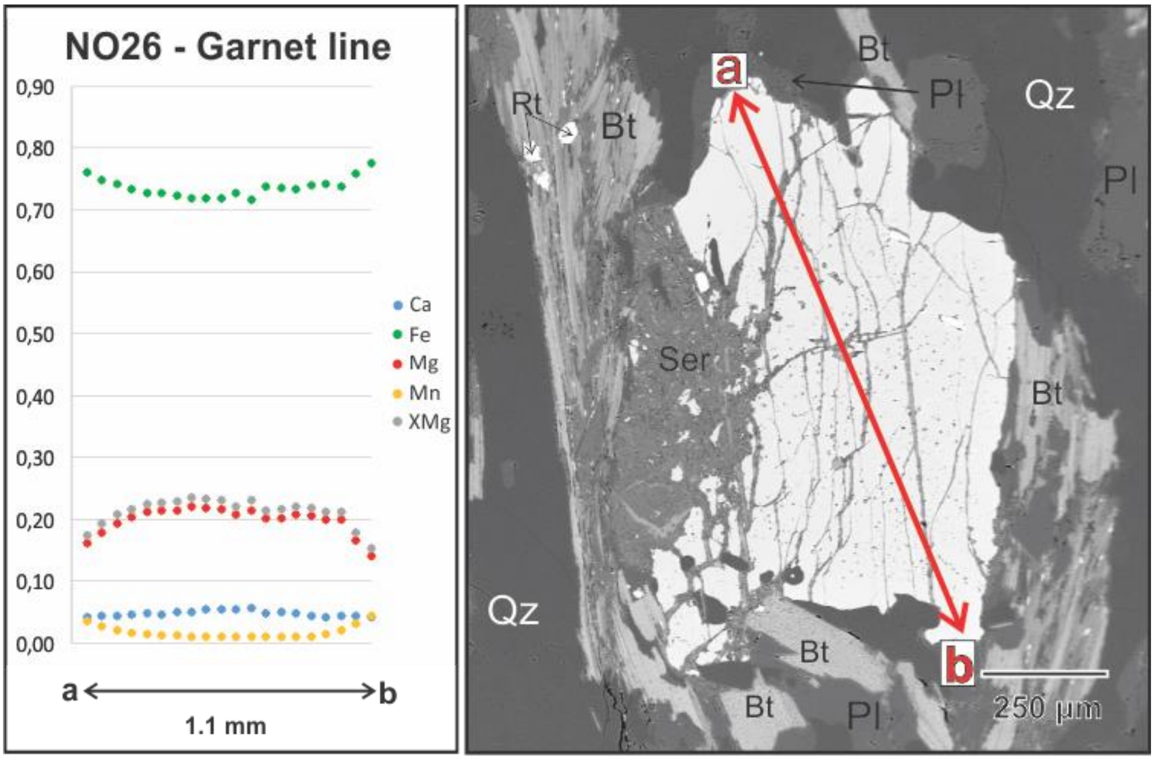

Figure 3.4.2-6 SEM image of garnet in sample NO26. The plot shows the mole fractions of divalent cations measured along the line a-b.

Skeletal kyanite aggregates (~5%) reach up to 1.5 mm in length. Cleavage planes of the crystals and elongation of aggregates are parallel with the main foliation, suggesting a syn-kinematic growth with respect to the foliation.

Only one single staurolite crystal is present in the thin section (Figure 3.4.2-7 (d)). It is oriented parallel with the main foliation (S1), and has one rutile inclusion that has the same orientation, suggesting a pre-kinematic growth with respect to the S1 fabric. Staurolite has X_{Mg} of 0.24 in the core, and 0.17 at the rim.

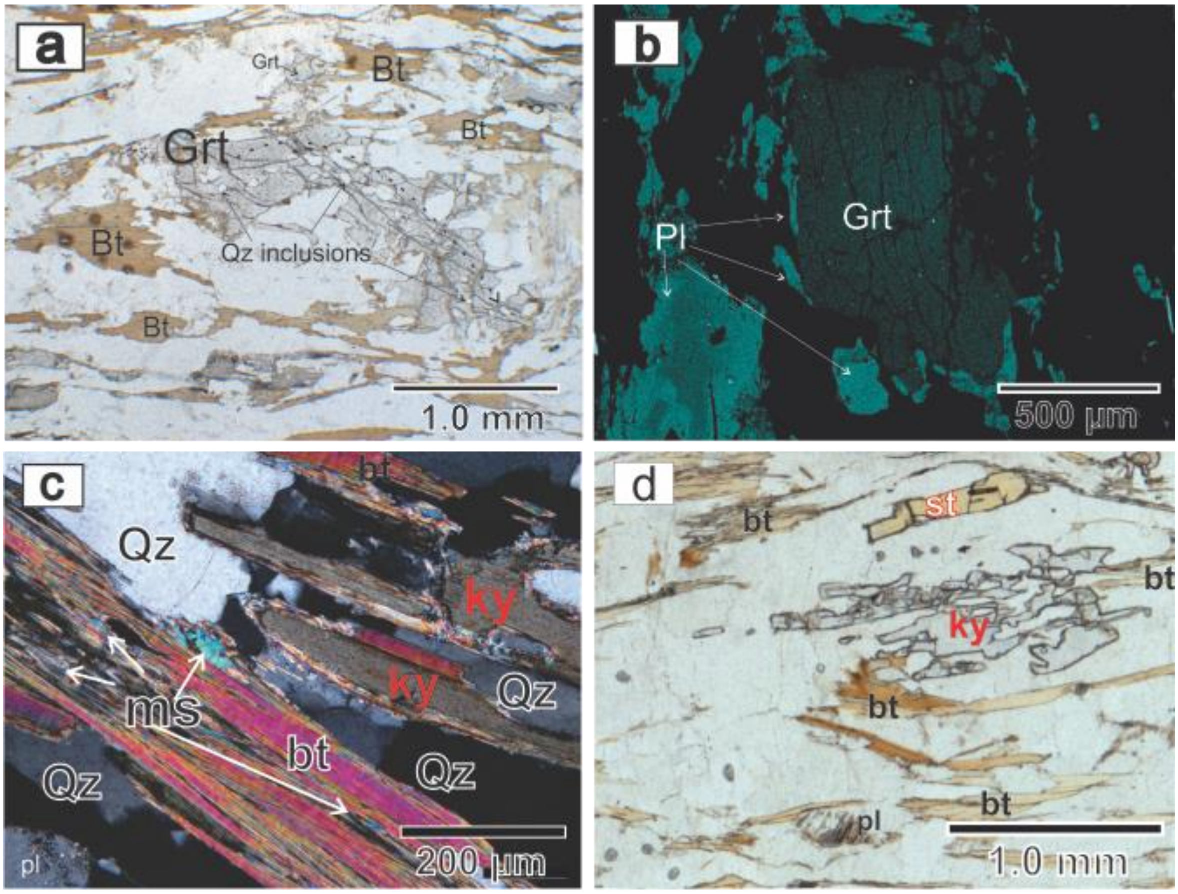

Figure 3.4.2-7 Textural relationships of the stable mineral assemblage in sample NO26. (a) Anhedral garnet porphyroblasts with inclusion trail of quartz. (b) SEM element map showing the relative proportion of Ca^{2+}. In the lower left corner: zoned plagioclase crystal show an increase in Ca^{2+} towards the rim. The plagioclase is consuming garnet, and forms a thin corona around the anhedral garnet. (c) Small amounts fine-grained muscovite is present together with biotite. (d) Kyanite, biotite and staurolite crystals oriented subparallel to each other (S1).

Thin-tabulate biotite reaches up to ~2.0 mm in length and it is homogeneously distributed through the sample. The biotite in the matrix has X_{Mg} values between 0.50-0.53, and a Si and Al content of 2.71-2.81 and 1.71-1.77 a.p.f.u., respectively. The biotite that consumes garnet shows a slightly higher X_{Mg} of 0.57.

Anhedral to subhedral plagioclase reaches up ~0.8 mm in length and shows a chemical zonation characterized by increase in Ca towards the rim (Figure 3.4.2-7 (b) and Appendix A). Plagioclase has a core-to-rim range in X_{An} from 0.12 to 0.23, and less than 1% K-feldspar component. Crystals show no specific orientation with respect to the matrix foliation.

White mica (<1 %) occurs together with biotite and is very fine grained. It has a Si and Al content of 3.06-3.15 and 2.45-2.86 a.p.f.u., respectively. The K / (K + Na) ratio is 0.76-0.96.

3.5 Phase equilibrium modelling

P-T conditions of formation of the six samples (described above) were estimated using phase equilibrium modelling by the Perple_X software package, version 6.7.0 (Connolly, 2005).The calculations of P-T pseudosections were performed in the MnNCKFMASHTi system with an internally consistent thermodynamic data set of Holland and Powell (1998:2004 upgrade). Whole-rock analyses of the studied samples (Table 3.3.1) were used as system compositions in the modelling. For samples containing no or negligible amounts of Fe_2O_3-bearing minerals, the FeO values were calculated from initial Fe_2O_3 by the use of formula (1).

$FeO = Fe_2O_3 * 0.8998$

For samples containing apatite (BB11, NO33, NQ21c and NO26), the corresponding amount of CaO bound to P_2O_5 in apatite formula was subtracted from the bulk composition.

For two samples containing compositionally zoned garnets (NO33 and NQ21c), the initial modelling did not give reasonable results. In both of the samples, garnet shows a prograde zoning pattern that suggests that the garnet core was progressively isolated from the system during growth (Figure 3.4.2-1 and Figure 3.4.2-3). Fractionation of garnet cores from the system progressively depletes the bulk composition by Fe, Mg, Mn, Ca, Al and Si. For this reason, a routine in Perple_X was used to fractionate garnet from the system. Such routine calculates a new bulk composition for the system along a pathway that is predefined in the problem definition. The pathway can be described by the following equation (2):

$P = (P_1/T_1) * T$

Where P_1 and T_1 is the starting pressure (P) and temperature (T) conditions at which the fractionation starts.

The fractionation routine calculates the stable mineral assemblage at predefined number of P-T points, and subtracts the estimated amount of garnet form the bulk composition.

As formula above implies, the fractionation routine requires information about at which point in the P-T space the fractionation starts, i.e. the point where garnet starts to crystallize. For this reason, the P-T conditions where garnets in the sample starts to develop is required. The loss of ignition is the best estimation of the water content at peak metamorphic conditions, but very likely does not represent the early stages of metamorphism, as rocks are progressively dehydrated during increasing pressure and temperature. For this reason, the estimated starting point (P_1 and T_1) and the effective bulk composition were calculated at H_2O saturated conditions.

Compositional zoning of minerals is one of many sources of error tied to phase equilibrium modelling, as it progressively changes the matrix system composition. The chemical composition of the modelled system will have an impact on the modelling results, as mineral stabilities are dependent on not only temperature and pressure changes, but also the availability of chemical components. Other sources of error might be partial disequilibrium in mineral assemblages, errors related to microprobe analyses of minerals, errors related to determination of bulk rock composition, errors associated with thermodynamic properties of endmember mineral phases and errors related to quality of solution models for mineral phases.

3.5.1 BB18 - Chlorite-bearing phyllite

Sample BB18 consists of muscovite, quartz, chlorite and ilmenite. The system composition used for modelling of this sample is (in wt%): SiO_2 = 57.24, TiO_2 = 1.03, Al_2O_3 = 21.51, FeO = 6.17, MgO = 0.93, MnO = 0.01, CaO = 0.01, K_2O = 7.19, Na_2O = 0.14, H_2O = 4.80.

The following mixing models were used for the modelling: garnet, staurolite, chlorite, chloritoid (Holland and Powell, 1998), biotite (Powell and Holland, 1999), ternary feldspar (Fuhrman and Lindsley, 1988), ilmenite (ideal solid solution of ilmenite (Fe), pyrophanite (Mn) and geikeielite (Mg) end-members) and white mica (hybrid model using the data of Chatterjee and Froese (1975) and an ideal phengite model described here:
http://www.esc.cam.ac.uk/astaff/holland/ds5/muscovites/mu.html).

The P-T pseudosection was calculated in the temperature interval between 300-550°C and pressure interval between 1-10 kbar (Figure 3.5.1-1). None of the mineral stability fields that the modelling predicts corresponds to the observed mineral assemblage of the sample. Compositional isopleths for measured X_{Mg} of chlorite and Si-content in muscovite were plotted in attempt to find the best fit for metamorphic P-T conditions. Compositional isopleths for chlorite X_{Mg} values constrain the temperature to ca. 375-475°C. Muscovite in the sample BB18 has a Si-content between 3.09 and 3.16 a.p.f.u. Compositional isopleths for the Si content in muscovite and the X_{Mg} of chlorite intersect in the pressure interval from 1.5 to 5.5 kbar, in the stability field of Chl + Ms + Ilm + Bt + Ttn + Qz + Rt + H_2O. The modelled stability field does not fit the observed mineral assemblage of the sample, hence the results are considered inconclusive.

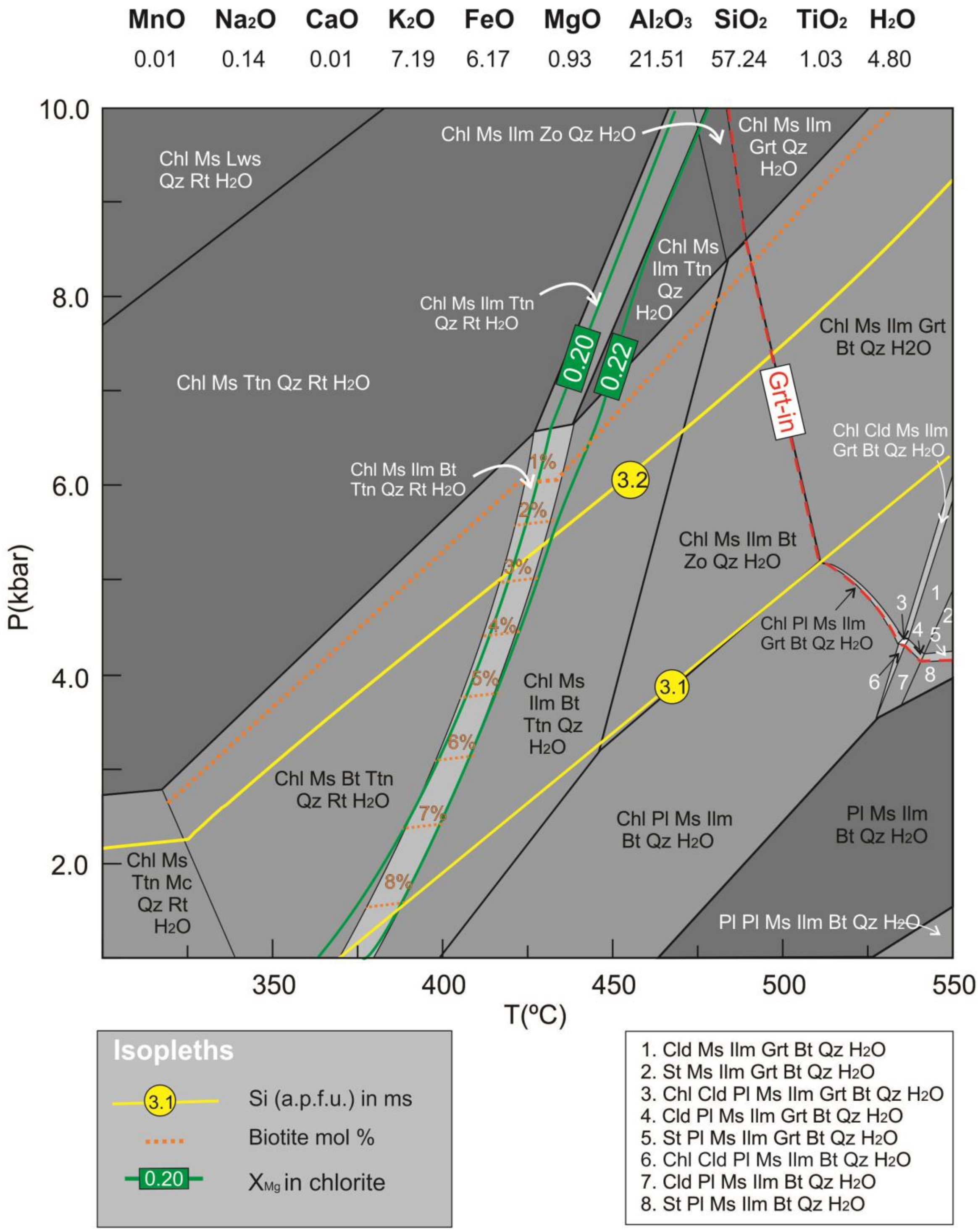

Figure 3.5.1-1- Calculated P-T pseudosection for the sample BB18. The bulk rock composition is indicated in top as weight % of oxides.

Comments on the result:

Due to a very small amount of CaO in the bulk chemical composition, negligible amounts of Ca-bearing phases (Ttn/Zo/Lws) are present in every stability field. By looking only at mineral stability without considering these phases, there is one field that contains the observed mineral assemblage of the sample (ca. 425-475°C and 6.5-10 kbar) but the composition of measured muscovite does not correspond to modelled composition within this P-T space.

The field that best fits with the measures chemical composition of chlorite and muscovite contains three mineral phases that were not observed during SEM analysis. The modelling predicts negligible amounts of both titanite and rutile (<<1 volume %) and between 3-8 % of biotite. In the exploratory stage of the modelling, three different mixing models for white mica were considered and they all gave very similar result: The Si-content of measured muscovite were stable together with the measured X_{Mg} of chlorite at pressures from ca. 1-5 kbar, in biotite-bearing stability fields.

Chlorite crystals were present only in some layers of the sample (see section 3.4.1.1) and absent from other layers. The non-homogeneous nature of the sample is most likely the cause of the inconclusive results. It is possible that the bulk chemical composition does not represent the chemical composition of the selected thin section area.

3.5.2 BA23 - Garnet-bearing quartzite

Sample BA23 consists of quartz, muscovite, magnetite, garnet, rutile, biotite and chlorite. The system composition used for modelling of this sample is (in wt%): SiO_2 = 72.66, TiO_2 = 0.24, Al_2O_3 = 7.11, FeO = 0.59, Fe_2O_3 = 14.40, MgO = 0.56, MnO = 0.52, CaO = 0.03, K_2O = 2.14, Na_2O = 0.11, H_2O = 1.40.

The following mixing models were used for the modelling: garnet (White et al., 2007), staurolite, chlorite, chloritoid (Holland and Powell, 1998), biotite (Powell and Holland, 1999), ternary feldspar (Fuhrman & Lindsley, 1988), ilmenite (ideal solid solution of ilmenite (Fe), pyrophanite (Mn) and geikeielite (Mg) end-members), magnetite (ideal magnesioferrite/magnetite model) and white mica (https://www.esc.cam.ac.uk/astaff/holland/ds5/muscovites/mu.html).

The P-T pseudosection was calculated in the temperature interval of 350-650 °C and pressure interval of 3-9 kbar and is presented in Figure 3.5.2-1 below. The modelling predicts that all mineral stability fields contain hematite (Fe_2O_3), which was not observed in the sample. Some stability fields contain magnetite (Fe_3O_4) in addition to hematite, but in very small amounts (<1%). This is considered to be the result of incorrect FeO/ Fe_2O_3 ratio in the bulk rock analysis. A possible explanation might be that part of the FeO has oxidized to Fe_2O_3 during the milling and subsequent storage of the sample prior to its chemical analysis.

From the measured Fe^{3+} content of minerals in the sample BA23 (Appendix A) the only phase containing a significant amount of Fe^{3+} is magnetite, and measured garnet in the sample has a relatively low content of Fe^{3+} (0.00-0.10 a.p.f.u.). The error with the FeO/Fe_2O_3 ratio affects the content of Fe^{3+} endmember (andradite) in modelled garnet, and also predicts two unsolvable garnets in some stability fields with very similar compositions. Thus, it is not possible to use the bulk chemical composition to model this sample. As it is hard to make any assumptions of the true FeO/Fe_2O_3 ratio of the sample, no further attempt on estimating the metamorphic conditions were made.

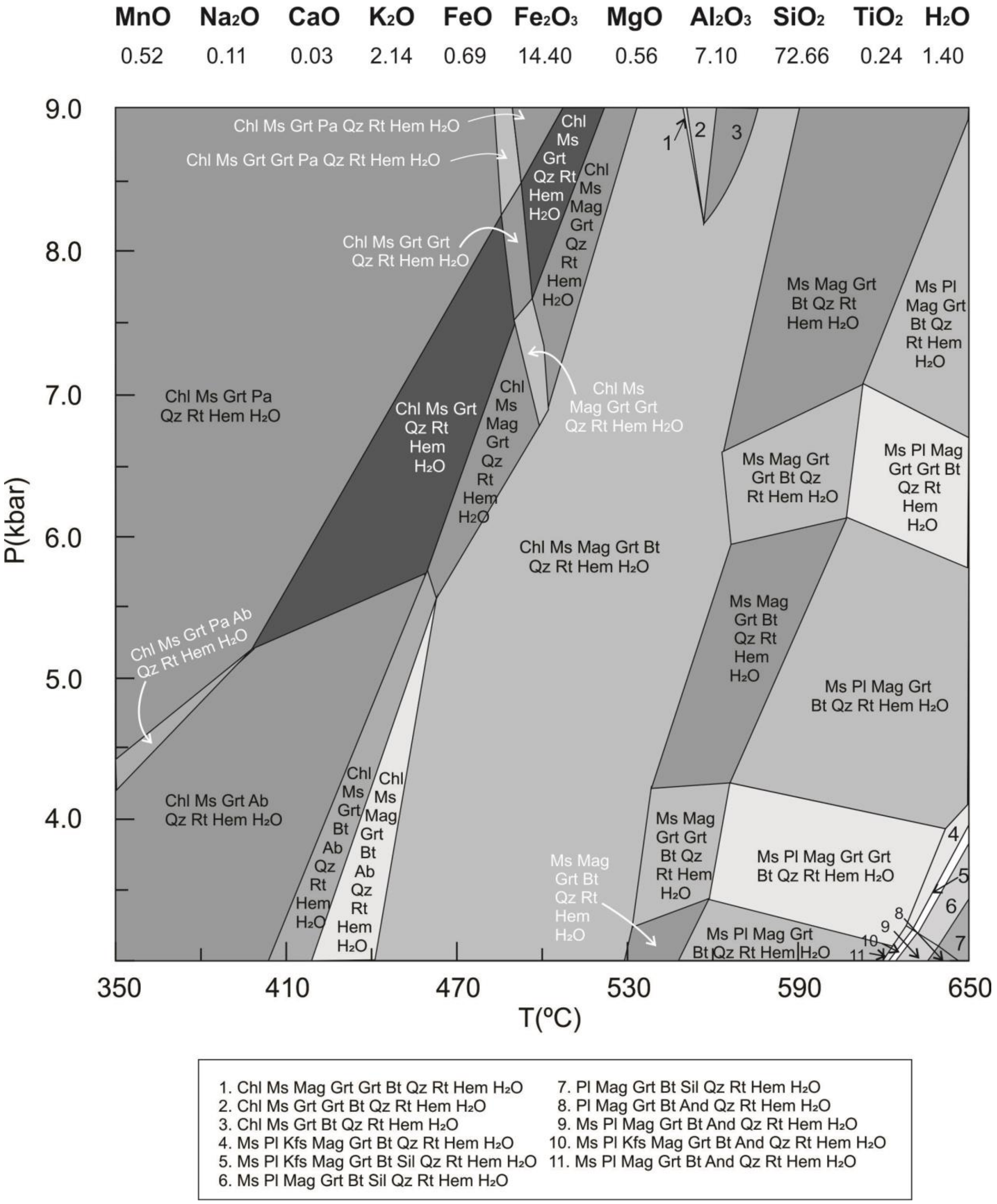

Figure 3.5.2-1- P-T-pseudosection calculated for sample BA23. The bulk rock composition is indicated in top as weight % of oxides.

3.5.3 BB11 - Garnet-mica-schist

The sample BB11 consists of garnet, chlorite, biotite, muscovite, quartz and ilmenite. Accessory amounts of plagioclase, k-feldspar and apatite were found during SEM analysis (Section 3.4.1.3). The system composition used for modelling of this sample is (in wt%): SiO_2 = 52.26, TiO_2 = 1.09, Al_2O_3 = 22.82, FeO = 8.70, MgO = 2.11, MnO = 0.11, CaO = 0.20, K_2O = 5.15, Na_2O = 0.99, H_2O = 5.00.

The following mixing models were used for the modelling: garnet, staurolite, chlorite, chloritoid (Holland and Powell, 1998), biotite (Powell and Holland, 1999), ternary feldspar (Fuhrman and Lindsley, 1988), ilmenite (ideal solid solution of ilmenite (Fe), pyrophanite (Mn) and geikeielite (Mg) end-members) and white mica (hybrid model using the data of Chatterjee and Froese (1975) and an ideal phengite model described here:
http://www.esc.cam.ac.uk/astaff/holland/ds5/muscovites/mu.html).

Compositional isopleths (X_{Sps}, X_{Grs} and X_{Alm}) for the garnet core composition constrain the beginning of garnet growth at ~510°C and 4.8 kbar in the stability field of the mineral assemblage: chlorite, plagioclase, muscovite, paragonite, ilmenite, garnet and quartz (Figure 3.5.3-1).

For estimation of peak metamorphic conditions, the compositional isopleths for the garnet rim composition (X_{Sps}, X_{Grs} and X_{Alm}) were plotted together with compositional isopleths for biotite and chlorite X_{Mg} values. The garnet in the sample BB11 shows a prograde zonation pattern with increase in X_{Mg} and decrease in Ca^{2+} and Mn^{2+} from core to rim (Figure 3.4.1-5), and for this reason the maximum measured X_{Alm} (=0.82) and the minimum measured X_{Grs} (=0.07) ± 1% was used to estimate the peak conditions. The compositional isopleths are shown in Figure 3.5.3-2 below.

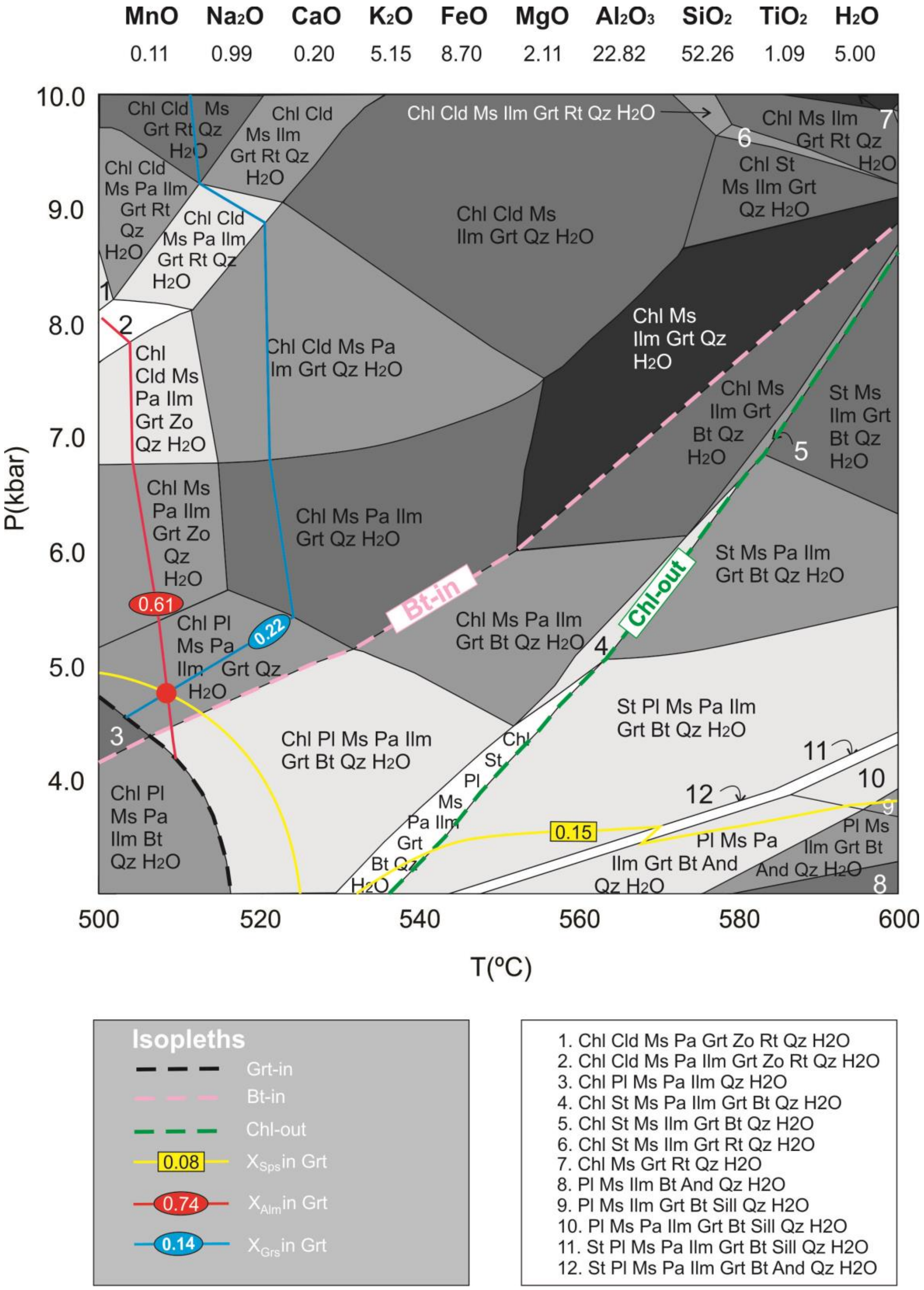

Figure 3.5.3-1 Calculated P-T pseudosection for the sample BB11 from 500-600 °C and 3-10 kbar. Isopleths for core composition of garnet in the sample are indicated with solid lines, and cross at ~510 °C and 4.8 kbar.

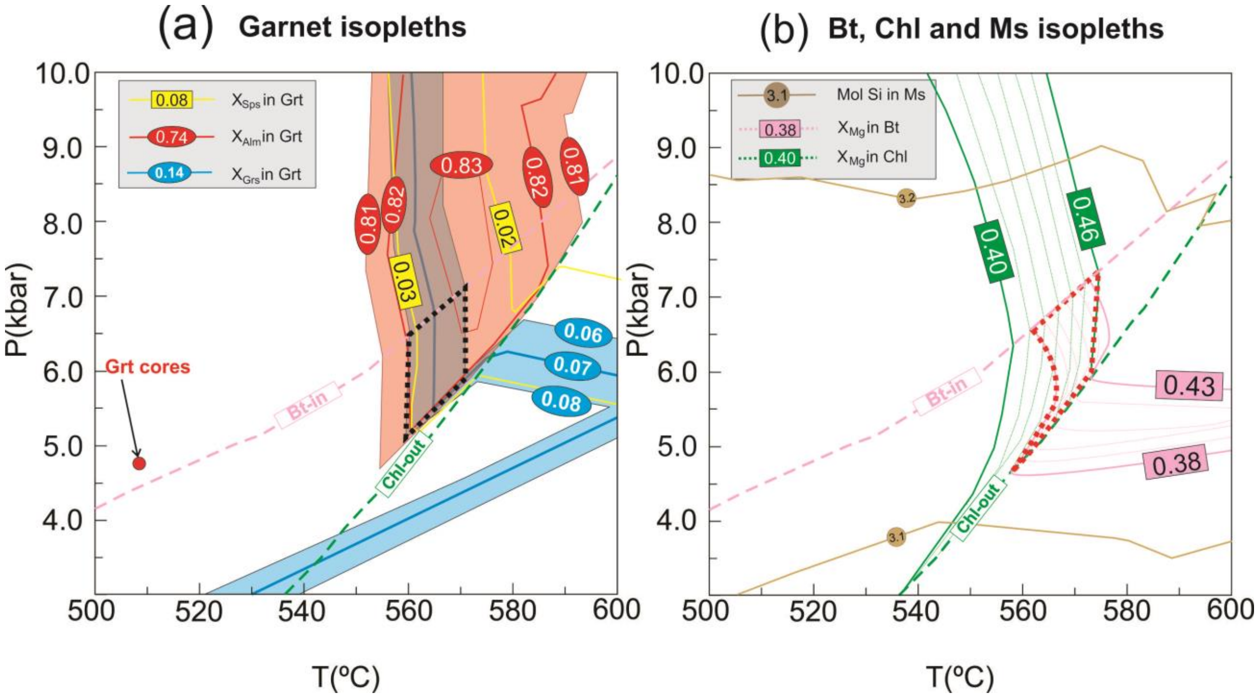

Figure 3.5.3-2 Compositional isopleths for mineral phases in the sample BB11. (a) Garnet rim composition in the sample BB11. The black dotted box shows the area where X_{Alm} and X_{Grs} in garnet rims (± 0.01) are stable in bt+chl-bearing stability fields. (b) The red dotted box shows the area where observed X_{Mg} of chlorite and biotite in the sample BB11 are stable together. The molar amount of Si in muscovite observed in sample BB11 fits well with the compositional isopleths for garnet rims, biotite and chlorite.

Compositional isopleths for garnet rim composition are widely spaced and vertical in the field where the biotite and chlorite are stable, which means that the composition of phases does not change very much within the stability field of the mineral assemblage observed in the sample BB11.

The compositional isopleths for garnet rim, as well as biotite and chlorite X_{Mg} values plot together in the field that shows the stable mineral assemblage: Chl + Ms + Ilm + Grt + Bt + Qz + H_2O. The combination of a paragonite-free mineral assemblage with compositional isopleths for garnet rim, biotite and chlorite suggest that the matrix mineral assemblage of the sample BB11 equilibrated at ca. 560-570°C and 6-7 kbar (Figure 3.5.3-3).

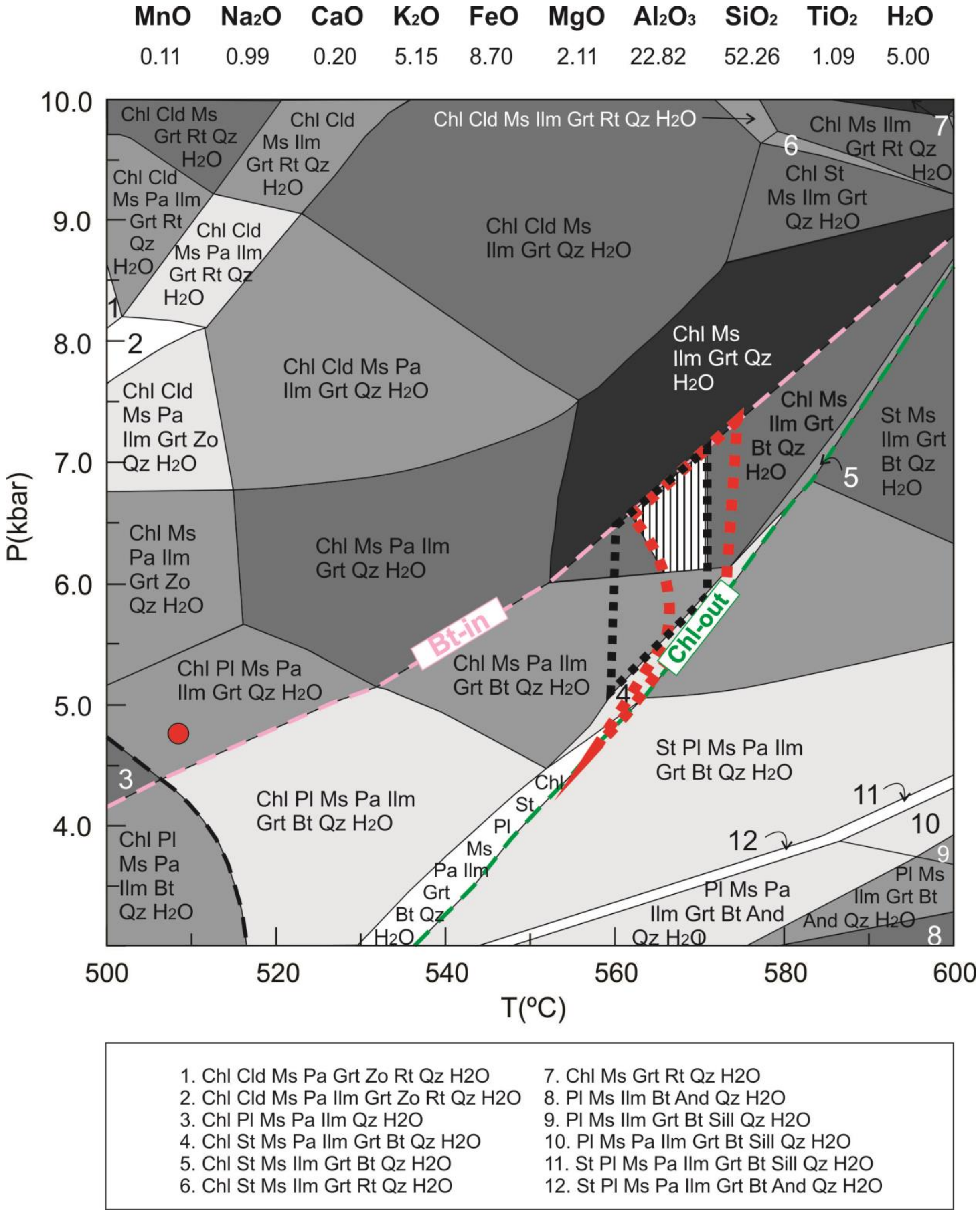

Figure 3.5.3-3- P-T pseudosection for sample BB11. The red circle indicates the P-T conditions at which garnet in the sample BB11 started to grow. The black dotted field indicates where garnet rim composition is stable together, and the red dotted line indicates the field where chlorite and biotite X_{Mg} in sample BB11 are stable together. The estimated peak conditions based on observed mineral assemblage and mineral chemistry are show with pattern fill.

Comments on the result:

WERAMI was used to constrain information about the system properties at the estimated peak conditions. At peak conditions, the system contains (in volume %): ~8 % Chl, ~55 % Ms, ~1% Ilm, ~7 % Grt, ~2 % Bt, ~21 % Qz and ~5 % H_2O. The volume percent of mineral phases at these conditions is not far from volume percent of minerals observed during petrographic study of the sample, except that modelling predicts lower content of biotite than observed (~7%).

Individual grains of anhedral plagioclase and K-feldspar were found during SEM analyses but are not stable at the estimated peak conditions. The modelling predicts that plagioclase was stable in the field where the garnet started to grow. Possibly, the plagioclase was not completely replaced during the metamorphism, or there is a small discrepancy in the bulk composition.

The chemical zonation pattern of garnet in the sample does confirm that there might be a slight error in the used system composition, as garnet cores are not in equilibrium with the matrix assemblage. However, the modelling of the sample BB11 gave reasonable results without considering this discrepancy. The garnets in the P-T field has X_{Sps} between 0.03 and 0.02, while the minimum measured $X_{Sps} = 0.00$. Fractionating of the garnet cores from the system could possibly further improve the results.

3.5.4 NO33 - Garnet-mica schist

Sample NO33 consists of garnet, biotite, chlorite, quartz and minor amounts of muscovite and ilmenite. Negligible amounts of apatite and magnetite were accounted for before calculations (section 3.5). An initial modelling for the sample NO33 did not give reasonable results for the matrix mineral assemblage, and thus changes in an effective bulk composition due to progressive fractionation of garnet was calculated in Perple_X. The following mixing models were used through all steps of the modelling: garnet, staurolite, chlorite, chloritoid (Holland and Powell, 1998), biotite (Powell and Holland, 1999), ternary feldspar (Fuhrman & Lindsley, 1988) and white mica (https://www.esc.cam.ac.uk/astaff/holland/ds5/muscovites/mu.html). The modelling of this sample required three steps.

Step 1: The beginning of garnet growth was estimated at H_2O-saturated conditions and with the bulk rock composition as the system composition. The P-T-pseudosection was calculated in the temperature interval of 450-600 °C and pressure interval of 3-11 kbar (Figure 3.5.4-1). Compositional isopleths (X_{Sps}, X_{Grs} and X_{Alm}) for the garnet core composition suggest that garnet started to growth at ca. 523 °C and ca. 4.5 kbar (Figure 3.5.4-1). The mineral assemblage at this stage was chlorite, muscovite, plagioclase, garnet, biotite, quartz and ilmenite.

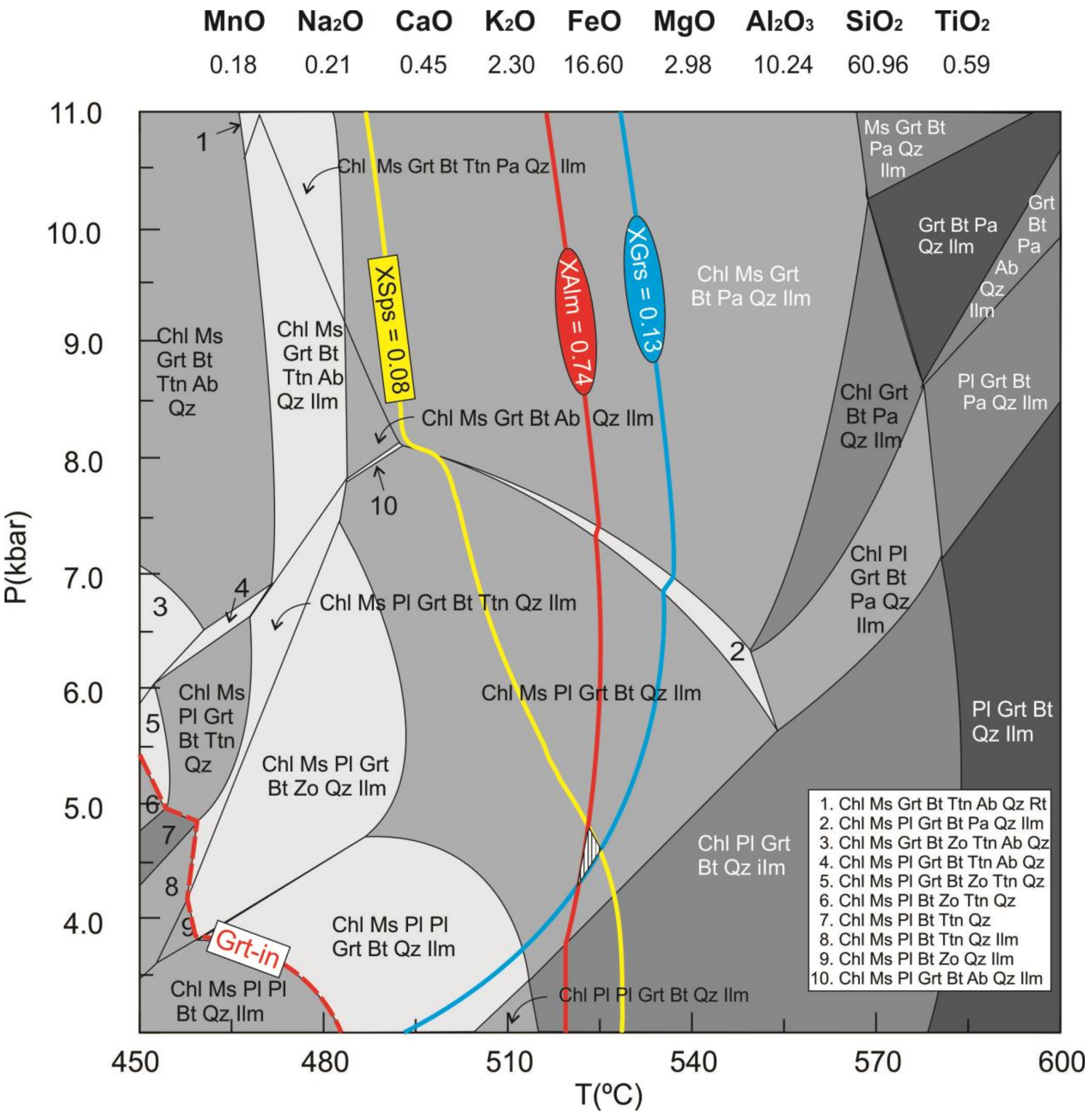

Figure 3.5.4-1 P-T pseudosection calculated for the sample NO33 at H_2O-saturated conditions. The bulk rock composition is indicated on top of the diagram as weight % of oxides. The pattern-filled triangle indicated where the compositional isopleths for garnet core composition overlap, hence the P-T field where garnets in sample NO33 started to develop.

Step 2: Fractionation of garnet out of the system was calculated from the temperature of 523 °C and the pressure of 4.5 kbar at H_2O-saturated conditions. The evolution of manganese content during the fractionation was used to decide which effective bulk composition to use for estimation of peak metamorphic conditions (Figure 3.5.4-2). Based on insignificant amount of manganese in the garnet rim, as well as in other mineral phases (See Appendix A and Figure 3.4.2-1), the effective bulk composition valid for the matrix mineral assemblage should be close to manganese free. The modelling of peak metamorphic conditions was done with the system composition read at 547 ºC, after fractionating garnet out of the system for 24 °C.

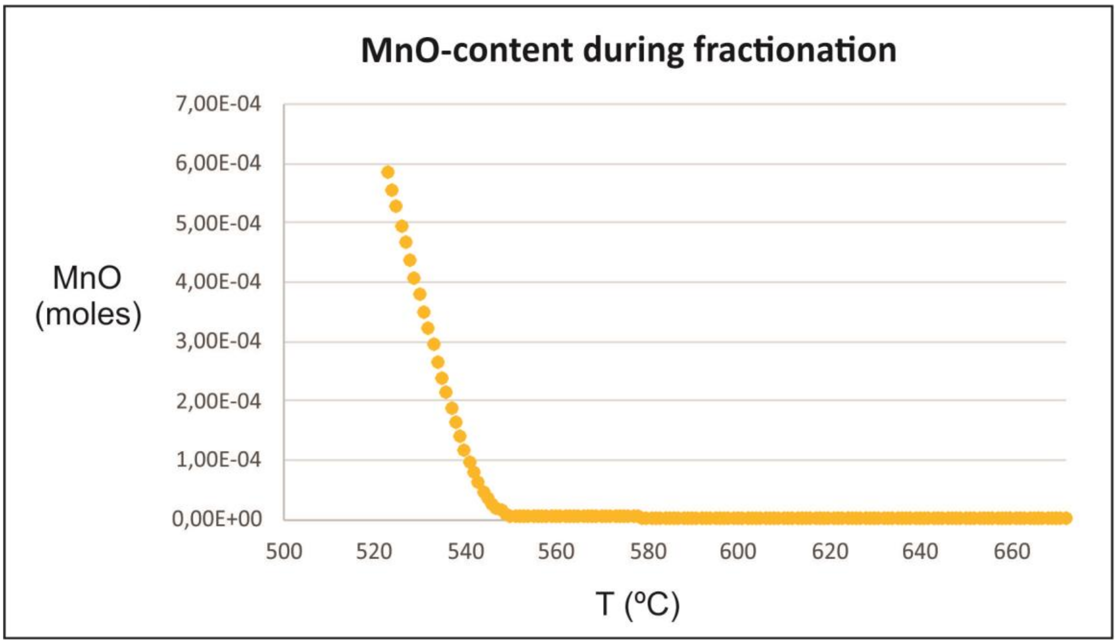

Figure 3.5.4-2 - Evolution of manganese content during garnet fractionation in the sample NO33.

<u>Step 3:</u> For estimation of peak metamorphic conditions, calculation was performed for the fractionated system composition. The water content of the system was constrained by the LOI from bulk rock analysis. This gives an effective system composition of (in wt%): SiO_2 = 58.30 TiO_2 = 0.59, Al_2O_3 = 8.74, FeO = 14.09, MgO = 2.92, MnO = 0.00, CaO = 0.15, K_2O = 2.30, Na_2O = 0.21, H_2O = 2.90.

The compositional isopleths for garnet rim (X_{Mg}, X_{Grs} and X_{Alm}) and X_{Mg} of biotite and chlorite were used to estimate the peak metamorphic conditions of the sample NO33. Compositional isopleths for the measured X_{Mg} of chlorite and garnet rim compositions constrain the temperature to ca. 540-560°C. The combination of a feldspar-free assemblage with the compositional isopleths suggests that the matrix mineral assemblage of the sample NO33 equilibrated at ca. 540-560°C and 6.5-9.0 kbar (Figure 3.5.4-3).

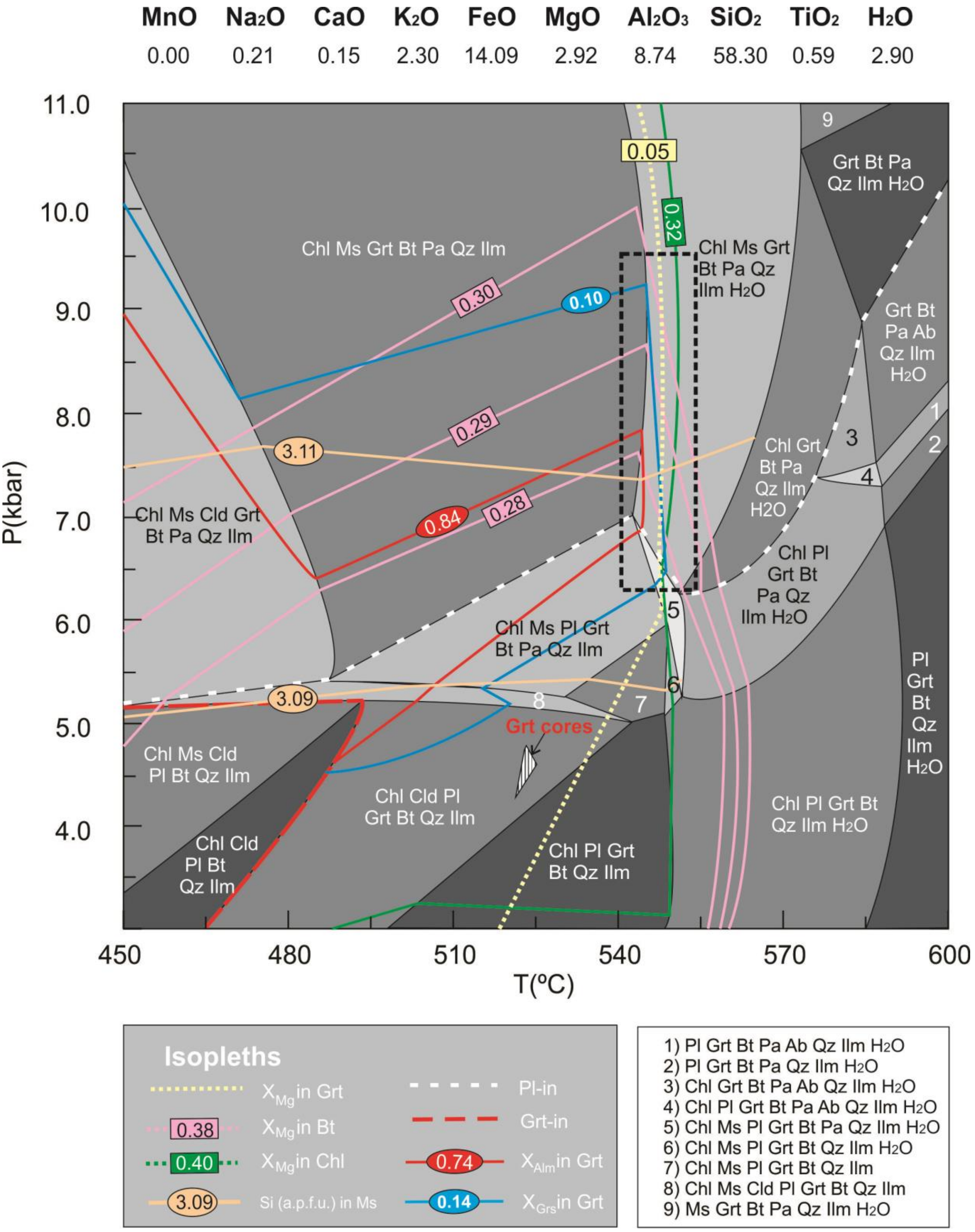

Figure 3.5.4-3 – P-T pseudosection for the sample NO33 calculated with the effective system composition after garnet fractionation. The pattern-filled triangle indicates the P-T conditions at which garnet in the sample NO33 started to grow at H_2O saturated conditions.

Comments on the results:

None of the mineral stability fields in the calculated pseudosection corresponds exactly to the mineral assemblage found during petrographic analysis as all stability fields contains some Na-bearing phase (plagioclase or paragonite).

The white mica mixing model that was used for the modelling seems to allow a low degree of mixing among the paragonite and muscovite endmembers. The measured muscovite for the sample NO33 has a $K^+ / (K^+ + Na^+)$ ratio of 0.83-0.85, while the modelled $K^+ / (K^+ + Na^+)$ in muscovite is ~0.90. This is most likely the reason for the presence of paragonite in the modelled stability fields, though this phase was not observed in the sample NO33. The Si-content of measured muscovite indicates that the matrix mineral assemblage probably equilibrated in the lower pressure part of the estimated peak conditions (<7.5 kbar) (Figure 3.5.4-3), but it was not used at due to the problem with the mica model.

3.5.5 NQ21c –Staurolite-garnet-mica schist

Sample NQ21c consists of garnet, biotite, staurolite, muscovite, quartz, plagioclase and accessory amounts of chlorite, apatite, ilmenite and rutile. An initial modelling for the sample did not give reasonable results for the matrix mineral assemblage, and thus changes in an effective bulk composition due to progressive fractionation of garnet was calculated in Perple_X. The following mixing models were used through all steps of the modelling: garnet, staurolite, chlorite, chloritoid (Holland and Powell, 1998), biotite (Powell and Holland, 1999), ternary feldspar (Fuhrman and Lindsley, 1988) and white mica (https://www.esc.cam.ac.uk/astaff/holland/ds5/muscovites/mu.html). The modelling of this sample required three steps.

Step 1: The beginning of garnet growth was estimated at H_2O-saturated conditions and with the bulk rock composition as the system composition. The P-T-pseudosection was calculated in the temperature interval of 500-650°C and pressure interval of 6-11 kbar (Figure 3.5.5-1). Compositional isopleths (X_{Sps}, X_{Grs} and X_{Alm}) for the garnet core composition suggest that garnet started to growth at ca. 564°C and ca. 6.6 kbar. The mineral assemblage at this stage was chlorite, muscovite, plagioclase, garnet, biotite, quartz and rutile (Figure 3.5.5-1).

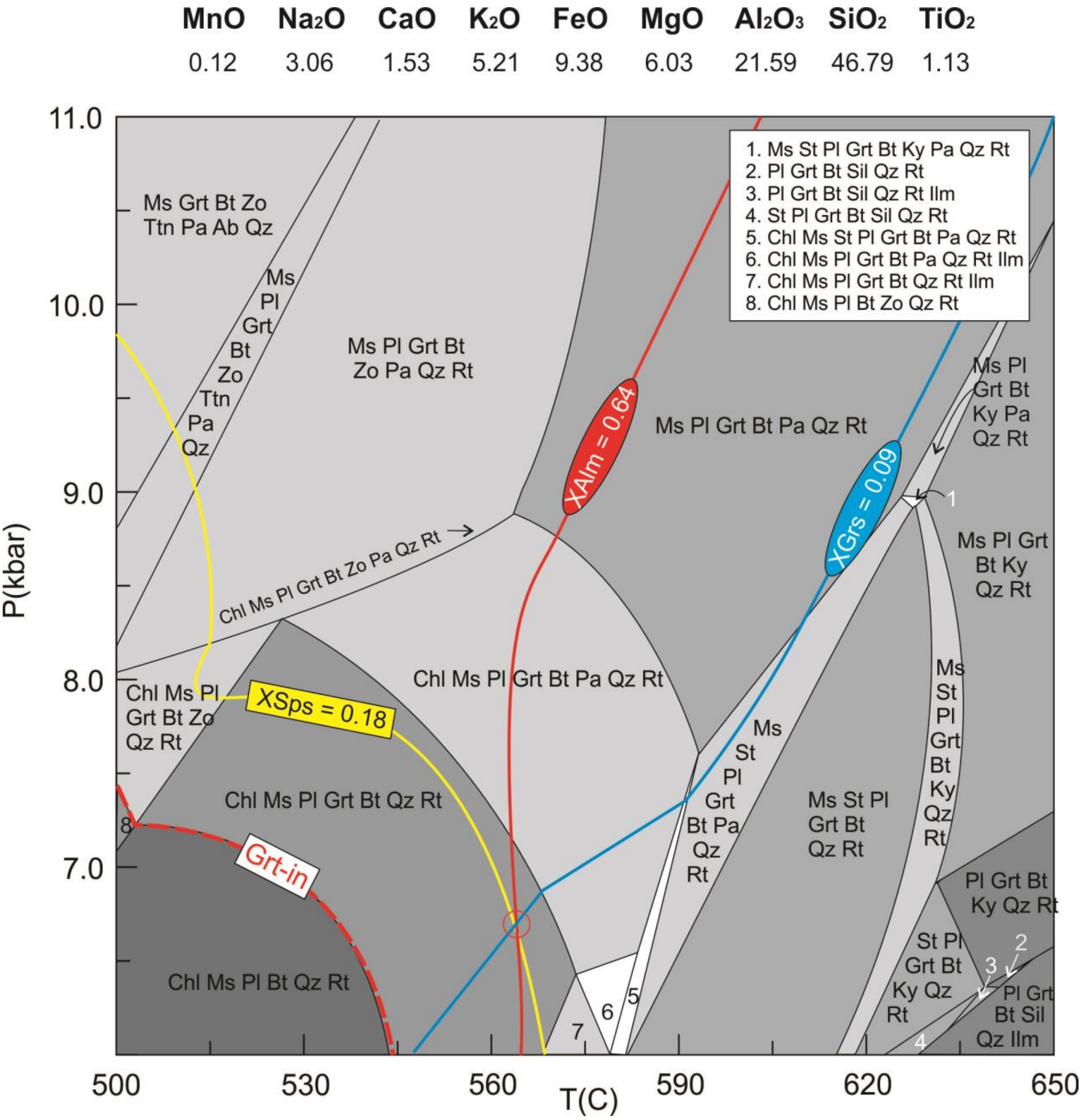

MnO	Na_2O	CaO	K_2O	FeO	MgO	Al_2O_3	SiO_2	TiO_2
0.12	3.06	1.53	5.21	9.38	6.03	21.59	46.79	1.13

Figure 3.5.5-1 P-T Pseudosection calculated for the sample NQ21c at H_2O-saturated conditions. The bulk rock composition is indicated at the top as weight % of oxides. The red circle indicates where the compositional isopleths for garnet core composition overlaps, hence the P-T conditions at which garnet in sample NQ21c started to develop.

Step 2: Fractionation of garnet out of the system was calculated from the temperature of 564 °C and the pressure of 6.6 kbar at H_2O saturated conditions. The modelling of garnet fractionation estimated that garnet growth continued up to the temperature of 585°C under the set conditions. The peak metamorphic conditions were modelled with the system composition read at 584°C, after fractionating garnet out of the system for 20°C and with the assumption that only the outermost part of the rim equilibrated with the system.

Step 3: For estimation of peak metamorphic conditions, calculation was performed for the fractionated system composition. The water content of the system was constrained by the LOI from bulk rock analyses. This gives an effective system composition of (in wt%): SiO_2 = 46.30 TiO_2 = 1.13, Al_2O_3 = 21.32, FeO = 8.98, MgO = 6.00, MnO = 0.04, CaO = 1.49, K_2O = 5.21, Na_2O = 3.06, H_2O = 3.10.

In addition to the calculated P-T pseudosection (Figure 3.5.5-3), compositional isopleths for garnet rims (X_{Prp}, X_{Sps}, X_{Grs} and X_{Alm}), plagioclase X_{An} and biotite X_{Mg} were used estimate peak metamorphic conditions.

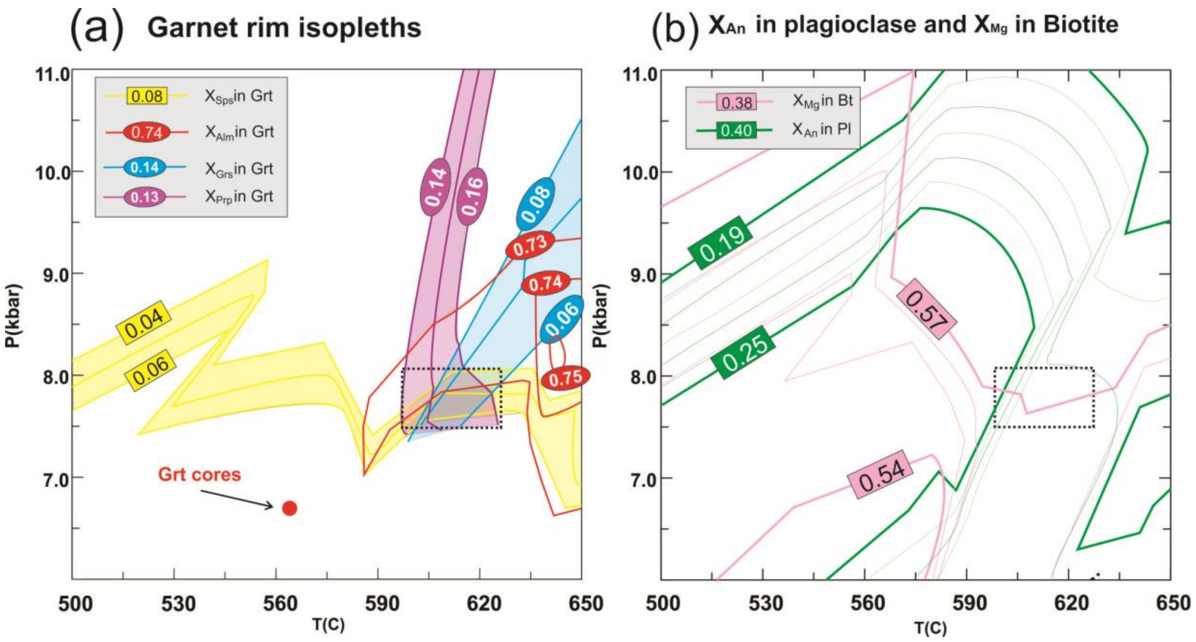

Figure 3.5.5-2 Compositional isopleths for mineral phases in the sample NQ21c. (a) Compositional isopleths for garnet rims in the sample NQ21c. The black dotted box shows the area where X_{Grs}, X_{Sps} and X_{Prp} in garnet rims (± 0.01) are stable together. (b) Compositional isopleths for biotite (X_{Mg}) and plagioclase X_{An} in the sample. The X_{An} of plagioclase is 0.21-0.25 and the X_{Mg} of biotite is ~0.57 in the area where garnet rim in the sample are stable.

The garnet in the sample shows a prograde zonation pattern with increase in X_{Mg} and decrease in Ca and Mn from core to rim (Figure 3.4.2-3). For this reason, the maximum measured X_{Alm} and X_{Prp}, and the minimum measured X_{Grs} and X_{Sps} ± 1% was used to estimate peak conditions. The modelling suggests that garnet rims equilibrated at ca. 595-630°C and at 7.4-8.1 kbar (Figure 3.5.5-2(a)). Compositional isopleths for X_{An} in plagioclase and X_{Mg} in biotite are shown in Figure 3.5.5-2(b) and correspond well with the estimations. The measured X_{Mg} of biotite in the sample is 0.54-0.56, and the modelled X_{Mg} is ~0.57.

The calculated P-T pseudosection (Figure 3.5.5-3) suggest that garnet rims equilibrated in the stability field containing the mineral assemblage(s): Ms + St + Pl + Grt + Bt + Qz + Rt + H_2O (± Pa).

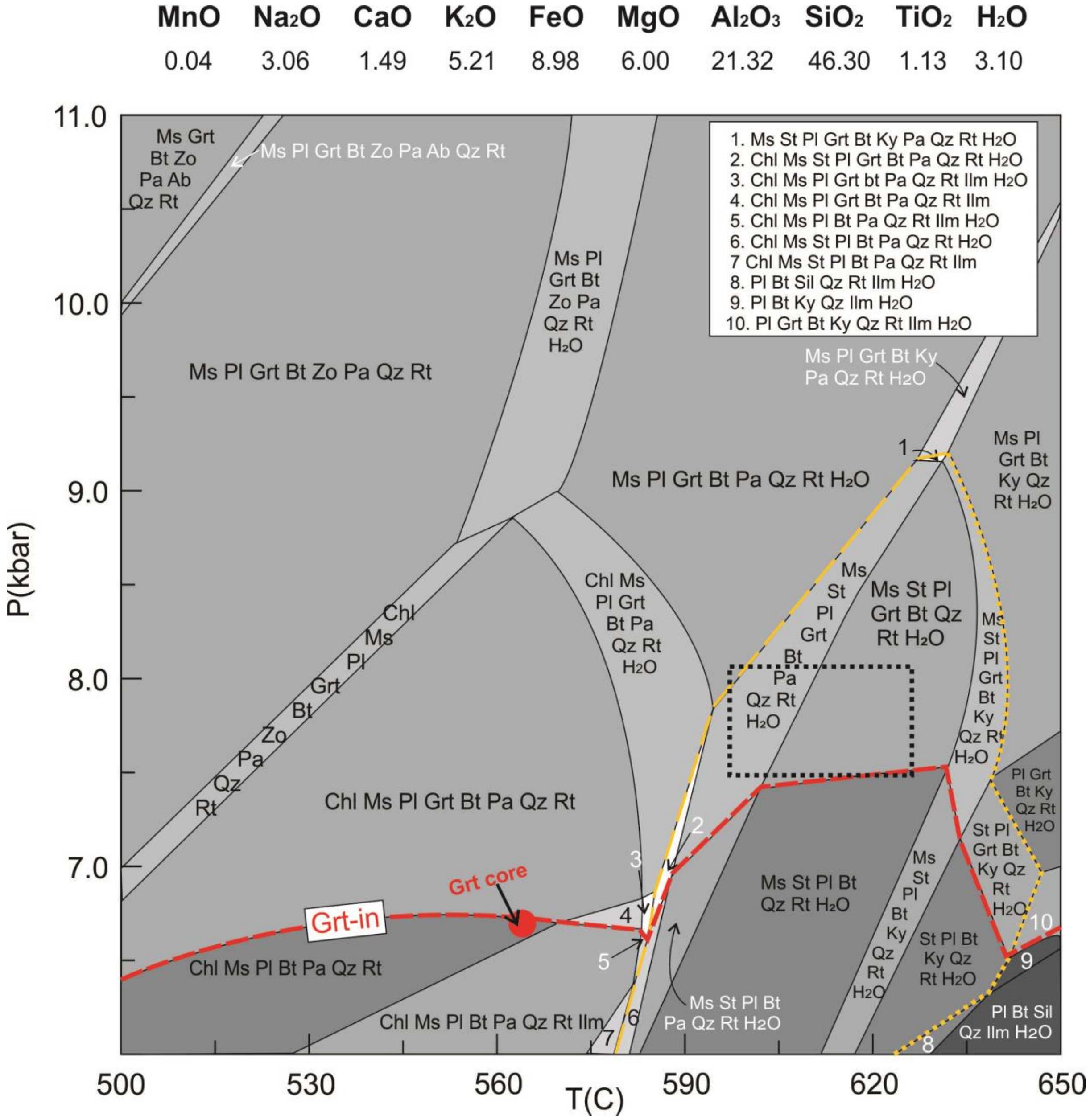

Figure 3.5.5-3- P-T pseudosection for the sample NQ21c calculated with the effective system composition after garnet fractionation. The red dot indicates the P-T conditions at which garnet in the sample NQ21c started to grow at H_2O-saturated conditions. The black dotted box indicates the estimated peak metamorphic conditions of the sample.

Comments on the result:

Minor amounts of ilmenite were found during SEM analyses but are not stable at the estimated peak conditions. One chlorite crystal was also found during petrographic study of the sample, but both the modelling and the petrographic study suggests that the chlorite is retrograde, as it is oriented parallel with crenulation cleavage, and chlorite is stable only at lower temperatures in the modelled P-T pseudosection.

The composition of other minerals in the sample NQ21c was considered during the modelling, but the best constrains for both the temperature and pressure were given by compositional isopleths of garnet. The modelling suggests that muscovite has a Si-content of between ca. 3.10 and 3.11 a.p.f.u., and a $K^+ / (K^+ + Na^+)$ ratio between 0.88 and 0.89 ratio at estimated peak metamorphic conditions. The modelled Si content is very close to the measured Si content of muscovite in the sample (3.07-3.10). The $K^+ / (K^+ + Na^+)$ ratio measured during SEM analyses was 0.74-0.81, i.e. lower than the modelled ratio, which seems to relate to the low degree of mixing among paragonite and muscovite endmember in the white mica solution model, as mentioned earlier. This makes the presence or absence of paragonite in stability field an invalid argument for further constrains on the peak metamorphic conditions. The presence of staurolite in the stability field corresponds to petrographic observations. The modelled X_{Mg} of staurolite is 0.18 and 0.17 at peak metamorphic conditions, which is not far from the measured X_{Mg} of staurolite (0.20-0.22) in the sample.

3.5.6 NO26 – Kyanite-quartzite

Sample NO26 mainly consists of quartz, plagioclase, kyanite, garnet, biotite and accessory muscovite, staurolite, rutile, ilmenite, apatite, zircon and monazite. The system composition of this sample is (in wt%): SiO_2 = 77.64, TiO_2 = 0.61, Al_2O_3 = 11.96, FeO = 2.60, MgO = 1.53, MnO = 0.02, CaO = 0.69, K_2O = 1.13, Na_2O = 1.79, H_2O = 1.30.

The following mixing models were used for the modelling: garnet, staurolite, chlorite (Holland and Powell, 1998), biotite (Powell and Holland, 1999), ternary feldspar (Fuhrman and Lindsley, 1988), white mica (https://www.esc.cam.ac.uk/astaff/holland/ds5/muscovites/mu.html) and cordierite (an ideal anhydrous/hydrous Mg/Fe model).

The P-T pseudosection was calculated in the temperature interval of 550-670°C and the pressure interval of 5-11 kbar. Garnet in the sample shows a reverse zoning pattern with decreasing X_{Mg} towards the rim. The reverse zoning pattern in garnet indicates that the garnet rim probably re-equilibrated with the matrix assemblage during cooling (Spear, 1993). The zoning profile also suggests that the re-equilibration only affected the garnet rim, as the garnet core profile is relatively flat. For this reason, the peak metamorphic conditions were estimated by using the garnet core composition in addition to the presence of kyanite in the sample.

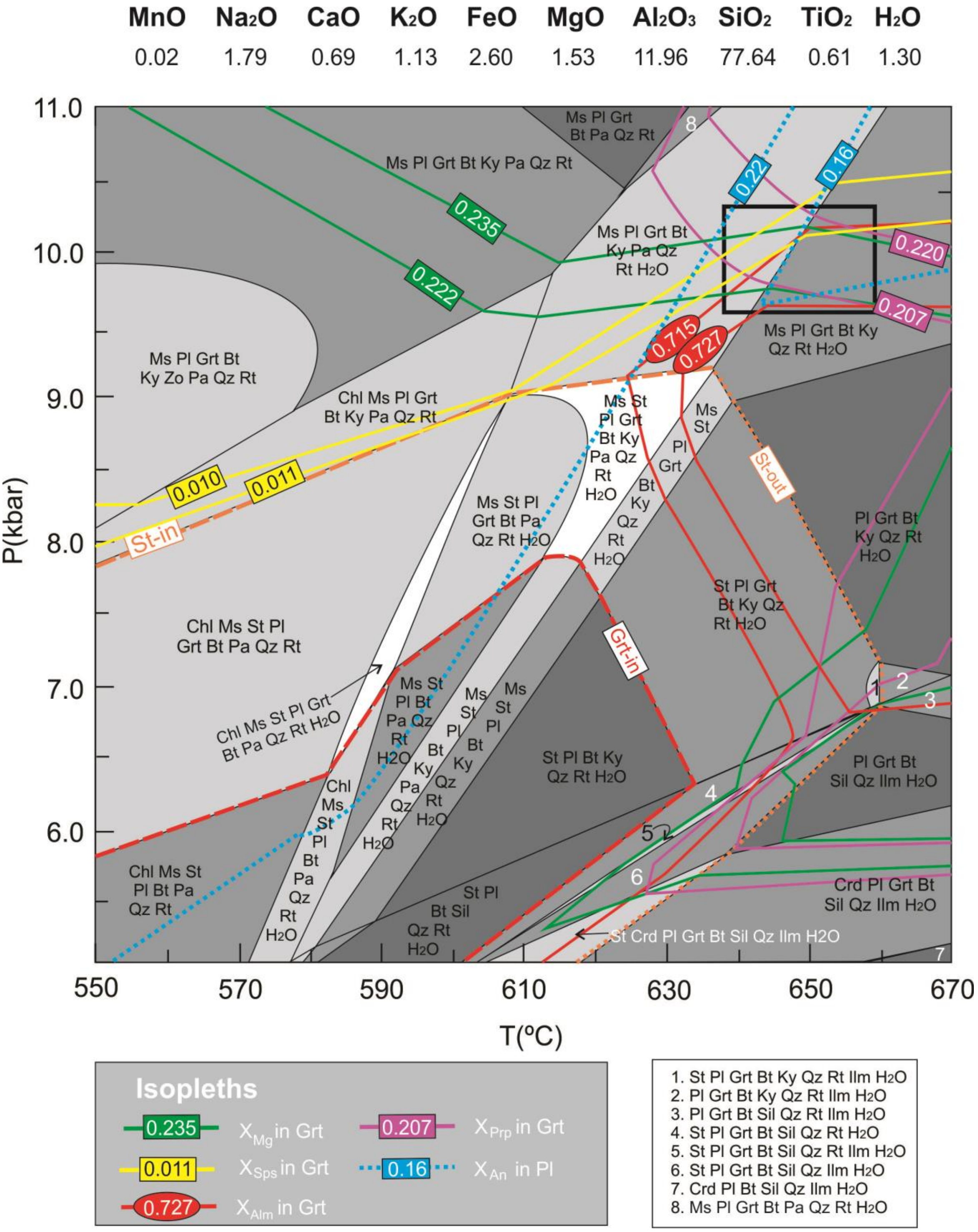

MnO	Na2O	CaO	K2O	FeO	MgO	Al2O3	SiO2	TiO2	H2O
0.02	1.79	0.69	1.13	2.60	1.53	11.96	77.64	0.61	1.30

1. St Pl Grt Bt Ky Qz Rt Ilm H_2O
2. Pl Grt Bt Ky Qz Rt Ilm H_2O
3. Pl Grt Bt Sil Qz Rt Ilm H_2O
4. St Pl Grt Bt Sil Qz Rt H_2O
5. St Pl Grt Bt Sil Qz Rt Ilm H_2O
6. St Pl Grt Bt Sil Qz Ilm H_2O
7. Crd Pl Bt Sil Qz Ilm H_2O
8. Ms Pl Grt Bt Pa Qz Rt H_2O

Figure 3.5.6-1 Calculated P-T pseudosection for the sample NO26. The black rectangle indicates where the compositional isopleths for garnet core composition overlaps.

Compositional isopleths for garnet cores (X_{Mg}, X_{Alm}, X_{Prp} and X_{Sps}) suggests that garnet cores in the sample equilibrated at ca. 630-660°C and 9.6-10.4 kbar, in the stability field of Ms + Pl + Grt + Bt + Ky + Qz + Rt + H_2O ± Pa.

Comments on the result:

At estimated peak conditions the X_{Grs} is 0.06, which is 1 % higher that the measured value. One staurolite crystal was found during petrographic studies of the sample. The plagioclase shows a zonation with increasing X_{An} towards the rim. The modeling suggests that the plagioclase grew/ re-equilibrated during decreasing temperature. The estimated peak metamorphic conditions is staurolite-free. The staurolite in the sample might have crystallized during cooling and decompression, or is a relict from a prograde stage that also re-equilibrated during retrogression.

Three of the compositional isopleths for garnet rims X_{Mg}, X_{Alm}, X_{Prp} also intersect at ca. 650°C and ca. 7.0 kbar pressure (Figure 3.5.6-1), but at this stage the X_{Sps} is ~0.05 and the X_{Grs} is ~0.02 which does not correspond to the measured garnet cores. The plagioclase X_{An} values at estimated peak conditions correspond well with the measured plagioclase in the sample. Both staurolite and plagioclase in the sample NO26 show variation in composition from core to rim. The modelling suggests that staurolite crystallized during decompression and cooling, both by the measured decrease in X_{Mg} towards the staurolite rim and by its stability in the modelled P-T pseudosection.

4 Discussion

4.1 The Brusque Metamorphic Complex

4.1.1 Metamorphism related to deformation events in the Brusque Metamorphic Complex

The structural data presented in this thesis do not allow for any conclusive reconstruction of the deformation history of the Brusque Metamorphic Complex. However, combining field observations with petrographic observations provides some information about how metamorphism relates to different deformation events.

Structural data collected from the BMC, together with previous studies by Basei et al. (2011) suggests that the dominant fabric across the BMC is a low-angle foliation, referred to as S1 in this thesis. Petrographic studies suggest that the peak metamorphic conditions in the Brusque Metamorphic Complex were reached during D1 event, as garnet porphyroblasts show a syn-kinematic growth with respect to the S1 fabric. Similar results were found in the study by Basei et al. (2011), which suggested that the S1 fabric (referred to as S2) was developed during early stages of the collision during NW directed low-angle thrusting.

The D2 event folded the S1 foliation and produced crenulation cleavage (S2). The S2 fabric was observed at many locations in the field and also during petrographic studies. However, the expression of the D2 deformation event deformation event varies across the studied area, which might be explained by differences in lithology (large amplitude folding in quartz rich lithologies and penetrative crenulation cleavage in mica rich lithologies), and/or due to a non-homogeneous distribution of the deformation.

Petrographic observations revealed growth of chlorite parallel with S2 crenulation cleavage planes (Figure 3.4.1-6). Such observations indicates that the D2 event was retrograde with respect to the peak mineral assemblage, because the thermodynamic modelling suggests growth of garnet at the expense of chlorite during the prograde metamorphism. However, the chemical composition of S2-parallel chlorites crystals in the sample BB11 is very similar to chemical composition of chlorite that is parallel with S1 fabric and thus interpreted as a part of the peak mineral assemblage (Appendix A).

Based on phase equilibrium modelling of the sample BB11, the P-T conditions during the D1 and D2 event were not far from each other (Figure 3.5.3-3).

4.1.2 Interpretation of the metamorphic grade of the Brusque Metamorphic Complex

The mineral assemblages in metapelitic rocks are often used as indicators of metamorphic conditions during orogenesis, as the succession of Fe-Mg-Al minerals in metapelitic rocks is largely dependent on temperature. This (Barrowian) mineral succession was first described by Barrow (1893) and is commonly used to describe the change in metamorphic grade through a field area. Interpretations are complicated by the fact that the appearances of index minerals are dependent on the bulk chemistry of the rock. However, based on observed mineral assemblages of samples collected from the south western part of the BMC, an interpretation of the change in metamorphic grade is possible here (Figure 4.1.2-1).

Petrographic observation of mineral assemblages indicates that the south-western part of the Brusque Metamorphic Complex can be subdivided into three zones in terms of metamorphic conditions. The distinction between different zones is based on phase equilibrium modelling of two samples and on observed mineral assemblages from additional samples in the area (Table 3.4.1)

Zone 1: Metapelitic samples collected south of the south-western limit of the Itajaí shear zone (BB16, BB18, BB19, BB23, BB24 and BB30) have mineral assemblages consisting of Qz + Ms ± Chl + Ilm + Hem. The observed mineral assemblages indicate that this zone experienced greenschist facies (chlorite zone) conditions during the development of S1 metamorphic foliation. Phase equilibrium modelling of one sample (BB18) from this zone might suggest that the sample equilibrated at temperatures between 375 and 475°C, nevertheless more accurate determination of metamorphic conditions was not possible.

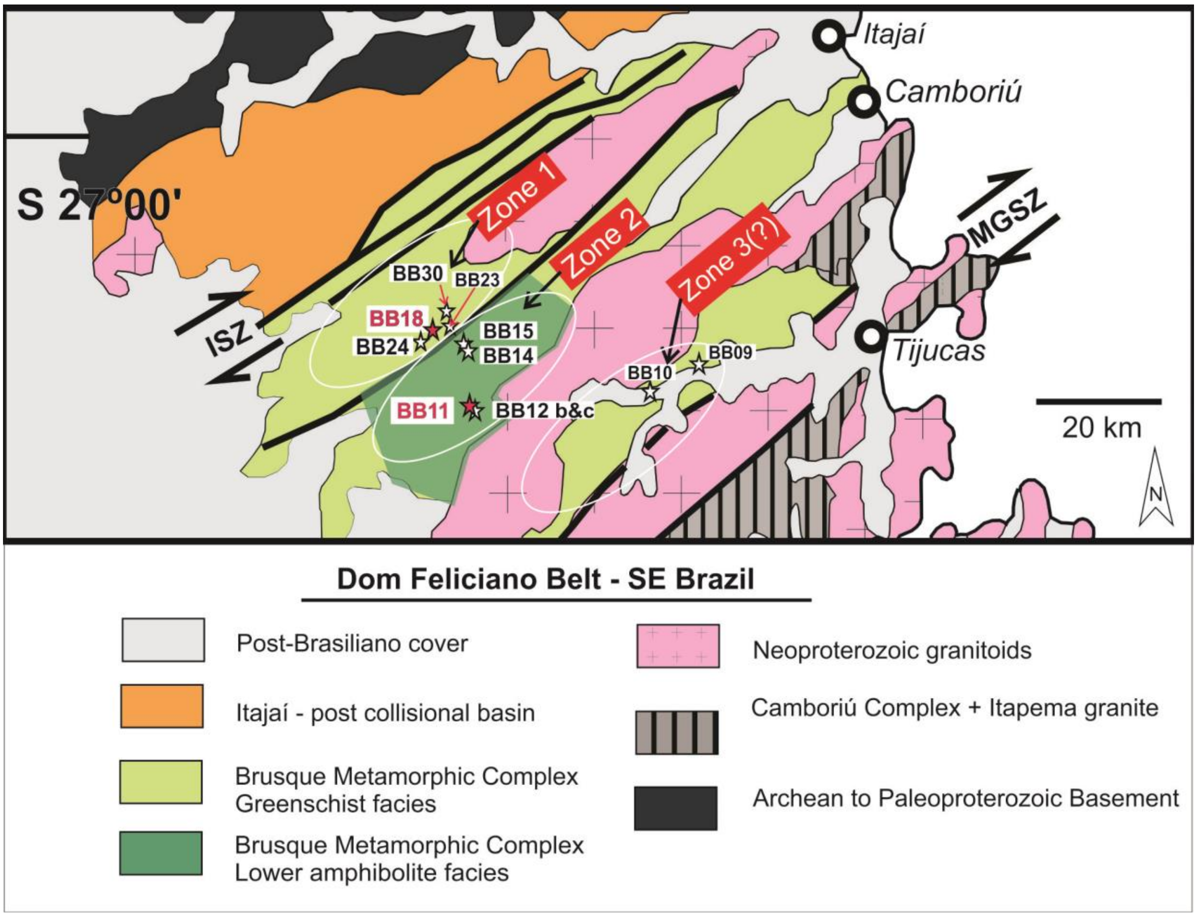

Figure 4.1.2-1 Simplified geological map of the Northernmost part of the Dom Feliciano Belt (from Figure 1.1.1-1). Sample locations are indicated by stars. Three different zones in terms of metamorphic grade were distinguished in the Brusque Metamorphic Complex based on petrographic studies and phase equilibrium modelling. ISZ: Itajaí shear zone, MGSZ: Major Gercino shear zone.

Zone 2: Metapelitic samples collected in the centre of the SW part of the Brusque Metamorphic Complex (Figure 4.1.2-1: BB11, BB12, BB14, BB15) contain garnet-bearing mineral assemblages, which gives a good indication that the metamorphic grade in this part of the complex is higher than the Zone 1. Phase equilibrium modelling of one sample (BB11) from this zone suggests that the matrix mineral assemblage equilibrated at temperatures of ca. 560-570°C and pressures of ca. 6.0-7.0 kbar, corresponding to lower amphibolite facies conditions (Figure 3.5.3-3). Assuming an average crustal density of 2.8 g/cm^3, the pressure conditions corresponds to depths of 22-26 km, which suggest an apparent thermal gradient of 22-26°C/km for metamorphism in this part of the BMC.

Zone 3: Two metapelitic samples from the area in close vicinity of the Major Gercino shear zone (Figure 4.1.2-1: BB09, BB10) contain the mineral assemblage: Qz + Ms + Bt + Opq ± Chl. Phase equilibrium modelling for samples from this part of the BMC has not been performed, however the stable mineral assemblage indicates that the Zone 3 corresponds to greenschist facies conditions (biotite zone).

Correlations with the eastern part of the BMC based on petrographic investigation:

Four samples were collected east of the area explained above (Figure 4.1.2-2: BB32, BB08, BB07, BB23). Sample BB32 contains the mineral assemblage: Grt + Ms + Bt + Qz + Ilm, which is similar to mineral assemblages in garnet-bearing samples from the western BMC (Zone 2). Assuming that the sample BB32 has a similar bulk composition as the sample BB11, this observation suggests that the unit of garnet-bearing mica schists continues further NE as a NE-SW trending zone in the centre of the BMC.

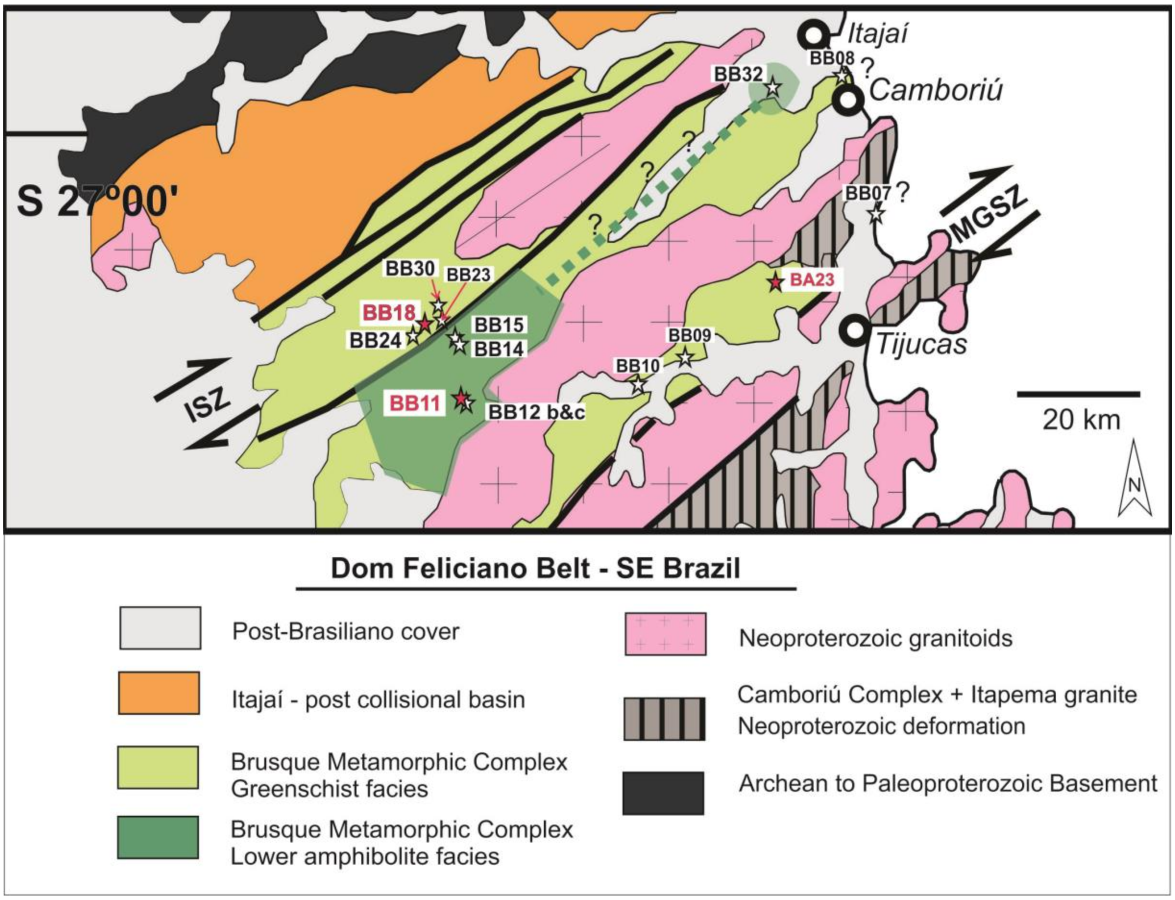

Figure 4.1.2-2 Simplified geological map of the Northernmost part of the Dom Feliciano Belt (from figure 1.1.1.-1). Sample locations are indicated by stars. The dotted line indicates a possible continuation of the garnet zone as a NE-SW trending thrust sheet. ISZ: Itajaí shear zone, MGSZ: Major Gercino shear zone.

Protoliths of the samples BB08, BB07 and BA23 did not have a pelitic composition, which makes a comparison of their mineral assemblages with assemblages in samples from SW part of the BMC difficult. Samples BB08 and BB07 contain significant amount of carbonate minerals and classify as metamorphosed calc-silicates. The parageneses of rocks containing carbonate minerals are largely dependent on chemical composition of fluids in the system during metamorphism, and do not follow the barrowian succession of Fe-Mg-Al minerals. Sample BA23 is a garnet-magnetite-quartzite with a high manganese content (Table 3.3.1). The position of the sample indicates that it should have a similar metamorphic grade as the samples form Zone 3 (biotite zone). The high manganese content is interpreted as the reason for the stabilization of garnet in the sample, as garnet develops at lower P-T conditions in manganese-rich systems than does garnet in systems with a normal metapelitic composition.

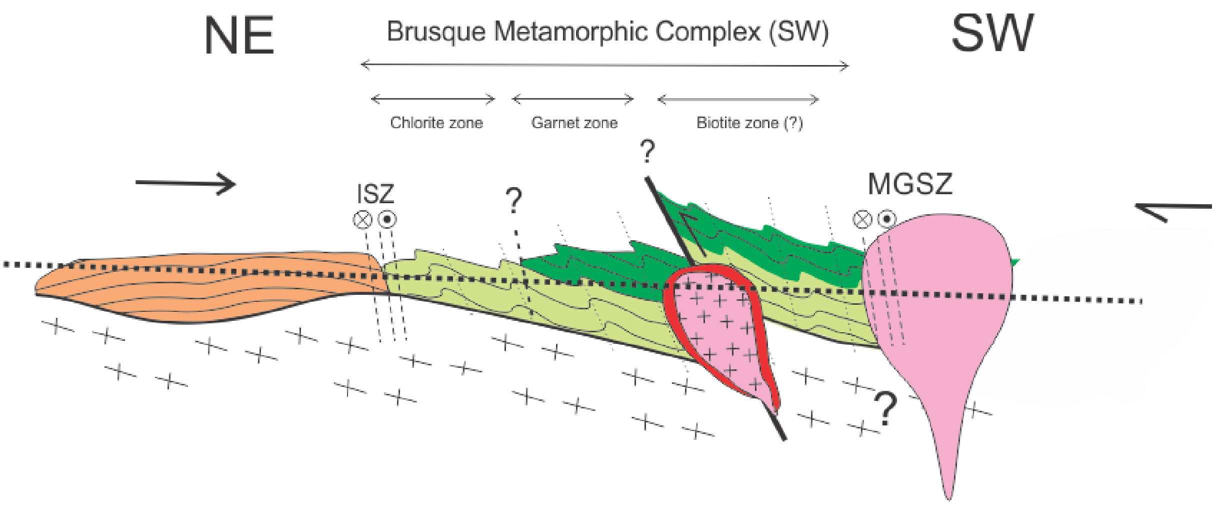

Figure 4.1.2-3 – Schematic cross-section of the south-western part of the Brusque Metamorphic Complex based on metamorphic grade of collected samples. This sketch only present one of several possible models that could be an explanation for the difference in metamorphic grades. The black dotted line represent the present erosional level.

Based on field observations, petrographic study of collected samples and thermodynamic modelling, the south-western Brusque Metamorphic Complex is represented by three contrasting metamorphic zones bound by shear zones and large-scale, elongated granitoid intrusions (Figure 4.1.2-1). Sharp boundaries between the individual zones might be the result of strike slip faulting that occurred during D2, as the orientation of the shear zones is parallel with S2 crenulation cleavage and axial planes of F2 folds. The ca. 620-590 Ma post-collisional granitoids that crosscut the BMC produced contact aureoles in adjacent parts of the BMC (Basei et al., 2011; Florisbal et al., 2012) (red areas in Figure 4.1.2-3). Although this metamorphic event has not been studied in detail, it is important to mention it, as it gives an upper age limit of the peak metamorphic event in the BMC, because the contact mineral assemblages overgrow S1 fabric. Dating of the peak metamorphic event of the BMC (and the other parts of the Schist Belt) still waits to be quantified. However, the high grade metamorphism in the Punta del Este Terrane (Oyhantçabal et al., 2009; Lenz et al., 2011), and the Coastal Terrane (Goscombe et al., 2005a; Konopásek et al., 2008), which are considered as the units with which the Schist Belt collided, does indicate that the collision started at ca. 650 Ma. These observations suggests that the peak of metamorphism in the Brusque Metamorphic Complex took place between ca. 650 and 620 Ma.

4.2 The Central Kaoko Zone

Three samples from the Kaoko Belt in Namibia were studied for comparison of metamorphic conditions on the western side (Brusque Metamorphic Complex) and the eastern side (Central Kaoko Zone). Based on the petrographic observations and dating of metamorphic garnet, Goscombe et al. (2003) stated that the peak metamorphic conditions in the Central Kaoko Zone were reached at ca. 575 Ma, i.e ca. 75-45 my later than on the South American side of the orogen.

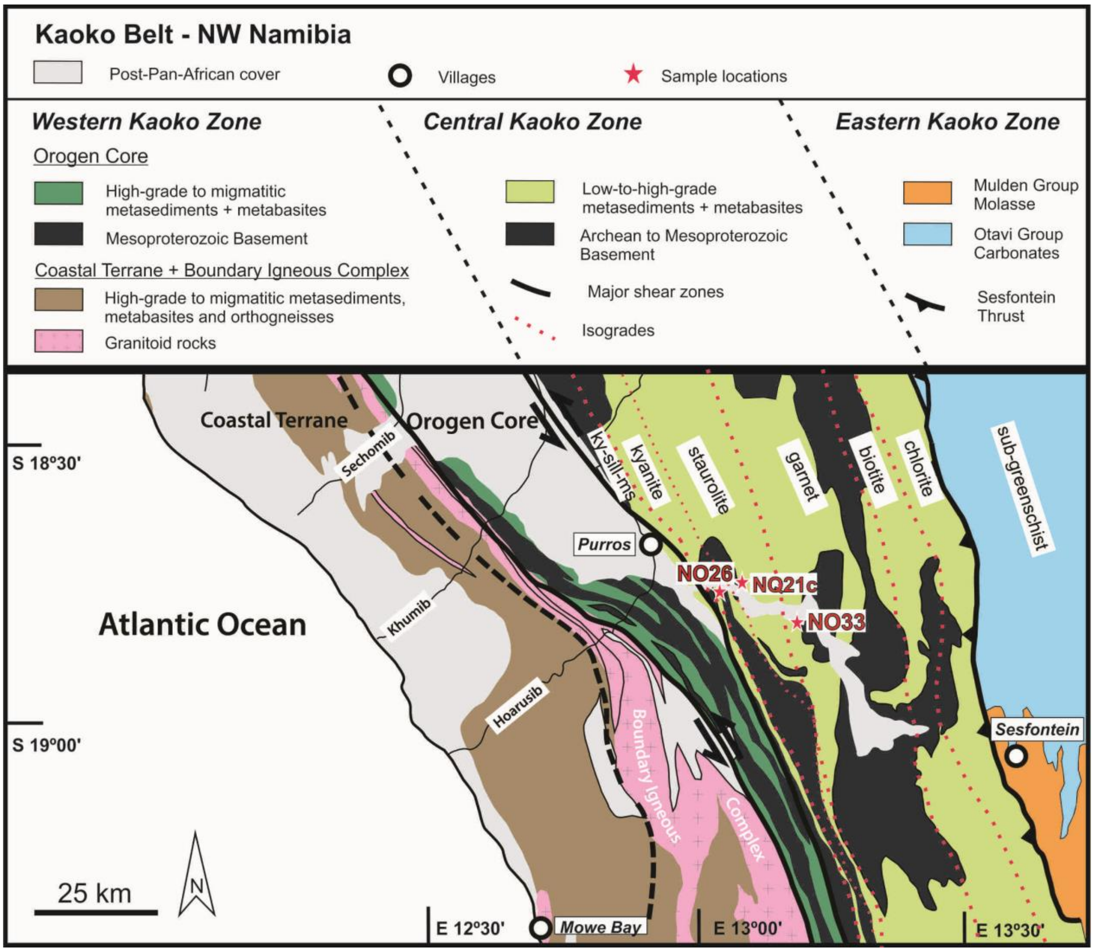

Figure 4.2.1 Simplified geological map of the Kaoko Belt in SW Namibia, modified after Ulrich et al.(2010) and Goscombe et al.(2003). Sample locations are marked with red stars.

4.2.1 Phase equilibrium modelling:

One sample from the garnet zone in the Central Kaoko Zone (Figure 4.1.1: NO33) suggests that the matrix mineral assemblage equilibrated at temperatures of ca 540-560°C and pressure of ca. 6.5-9.0 kbar (Figure 3.5.4-3). These pressure conditions corresponds to depths of ca. 24-33 km assuming an average crust density of 2.8 g/cm^3. This suggest an apparent thermal gradient of 16-23°C/km for the metamorphism in the garnet zone of the Central Kaoko Zone.

Sample NQ21c (Figure 4.1.1) from the staurolite zone in the Central Kaoko Zone suggests that the matrix mineral assemblage equilibrated at temperatures of ca. 595-630°C and pressure of ca. 7.4-8.1 kbar (Figure 3.5.5-3). These conditions corresponds to depth of ca. 27-30 km assuming an average crust density of 2.8 g/cm^3, and suggest a thermal gradient of ca. 20-23°C/km during metamorphic peak in the staurolite zone of the Central Kaoko Zone.

The matrix mineral assemblage in the sample NO26 (Figure 4.1.1) seems to have re-equilibrated during retrogression, resulting in a decrease in X_{Mg} of garnet rims. The peak metamorphic conditions for the sample were estimated by the use of compositional isopleths for garnet core composition. The result suggested that the garnet equilibrated at temperatures of ca. 630-660°C and pressure of ca. 9.6-10.4 kbar (Figure 3.5.6-1). Assuming an average crust density of 2.8 g/cm^3, these pressure conditions corresponds to depths of 35-38 km, which suggest an apparent thermal gradient of 17-19°C/km during metamorphic peak in the kyanite zone.

The estimated apparent thermal gradients for the individual metamorphic zones range between 16 and 23°C/km, which are values very similar to thermal gradients found by Goscombe et al. (2003) (17-24°C/km).

4.3 Comparison of samples

As mentioned in the introductory section, the Brusque Metamorphic Complex can be considered as an equivalent of the Central Kaoko Zone in terms of pre-collisional origin and tectonic position during the collision. However, the collision and peak metamorphism took place ca. 75-45 Ma earlier on the Brazilian side than on the African side of the orogenic system.

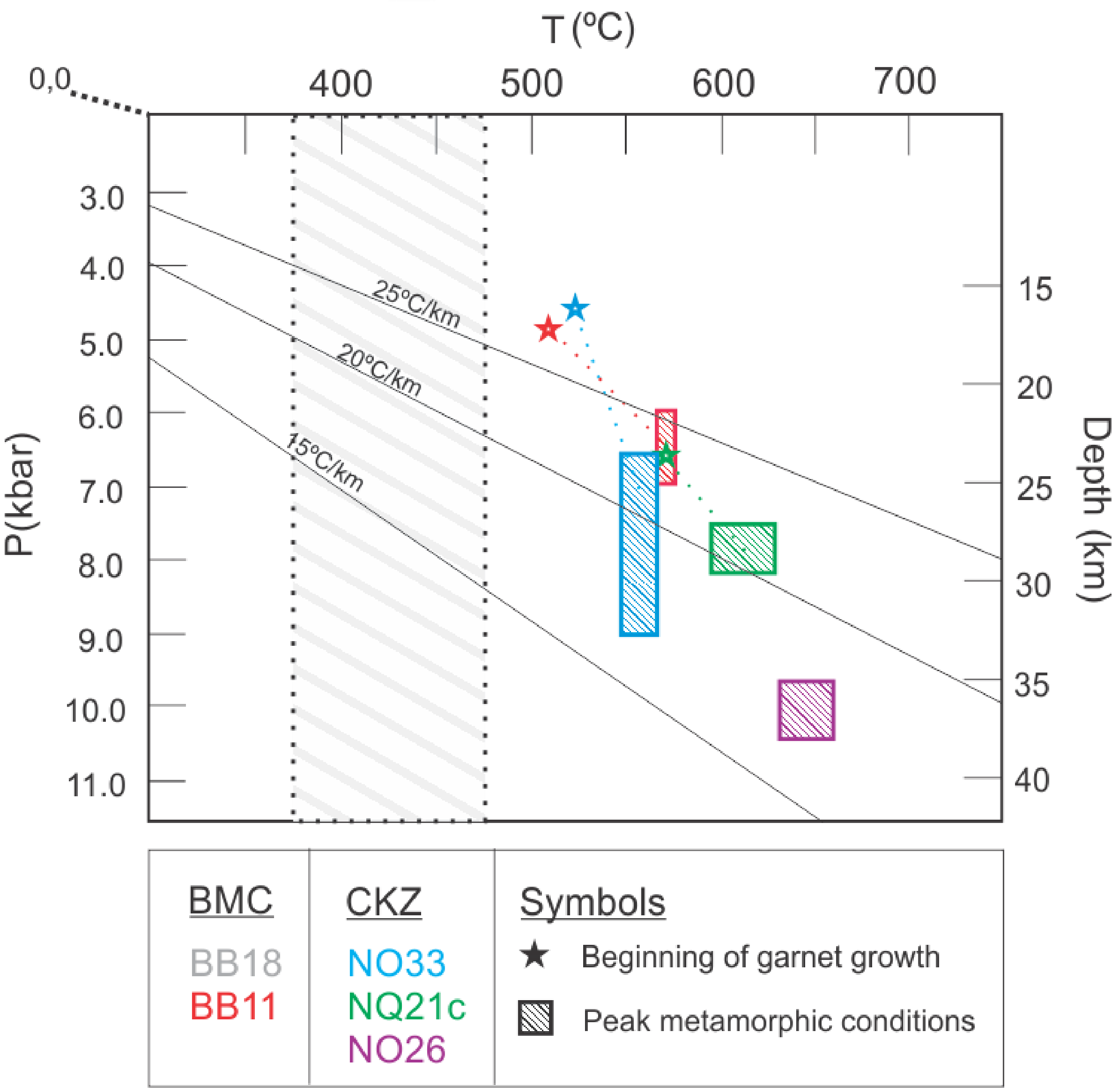

Figure 4.3.1 Summary of P-T conditions for two samples from the Brusque Metamorphic Complex and three samples from the Central Kaoko Zone.

Phase equilibrium modelling of three samples from the Central Kaoko Zone in the Kaoko Belt suggests apparent crustal thermal gradients of 16-23°C/km during peak metamorphic conditions. P-T modelling from one sample from the garnet zone in the Brusque Metamorphic Complex suggests an apparent crustal thermal gradient of 22-26 °C/km, which overlaps with modelled thermal gradients for the Central Kaoko Zone. Such results suggests that despite the difference in timing of metamorphism, the thermal conditions in the crust were similar during underthrusting of the western and eastern margin of the northern Dom Feliciano-Kaoko belt (Figure 4.3.1).

4.4 Evolutionary model

The results presented in this thesis, as well as previously published works can be combined in a schematic model that summarize the pre-, syn- and post-collisional evolution of the Dom Feliciano-Kaoko orogen.

Pre-collisional setting:

Figure 4.4.1 A) shows a schematic view of the pre-collisional setting of the Dom Feliciano-Kaoko belt. Many different interpretations and discussions have been published about the pre-collisional setting of the studied area. Most of these models suggested continental rifting that proceeded into the development of an oceanic domain (Adamasor Ocean) and assumed that the oceanic crust was subducted either westwards, eastwards or both ways during the Neoproterozoic convergence (Basei et al., 2000; Goscombe and Gray, 2007; Frimmel et al., 2011; Chemale Jr et al., 2012). Konopásek et al. (2017) recently argued that the pre-collisional setting did not involve any long-lived subduction system and proposed that the orogenic system formed during inversion of a continental rift called the Adamasor Rift. The pre-collisional setting proposed by Konopásek et al. (2017) is the starting point of the evolutionary model proposed in this thesis.

The rift initiated in early Neoproterozoic at ca. 820 Ma. Detrital material that formed by erosion of surrounding cratons and products of syn-sedimentary bimodal volcanism were filling in the axial part of the rift (i.e. future Coastal-Punta del Este Terrane) between ca. 820-785 Ma. The active continental stretching progressively moved towards the basin shoulders, expanded the rift system, and the deposition continued up to ca. 680-660 Ma (Konopásek et al. (2017) and references therein).

650-580(?) Ma collision on the western margin of the orogenic system:

With the change of tectonic forces from extensional to compressional in late Neoproterozoic, the collision started in west at around 650 Ma (Figure 4.4.1 B)). The collision resulted in high-grade metamorphism and migmatization in the Coastal-Punta del Este Terrane (Oyhantçabal et al., 2009; Lenz et al., 2011; Konopásek et al., 2008; Goscombe et al., 2005a) and the volcano-sedimentary rocks deposited on top of the Luis Alves microplate during the rifting stage were continuously metamorphosed and deformed during the collision. Direct dating of the peak metamorphism in the Brusque Metamorphic Complex still waits to be done. However, the minimum age of the peak metamorphic event (D1) in the northern Dom Feliciano Belt can be inferred from the presence of post collisional granitoids intruding the BMC at ca. 620 Ma. Brusque Metamorphic Complex may be regarded as a fold-and thrust belt that has developed during the collision, and phase equilibrium presented in this thesis suggests that the central part of the BMC reached maximum depths of ca. 22-26 km before exhumation.

580-550 Ma collision in the eastern part of the orogenic system:

Figure 4.4.1 C) show a schematic view of the collision in the eastern part of the orogenic system. Dating of syn-collisional granitoids and garnet porphyroblasts from peak metamorphic assemblages constrains the collisional event to ca. 580-550 Ma throughout the Kaoko Belt, except for the Coastal Terrain. The collision caused high-grade metamorphism and migmatization in the Orogen Core, and the emplacement of the ca. 580-550 Boundary Igneous Complex (Konopásek et al., 2008; Goscombe et al., 2003; Goscombe et al., 2005b).

The Central Kaoko Zone reached peak metamorphic conditions at ca. 575 Ma during the first stage of the collision which Goscombe et al. (2003) defined as the transpressional phase. P-T modelling suggests that the garnet, staurolite and kyanite- zone reached maximum depths of ca. 24-33 km, 27-30 km and 35-38 km before exhumation, respectively. During the compressional phase, the Central Kaoko Zone was folded and thrust over the Eastern Kaoko Zone.

Despite the large time difference between the peak metamorphic event in the Brusque Metamorphic Complex and in the Central Kaoko Zone, the thermal conditions in the crust remained more or less the same in these parts of the orogenic system and corresponds to apparent thermal gradients commonly observed during orogenesis (Spear, 1993). Collision on both margins of the orogenic system were accompanied by high-grade metamorphism and migmatization in the core of the orogen (i.e. the Orogen Core and the Coastal-Punta del Este Terrane) and lead to formation of granitoid intrusions. Such processes bring heat to the system, and might be responsible for the similar thermal state of the crust on both sides of the orogenic system.

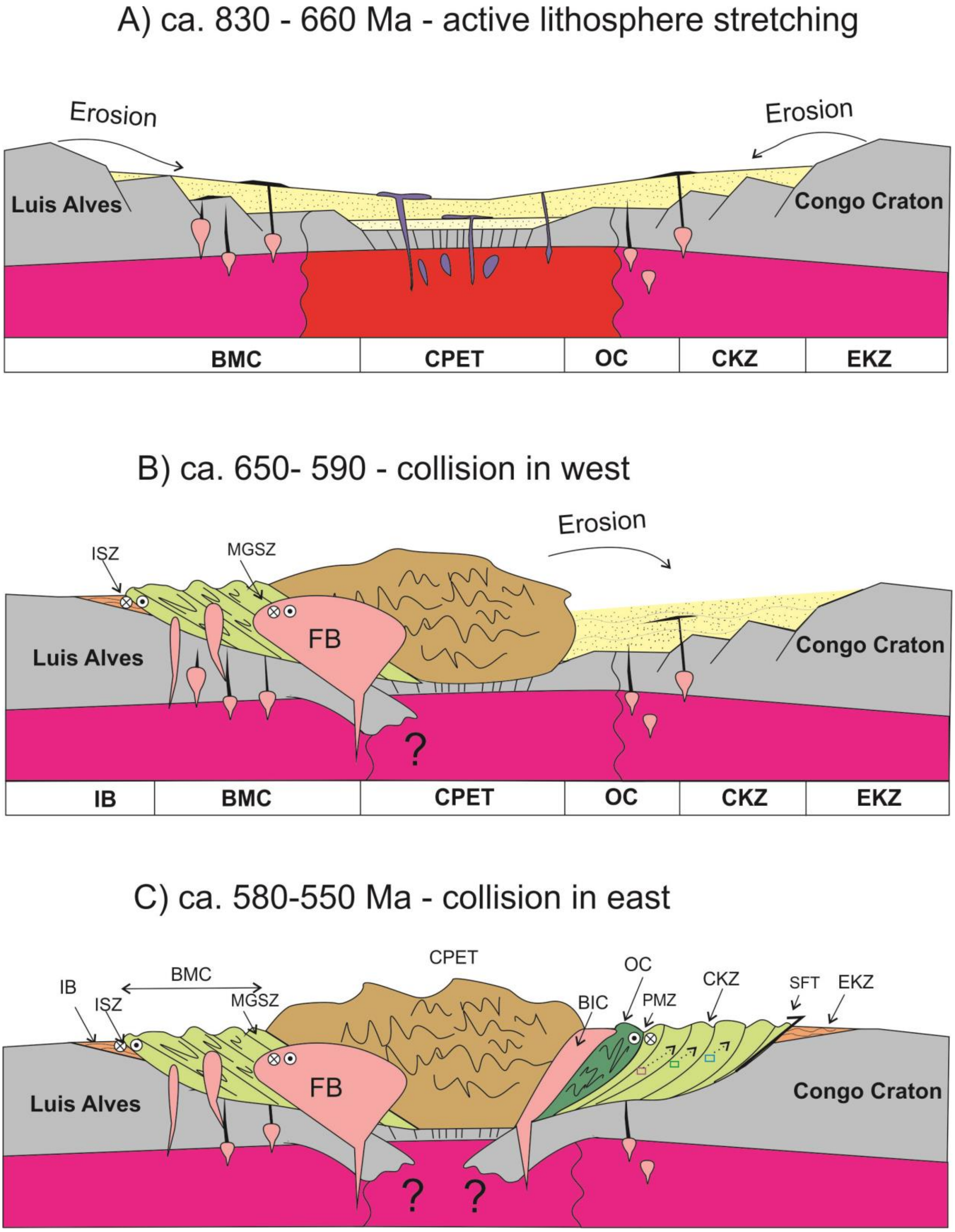

A) ca. 830 - 660 Ma - active lithosphere stretching

B) ca. 650- 590 - collision in west

C) ca. 580-550 Ma - collision in east

Figure 4.4.1 Schematic view of the evolution of the Dom Feliciano-Kaoko Belt. IB: Itajaí Basin, ISZ: Itajaí shear zone, BMC: Brusque Metamorphic Complex, MGSZ: Major Gercino shear zone, CPET: Coastal-Punta del Este Terrane, OC: Orogen Core, PMZ: Purros Mylonite Zone, CKZ: Central Kaoko Zone, SFT: Sesfontein Thrust, EKZ: Eastern Kaoko Zone.

5 Conclusions

- Metapelitic samples collected from the western part of the Brusque Metamorphic Complex contain mineral assemblages suggesting that the central part has a higher metamorphic grade (lower amphibolite facies) than the north and south zones (greenschist facies).

- P-T modelling of one sample from the central part of the western Brusque Metamorphic Complex suggested an apparent thermal gradient of 22-26 °C/km during metamorphic peak, and P-T modelling of three samples from the Central Kaoko Zones suggested thermal gradients between 16 and 23°C/km.

- The conclusion of this thesis is that the thermal state of the crust was similar on both sides of the orogenic system despite a large time difference between the peak metamorphic event in the Brusque Metamorphic Complex and in the Central Kaoko Zone.

Work cited

BARROW, G. 1893. On an Intrusion of Muscovite-biotite Gneiss in the South-eastern Highlands of Scotland, and its accompanying Metamorphism. *Quarterly Journal of the Geological Society,* 49**,** 330-358.

BASEI, M., NETO, M. C., CASTRO, N., NUTMAN, A., WEMMER, K., YAMAMOTO, M., HUECK, M., OSAKO, L., SIGA, O. & PASSARELLI, C. 2011. Tectonic evolution of the Brusque Group, Dom Feliciano belt, Santa Catarina, Southern Brazil. *Journal of South American Earth Sciences,* 32**,** 324-350.

BASEI, M., SIGA JR, O., MASQUELIN, H., HARARA, O., REIS NETO, J. & PRECIOZZI, F. 2000. The Dom Feliciano Belt of Brazil and Uruguay and its Foreland Domain the Rio de la Plata Craton: framework, tectonic evolution and correlation with similar provinces of Southwestern Africa. *Tectonic Evolution of South America,* 1**,** 311-334.

CHATTERJEE, N. & FROESE, E. 1975. Thermodynamic study of pseudobinary join muscovite-paragonite in system KAlSi3O8-NaAlSi3O8-Al2O3-SiO2-H2O. *American Mineralogist,* 60**,** 985-993.

CHEMALE JR, F., MALLMANN, G., DE FÁTIMA BITENCOURT, M. & KAWASHITA, K. 2012. Time constraints on magmatism along the Major Gercino Shear Zone, southern Brazil: implications for West Gondwana reconstruction. *Gondwana Research,* 22**,** 184-199.

CONNOLLY, J. A. 2005. Computation of phase equilibria by linear programming: a tool for geodynamic modeling and its application to subduction zone decarbonation. *Earth and Planetary Science Letters,* 236**,** 524-541.

DE CAMPOS, R. S., PHILIPP, R. P., MASSONNE, H.-J. & CHEMALE, F. 2012a. Early post-collisional Brasiliano magmatism in Botuverá region, Santa Catarina, southern Brazil: Evidence from petrology, geochemistry, isotope geology and geochronology of the diabase and lamprophyre dikes. *Journal of South American Earth Sciences,* 37**,** 266-278.

DE CAMPOS, R. S., PHILIPP, R. P., MASSONNE, H.-J., CHEMALE JR, F. & THEYE, T. 2012b. Petrology and isotope geology of mafic to ultramafic metavolcanic rocks of the Brusque Metamorphic Complex, southern Brazil. *International Geology Review,* 54**,** 686-713.

FLORISBAL, L. M., DE ASSIS JANASI, V., DE FÁTIMA BITENCOURT, M. & HEAMAN, L. M. 2012. Space–time relation of post-collisional granitic magmatism in Santa Catarina, southern Brazil: U–Pb LA-MC-ICP-MS zircon geochronology of coeval mafic–felsic magmatism related to the Major Gercino Shear Zone. *Precambrian Research,* 216**,** 132-151.

FRANZ, L., ROMER, R. L. & DINGELDEY, D. P. 1999. Diachronous Pan-African granulite-facies metamorphism (650 Ma and 550 Ma) in the Kaoko belt, NW Namibia. *European Journal of Mineralogy,* 11**,** 167-180.

FRIMMEL, H., BASEI, M. & GAUCHER, C. 2011. Neoproterozoic geodynamic evolution of SW-Gondwana: a southern African perspective. *International Journal of Earth Sciences,* 100**,** 323-354.

GOSCOMBE, B., GRAY, D., ARMSTRONG, R., FOSTER, D. A. & VOGL, J. 2005a. Event geochronology of the Pan-African Kaoko Belt, Namibia. *Precambrian Research,* 140**,** 103. e1-103. e41.

GOSCOMBE, B., GRAY, D. & HAND, M. 2005b. Extrusional tectonics in the core of a transpressional orogen; the Kaoko Belt, Namibia. *Journal of Petrology,* 46**,** 1203-1241.

GOSCOMBE, B. & GRAY, D. R. 2007. The Coastal Terrane of the Kaoko Belt, Namibia: outboard arc-terrane and tectonic significance. *Precambrian Research,* 155**,** 139-158.

GOSCOMBE, B., HAND, M., GRAY, D. & MAWBY, J. 2003. The metamorphic architecture of a transpressional orogen: the Kaoko Belt, Namibia. *Journal of Petrology,* 44**,** 679-711.

GRAY, D. R., FOSTER, D., MEERT, J., GOSCOMBE, B., ARMSTRONG, R., TROUW, R. & PASSCHIER, C. 2008. A Damara orogen perspective on the assembly of southwestern Gondwana. *Geological Society, London, Special Publications,* 294**,** 257-278.

GUADAGNIN, F., CHEMALE, F., DUSSIN, I. A., JELINEK, A. R., DOS SANTOS, M. N., BORBA, M. L., JUSTINO, D., BERTOTTI, A. L. & ALESSANDRETTI, L. 2010. Depositional age and provenance of the Itajaí Basin, Santa Catarina State, Brazil: implications for SW Gondwana correlation. *Precambrian Research,* 180**,** 156-182.

HARTMANN, L. A., DE FÁTIMA BITENCOURT, M., SANTOS, J. O. S., MCNAUGHTON, N. J., RIVERA, C. B. & BETIOLLO, L. 2003. Prolonged Paleoproterozoic magmatic participation in the Neoproterozoic Dom Feliciano belt, Santa Catarina, Brazil, based on zircon U–Pb SHRIMP geochronology. *Journal of South American Earth Sciences,* 16**,** 477-492.

HOLLAND, T. & POWELL, R. 1998. An internally consistent thermodynamic data set for phases of petrological interest. *Journal of metamorphic Geology,* 16**,** 309-343.

JUNG, S., BRANDT, S., NEBEL, O., HELLEBRAND, E., SETH, B. & JUNG, C. 2014. The P–T–t paths of high-grade gneisses, Kaoko Belt, Namibia: Constraints from mineral data, U–Pb allanite and monazite and Sm–Nd/Lu–Hf garnet ages and garnet ion probe data. *Gondwana Research,* 25**,** 775-796.

KONOPÁSEK, J., JANOUŠEK, V., OYHANTÇABAL, P., SLÁMA, J. & ULRICH, S. 2017. Did the circum-Rodinia subduction trigger the Neoproterozoic rifting along the Congo–Kalahari Craton margin? *International Journal of Earth Sciences***,** 1-36.

KONOPÁSEK, J., KOŠLER, J., SLÁMA, J. & JANOUŠEK, V. 2014. Timing and sources of pre-collisional Neoproterozoic sedimentation along the SW margin of the Congo Craton (Kaoko Belt, NW Namibia). *Gondwana Research,* 26**,** 386-401.

KONOPÁSEK, J., KOŠLER, J., TAJČMANOVÁ, L., ULRICH, S. & KITT, S. L. 2008. Neoproterozoic igneous complex emplaced along major tectonic boundary in the Kaoko Belt (NW Namibia): ion probe and LA-ICP-MS dating of magmatic and metamorphic zircons. *Journal of the Geological Society,* 165**,** 153-165.

KONOPÁSEK, J., SLÁMA, J. & KOŠLER, J. 2016. Linking the basement geology along the Africa-South America coasts in the South Atlantic. *Precambrian Research,* 280**,** 221-230.

LENZ, C., FERNANDES, L., MCNAUGHTON, N., PORCHER, C. & MASQUELIN, H. 2011. U–Pb SHRIMP ages for the Cerro Bori Orthogneisses, Dom Feliciano Belt in Uruguay: Evidences of a∼ 800Ma magmatic and∼ 650Ma metamorphic event. *Precambrian Research,* 185**,** 149-163.

LI, Z.-X., BOGDANOVA, S., COLLINS, A., DAVIDSON, A., DE WAELE, B., ERNST, R., FITZSIMONS, I., FUCK, R., GLADKOCHUB, D. & JACOBS, J. 2008. Assembly, configuration, and break-up history of Rodinia: a synthesis. *Precambrian research,* 160**,** 179-210.

MILLER, R. M. 1983. The Pan-African Damara Orogen of South West Africa/Namibia. *Evolution of the Damara Orogen of South West Africa/Namibia.*

OYHANTÇABAL, P., SIEGESMUND, S., WEMMER, K., PRESNYAKOV, S. & LAYER, P. 2009. Geochronological constraints on the evolution of the southern Dom Feliciano Belt (Uruguay). *Journal of the Geological Society,* 166**,** 1075-1084.

PISAREVSKY, S. A., WINGATE, M. T., POWELL, C. M., JOHNSON, S. & EVANS, D. A. 2003. Models of Rodinia assembly and fragmentation. *Geological Society, London, Special Publications,* 206**,** 35-55.

PORADA, H. 1979. The damara-ribeira orogen of the Pan-Africanbrasiliano cycle in Namibia (Southwest Africa) and Brazil as interpreted in terms of continental collision. *Tectonophysics,* 57**,** 237-265.

POWELL, R. & HOLLAND, T. 1999. Relating formulations of the thermodynamics of mineral solid solutions; activity modeling of pyroxenes, amphiboles, and micas. *American Mineralogist,* 84**,** 1-14.

PRECIOZZI, F., MASQUELIN, H. & BASEI, M. A. S. The Namaqua/Grenville Terrane of eastern Uruguay. II South American Symposium on Isotope Geology, Carlos Paz, 1999.

SETH, B., KRÖNER, A., MEZGER, K., NEMCHIN, A., PIDGEON, R. & OKRUSCH, M. 1998. Archaean to Neoproterozoic magmatic events in the Kaoko belt of NW Namibia and their geodynamic significance. *Precambrian Research,* 92**,** 341-363.

SPEAR, F. S. 1993. *Metamorphic phase equilibria and pressure-temperature-time paths,* Mineralogical Society of America Washington, DC.

ULRICH, S., KONOPÁSEK, J., JEŘÁBEK, P. & TAJČMANOVÁ, L. 2011. Transposition of structures in the Neoproterozoic Kaoko Belt (NW Namibia) and their absolute timing. *International Journal of Earth Sciences,* 100**,** 415-429.

WHITE, R., POWELL, R. & HOLLAND, T. 2007. Progress relating to calculation of partial melting equilibria for metapelites. *Journal of metamorphic Geology,* 25**,** 511-527.

WILL, T., OKRUSCH, M. & GRUNER, B. 2004. Barrovian and Buchan type metamorphism in the Pan-African Kaoko belt, Namibia: implications for its geotectonic position within the framework of Western Gondwana. *South African Journal of Geology,* 107**,** 431-454.

Appendix A

Sample	**BB18**								
Mineral	**Muscovite**					**Chlorite**		**Ilmenite**	
Fabric	**S1**					**S1**		**S1**	
Point	26 / 1 .	30 / 1 .	31 / 1 .	27 / 1 .	32 / 1 .	24 / 1 .	25 / 1 .	28 / 1 .	29 / 1 .
Position	Chl layer			Qz layer					
Wt %									
SiO_2	46,20	47,17	45,61	46,98	46,05	22,25	23,79	3,76	1,76
TiO_2	0,06	0,07	0,06	0,06	0,06	0,05	0,03	51,99	51,36
Cr_2O_3	0,00	0,00	0,00	0,02	0,03	0,01	0,00	0,01	0,05
Al_2O_3	31,70	31,59	31,78	31,34	31,52	19,66	20,91	0,89	0,86
Fe_2O_3	4,03	3,53	4,85	2,99	4,39	2,23	0,00	0,00	0,00
FeO	0,96	0,87	0,41	1,31	0,58	37,99	37,59	42,76	42,86
MnO	0,03	0,06	0,04	0,03	0,08	0,04	0,04	0,47	0,50
MgO	1,23	1,51	1,04	1,51	1,33	5,20	5,79	0,01	0,05
CaO	0,05	0,00	0,03	0,00	0,00	0,05	0,02	0,03	0,16
Na_2O	0,61	0,59	0,57	0,56	0,55	0,00	0,00	0,00	0,00
K_2O	10,33	10,56	10,48	10,44	10,45	0,02	0,02	0,00	0,00
Total	95,20	95,94	94,87	95,24	95,03	87,49	88,19	99,92	97,60
No. O	11,00	11,00	11,00	11,00	11,00	14,00	14,00	11,00	11,00
Si	3,12	3,15	3,09	3,16	3,11	2,56	2,69	0,09	0,05
Ti	0,00	0,00	0,00	0,00	0,00	0,00	0,00	0,98	0,99
Cr	0,00	0,00	0,00	0,00	0,00	0,00	0,00	0,00	0,00
Al	2,52	2,49	2,54	2,49	2,51	2,67	2,78	0,03	0,03
Fe^{3+}	0,20	0,18	0,25	0,15	0,22	0,19	0,00	0,00	0,00
Fe^{2+}	0,05	0,05	0,02	0,07	0,03	3,66	3,55	0,89	0,92
Mn	0,00	0,00	0,00	0,00	0,00	0,00	0,00	0,01	0,01
Mg	0,12	0,15	0,11	0,15	0,13	0,89	0,97	0,00	0,00
Ca	0,00	0,00	0,00	0,00	0,00	0,01	0,00	0,00	0,00
Na	0,08	0,08	0,08	0,07	0,07	0,00	0,00	0,00	0,00
K	0,89	0,90	0,91	0,90	0,90	0,00	0,00	0,00	0,00
Total	7,00	7,00	7,00	7,00	7,00	10,00	10,00	2,00	2,00
X_{Mg}						0,20	0,22		

Sample	**BA23**																	
Mineral	**Garnet**							**Biotite**		**Muscovite**						**Magnetite**		
Fabric	**S1**							**S1**		**S1**						**S1**		
Point	56 / 1 .	57 / 1 .	58 / 1 .	59 / 1 .	45 / 1 .	53 / 1 .	39 / 1 .	40 / 1 .	42 / 1 .	34 / 1 .	35 / 1 .	38 / 1 .	39 / 1 .	44 / 1 .	45 / 1 .	36 / 1 .	37 / 1 .	54 / 1 .
Position	Core	Rim	Core	Rim	Core	Rim	Rim											
Wt %																		
SiO_2	36,87	36,94	37,24	37,31	37,09	37,29	36,94	38,97	38,75	46,51	46,20	46,98	47,17	45,61	46,05	0,07	0,06	0,03
TiO_2	0,05	0,06	0,03	0,04	0,06	0,05	0,05	0,28	0,35	0,06	0,06	0,06	0,07	0,06	0,06	0,01	2,17	2,21
Cr_2O_3	0,00	0,03	0,01	0,00	0,01	0,03	0,01	0,03	0,00	0,00	0,00	0,02	0,00	0,00	0,03	0,01	0,04	0,00
Al_2O_3	20,00	20,20	20,67	20,34	20,15	20,33	20,15	19,19	19,47	31,50	31,70	31,34	31,59	31,78	31,52	0,10	0,24	0,15
Fe_2O_3	0,74	1,64	0,19	0,00	0,87	0,30	0,81	0,00	0,00	3,15	4,03	2,99	3,53	4,85	4,39	68,66	63,90	63,92
FeO	8,02	9,72	10,94	11,16	8,81	10,82	10,64	10,27	10,27	1,31	0,96	1,31	0,87	0,41	0,58	30,44	32,85	32,35
MnO	30,92	27,07	26,81	26,95	29,96	26,80	27,53	0,76	1,01	0,02	0,03	0,03	0,06	0,04	0,08	0,50	0,07	0,45
MgO	1,05	2,59	2,88	2,63	1,46	2,52	2,22	16,18	16,13	1,27	1,23	1,51	1,51	1,04	1,33	0,05	0,00	0,03
CaO	2,21	1,79	1,02	1,11	1,90	1,70	1,20	0,18	0,12	0,03	0,05	0,00	0,00	0,03	0,00	0,00	0,02	0,03
Na_2O	0,02	0,04	0,00	0,01	0,05	0,00	0,04	0,18	0,28	0,53	0,61	0,56	0,59	0,57	0,55	0,00	0,00	0,00
K_2O	0,00	0,00	0,01	0,00	0,00	0,00	0,00	7,66	8,39	10,47	10,33	10,44	10,56	10,48	10,45	0,03	0,00	0,00
Total	99,87	100,08	99,81	99,55	100,35	99,83	99,58	93,70	94,77	94,84	95,20	95,24	95,94	94,87	95,03	99,87	99,34	99,17
No. O	12,00	12,00	12,00	12,00	12,00	12,00	12,00	11,00	11,00	11,00	11,00	11,00	11,00	11,00	11,00	4,00	4,00	4,00
Si	3,01	2,99	3,01	3,03	3,01	3,02	3,01	2,96	2,90	3,15	3,12	3,16	3,15	3,09	3,11	0,00	0,00	0,00
Ti	0,00	0,00	0,00	0,00	0,00	0,00	0,00	0,02	0,02	0,00	0,00	0,00	0,00	0,00	0,00	0,00	0,06	0,06
Cr	0,00	0,00	0,00	0,00	0,00	0,00	0,00	0,00	0,00	0,00	0,00	0,00	0,00	0,00	0,00	0,00	0,00	0,00
Al	1,93	1,92	1,97	1,95	1,93	1,94	1,93	1,72	1,72	2,51	2,52	2,49	2,49	2,54	2,51	0,00	0,01	0,01
Fe^{3+}	0,05	0,10	0,01	0,00	0,05	0,02	0,05	0,00	0,00	0,16	0,20	0,15	0,18	0,25	0,22	1,99	1,86	1,86
Fe^{2+}	0,55	0,66	0,74	0,76	0,60	0,73	0,72	0,65	0,64	0,07	0,05	0,07	0,05	0,02	0,03	0,98	1,06	1,05
Mn	2,14	1,85	1,83	1,85	2,06	1,84	1,90	0,05	0,06	0,00	0,00	0,00	0,00	0,00	0,00	0,02	0,00	0,01
Mg	0,13	0,31	0,35	0,32	0,18	0,30	0,27	1,83	1,80	0,13	0,12	0,15	0,15	0,11	0,13	0,00	0,00	0,00
Ca	0,19	0,16	0,09	0,10	0,17	0,15	0,10	0,01	0,01	0,00	0,00	0,00	0,00	0,00	0,00	0,00	0,00	0,00
Na	0,00	0,01	0,00	0,00	0,01	0,00	0,01	0,03	0,04	0,07	0,08	0,07	0,08	0,08	0,07	0,00	0,00	0,00
K	0,00	0,00	0,00	0,00	0,00	0,00	0,00	0,74	0,80	0,90	0,89	0,90	0,90	0,91	0,90	0,00	0,00	0,00
Total	8,00	8,00	8,00	8,00	8,00	8,00	8,00	8,00	8,00	7,00	7,00	7,00	7,00	7,00	7,00	3,00	3,00	3,00
X_{Mg}	0,19	0,32	0,32	0,30	0,23	0,29	0,27	0,74	0,74									
X_{Prp}	0,04	0,10	0,12	0,11	0,06	0,10	0,09											
X_{Alm}	0,18	0,22	0,25	0,25	0,20	0,24	0,24											
X_{Grs}	0,06	0,05	0,03	0,03	0,06	0,05	0,04											
X_{Sps}	0,71	0,62	0,61	0,61	0,69	0,61	0,63											

Sample	**BB11**																
Mineral	**Garnet**						**Biotite**						**White mica**				
Fabric	**S1**						**S1**				**S2?**		**S1**				
Point	120 / 1 .	122 / 1 .	83 / 1 .	117 / 1 .	118 / 1 .	119 / 1 .	5 / 1 .	6 / 1 .	13 / 1 .	14 / 1 .	25 / 1 .	26 / 1 .	11 / 1 .	17 / 1 .	23 / 1 .	24 / 1 .	29 / 1 .
Position	Core	Rim	Core	Rim	Rim	Rim	Center	Center	Core	Rim	Center	Rim					
Wt %																	
SiO_2	37,51	37,66	37,78	37,75	37,58	37,77	37,90	37,25	37,20	36,03	37,37	37,50	47,78	47,85	47,15	46,79	47,11
TiO_2	0,13	0,02	0,12	0,07	0,03	0,03	1,76	1,67	1,72	1,55	1,69	1,66	0,29	0,31	0,28	0,34	0,28
Cr_2O_3	0,01	0,02	0,01	0,01	0,01	0,00	0,01	0,03	0,01	0,02	0,02	0,02	0,02	0,04	0,01	0,01	0,05
Al_2O_3	20,45	20,81	20,69	20,44	20,90	20,78	18,71	18,55	18,87	18,17	18,83	18,66	34,38	33,45	35,97	35,91	34,03
Fe_2O_3	1,14	0,00	0,28	0,66	1,05	0,55	0,00	0,00	0,00	0,00	0,00	0,00	0,00	0,00	0,00	0,00	0,00
FeO	27,20	36,91	27,49	33,41	36,56	36,40	19,01	21,00	19,46	22,66	19,78	19,43	1,54	1,85	1,02	1,14	1,82
MnO	6,43	0,10	6,53	1,01	0,09	0,12	0,02	0,06	0,00	0,05	0,04	0,05	0,00	0,00	0,01	0,00	0,00
MgO	0,77	2,56	0,73	1,48	2,52	2,48	7,44	7,48	8,01	7,88	8,19	8,24	0,87	1,15	0,56	0,54	0,86
CaO	7,55	2,62	7,63	6,25	2,77	3,14	0,12	0,08	0,04	0,03	0,05	0,07	0,02	0,03	0,01	0,04	0,02
Na_2O	0,04	0,01	0,02	0,03	0,04	0,03	0,09	0,20	0,04	0,18	0,09	0,15	0,70	1,04	2,17	1,68	0,86
K_2O	0,00	0,00	0,00	0,00	0,03	0,02	8,62	8,45	8,42	8,45	8,54	8,74	9,79	9,36	8,35	9,11	9,64
Total	101,24	100,71	101,28	101,12	101,57	101,32	93,67	94,76	93,77	95,02	94,61	94,52	95,39	95,08	95,54	95,54	94,67
No. O	12,00	12,00	12,00	12,00	12,00	12,00	11,00	11,00	11,00	11,00	11,00	11,00	11,00	11,00	11,00	11,00	11,00
Si	3,00	3,02	3,01	3,02	2,99	3,01	3,05	2,97	2,98	2,87	2,97	2,97	3,19	3,20	3,10	3,09	3,16
Ti	0,01	0,00	0,01	0,00	0,00	0,00	0,11	0,10	0,10	0,09	0,10	0,10	0,01	0,02	0,01	0,02	0,01
Cr	0,00	0,00	0,00	0,00	0,00	0,00	0,00	0,00	0,00	0,00	0,00	0,00	0,00	0,00	0,00	0,00	0,00
Al	1,93	1,97	1,95	1,92	1,96	1,95	1,77	1,74	1,78	1,70	1,76	1,74	2,70	2,63	2,79	2,79	2,69
Fe^{3+}	0,07	0,00	0,02	0,04	0,06	0,03	0,00	0,00	0,00	0,00	0,00	0,00	0,00	0,00	0,00	0,00	0,00
Fe^{2+}	1,82	2,47	1,83	2,23	2,43	2,43	1,28	1,40	1,30	1,51	1,31	1,29	0,09	0,10	0,06	0,06	0,10
Mn	0,44	0,01	0,44	0,07	0,01	0,01	0,00	0,00	0,00	0,00	0,00	0,00	0,00	0,00	0,00	0,00	0,00
Mg	0,09	0,31	0,09	0,18	0,30	0,30	0,89	0,89	0,96	0,93	0,97	0,97	0,09	0,11	0,06	0,05	0,09
Ca	0,65	0,22	0,65	0,54	0,24	0,27	0,01	0,01	0,00	0,00	0,00	0,01	0,00	0,00	0,00	0,00	0,00
Na	0,01	0,00	0,00	0,00	0,01	0,01	0,01	0,03	0,01	0,03	0,01	0,02	0,09	0,13	0,28	0,22	0,11
K	0,00	0,00	0,00	0,00	0,00	0,00	0,88	0,86	0,86	0,86	0,86	0,88	0,83	0,80	0,70	0,77	0,83
Total	8,00	8,00	8,00	8,00	8,00	8,00	8,00	8,00	8,00	8,00	8,00	8,00	7,00	7,00	7,00	7,00	7,00
X_{Mg}	0,05	0,11	0,05	0,07	0,11	0,11	0,41	0,39	0,42	0,38	0,42	0,43					
X_{Prp}	0,03	0,10	0,03	0,06	0,10	0,10											
X_{Alm}	0,61	0,82	0,61	0,74	0,82	0,81											
X_{Grs}	0,22	0,07	0,22	0,18	0,08	0,09											
X_{Sps}	0,15	0,00	0,15	0,02	0,00	0,00											

Sample	**BB11**																
Mineral	**Chlorite**										**Plagioclase**			**K-feldspare**	**Ilmenite**		
Fabric	**S1**						**S2**				**S1**			**S1**	**S1**		
Point	18/ 1	19/ 1	20/ 1	21 / 1.	27/ 1	28/ 1	3/ 1	4/ 1	9/ 1	10/ 1	7/ 1	19/ 1	20/ 1	21/ 1	22 / 1 .	32 / 1 .	33 / 1 .
Position	Core	Rim	Core	Rim	Core	Rim	Core	Rim	Core	Rim	Core	Core	Core				
Wt %																	
SiO_2	24,72	25,00	25,05	24,74	25,08	25,30	24,84	25,18	25,33	24,90	68,06	65,46	68,08	65,59	0,06	0,06	0,02
TiO_2	0,10	0,11	0,07	0,06	0,07	0,09	0,08	0,09	0,08	0,04	0,00	0,00	0,00	0,00	54,94	54,39	52,91
Cr_2O_3	0,04	0,00	0,04	0,05	0,03	0,01	0,02	0,03	0,05	0,04	0,00	0,00	0,00	0,00	0,01	0,02	0,02
Al_2O_3	21,92	22,39	21,87	22,24	22,04	22,18	22,37	22,44	22,35	22,72	20,57	22,32	21,06	18,42	0,00	0,00	0,02
Fe_2O_3	0,00	0,00	0,00	0,00	0,00	0,00	0,00	0,00	0,00	0,00	0,00	0,14	0,00	0,00	0,00	0,00	0,00
FeO	29,90	28,30	30,32	29,65	28,61	29,21	30,13	27,93	27,38	29,82	0,06	0,00	0,05	0,01	45,07	45,35	45,92
MnO	0,09	0,08	0,10	0,07	0,11	0,09	0,08	0,06	0,06	0,08	0,00	0,00	0,00	0,00	0,82	0,75	0,87
MgO	11,52	12,92	11,77	11,80	12,98	12,03	11,47	12,99	13,08	11,76	0,00	0,00	0,00	0,00	0,04	0,02	0,03
CaO	0,01	0,03	0,01	0,03	0,00	0,04	0,01	0,02	0,01	0,02	1,33	3,16	1,60	0,00	0,01	0,00	0,00
Na_2O	0,00	0,01	0,00	0,00	0,00	0,03	0,00	0,00	0,00	0,00	10,95	10,64	10,95	0,27	0,00	0,00	0,00
K_2O	0,00	0,00	0,02	0,00	0,00	0,05	0,00	0,01	0,01	0,01	0,08	0,11	0,10	16,43	0,00	0,00	0,00
Total	88,28	88,83	89,26	88,64	88,90	89,02	88,99	88,75	88,37	89,38	101,04	101,83	101,83	100,72	100,94	100,58	99,77
No. O	14,00	14,00	14,00	14,00	14,00	14,00	14,00	14,00	14,00	14,00	8,00	8,00	8,00	8,00	3,00	3,00	3,00
Si	2,66	2,65	2,67	2,65	2,65	2,69	2,65	2,66	2,69	2,64	2,96	2,82	2,93	3,01	0,00	0,00	0,00
Ti	0,01	0,01	0,01	0,00	0,01	0,01	0,01	0,01	0,01	0,00	0,00	0,00	0,00	0,00	1,04	1,03	1,01
Cr	0,00	0,00	0,00	0,00	0,00	0,00	0,00	0,00	0,00	0,00	0,00	0,00	0,00	0,00	0,00	0,00	0,00
Al	2,78	2,79	2,74	2,80	2,75	2,78	2,82	2,80	2,80	2,84	1,05	1,13	1,07	1,00	0,00	0,00	0,00
Fe^{3+}	0,00	0,00	0,00	0,00	0,00	0,00	0,00	0,00	0,00	0,00	0,00	0,00	0,00	0,00	0,00	0,00	0,00
Fe^{2+}	2,69	2,50	2,70	2,65	2,53	2,60	2,69	2,47	2,43	2,64	0,00	0,00	0,00	0,00	0,94	0,95	0,97
Mn	0,01	0,01	0,01	0,01	0,01	0,01	0,01	0,01	0,01	0,01	0,00	0,00	0,00	0,00	0,02	0,02	0,02
Mg	1,85	2,04	1,87	1,88	2,05	1,90	1,82	2,05	2,07	1,86	0,00	0,00	0,00	0,00	0,00	0,00	0,00
Ca	0,00	0,00	0,00	0,00	0,00	0,00	0,00	0,00	0,00	0,00	0,06	0,15	0,07	0,00	0,00	0,00	0,00
Na	0,00	0,00	0,00	0,00	0,00	0,01	0,00	0,00	0,00	0,00	0,92	0,89	0,91	0,02	0,00	0,00	0,00
K	0,00	0,00	0,00	0,00	0,00	0,01	0,00	0,00	0,00	0,00	0,00	0,01	0,01	0,96	0,00	0,00	0,00
Total	10,00	10,00	10,00	10,00	10,00	10,00	10,00	10,00	10,00	10,00	5,00	5,00	5,00	5,00	2,00	2,00	2,00
X_{Mg}	0,41	0,45	0,41	0,42	0,45	0,42	0,40	0,45	0,46	0,41							
X_{An}											0,06	0,14	0,07				

Sample	**NO33**																			
Mineral	**Garnet**				**Biotite**				**Chlorite**				**Muscovite**			**Ilmenite**		**Magnetite**	
Fabric	**S1**				**S2**	**S1**			**S1**				**S1**						
Point	101 / 1 .	139 / 1 .	151 / 1 .	153 / 1 .	146 / 1 .	148 / 1 .	149 / 1 .	150 / 1 .	142 / 1 .	143 / 1 .	144 / 1 .	145 / 1 .	156 / 1 .	157 / 1 .	158 / 1 .	141 / 1 .	147 / 1 .	154 / 1 .	155 / 1 .
Position	Core	Rim	Rim	Rim					Grt rim							in grt	Matrix	in bt	in bt
Wt %																			
SiO_2	37,24	37,07	36,92	36,99	35,02	35,16	34,85	35,16	23,59	23,43	23,32	23,52	46,36	46,82	45,83	0,03	0,04	0,05	0,04
TiO_2	0,05	0,02	0,08	0,04	1,80	1,79	1,80	1,69	0,08	0,04	0,07	0,06	0,21	0,21	0,25	47,72	48,83	0,14	0,09
Cr_2O_3	0,00	0,00	0,02	0,01	0,03	0,04	0,07	0,02	0,01	0,04	0,00	0,01	0,04	0,03	0,03	0,01	0,03	0,21	0,22
Al_2O_3	20,71	20,76	20,73	20,61	18,62	18,22	18,00	18,00	22,13	21,68	21,92	22,35	34,19	34,63	34,53	0,02	0,01	0,06	0,05
Fe_2O_3	0,01	0,00	0,71	0,24	0,00	0,00	0,00	0,00	0,00	0,00	0,00	0,12	1,07	0,00	0,00	8,06	5,68	71,56	71,40
FeO	33,08	36,88	34,91	35,62	25,20	25,02	26,29	26,12	33,74	33,86	33,66	33,88	2,07	2,98	2,76	42,39	43,46	32,67	32,47
MnO	3,67	0,67	1,11	0,68	0,03	0,00	0,01	0,00	0,04	0,03	0,02	0,02	0,01	0,00	0,00	0,13	0,42	0,00	0,00
MgO	0,96	1,11	1,04	1,09	6,04	6,00	5,81	6,14	8,89	8,79	8,87	9,01	0,63	0,66	0,53	0,17	0,04	0,02	0,01
CaO	4,65	3,53	4,91	4,71	0,01	0,05	0,02	0,00	0,00	0,02	0,00	0,02	0,00	0,04	0,00	0,09	0,00	0,00	0,01
Na_2O	0,02	0,01	0,00	0,00	0,19	0,22	0,23	0,19	0,04	0,00	0,00	0,04	1,24	1,15	1,09	0,00	0,00	0,00	0,00
K_2O	0,01	0,01	0,01	0,00	9,19	9,38	9,09	9,08	0,00	0,02	0,02	0,00	9,43	9,36	9,34	0,00	0,00	0,00	0,00
Total	100,39	100,06	100,45	99,98	96,11	95,89	96,16	96,40	88,52	87,91	87,89	89,02	95,26	95,87	94,36	98,60	98,51	104,70	104,28
No. O	12,00	12,00	12,00	12,00	11,00	11,00	11,00	11,00	12,00	12,00	12,00	12,00	11,00	11,00	11,00	3,00	3,00	4,00	4,00
Si	3,01	3,01	2,99	3,00	2,79	2,80	2,78	2,80	2,58	2,59	2,57	2,56	3,10	3,11	3,09	0,00	0,00	0,00	0,00
Ti	0,00	0,00	0,00	0,00	0,11	0,11	0,11	0,10	0,01	0,00	0,01	0,00	0,01	0,01	0,01	0,92	0,94	0,00	0,00
Cr	0,00	0,00	0,00	0,00	0,00	0,00	0,00	0,00	0,00	0,00	0,00	0,00	0,00	0,00	0,00	0,00	0,00	0,01	0,01
Al	1,97	1,99	1,98	1,97	1,75	1,71	1,69	1,69	2,86	2,82	2,85	2,87	2,69	2,71	2,74	0,00	0,00	0,00	0,00
Fe^{3+}	0,00	0,00	0,04	0,01	0,00	0,00	0,00	0,00	0,00	0,00	0,00	0,01	0,05	0,00	0,00	0,16	0,11	1,98	1,98
Fe^{2+}	2,24	2,51	2,36	2,42	1,68	1,67	1,76	1,74	3,09	3,13	3,11	3,08	0,12	0,17	0,16	0,91	0,93	1,00	1,00
Mn	0,25	0,05	0,08	0,05	0,00	0,00	0,00	0,00	0,00	0,00	0,00	0,00	0,00	0,00	0,00	0,00	0,01	0,00	0,00
Mg	0,12	0,13	0,13	0,13	0,72	0,71	0,69	0,73	1,45	1,45	1,46	1,46	0,06	0,06	0,05	0,01	0,00	0,00	0,00
Ca	0,40	0,31	0,43	0,41	0,00	0,00	0,00	0,00	0,00	0,00	0,00	0,00	0,00	0,00	0,00	0,00	0,00	0,00	0,00
Na	0,00	0,00	0,00	0,00	0,03	0,03	0,04	0,03	0,01	0,00	0,00	0,01	0,16	0,15	0,14	0,00	0,00	0,00	0,00
K	0,00	0,00	0,00	0,00	0,93	0,95	0,93	0,92	0,00	0,00	0,00	0,00	0,80	0,79	0,80	0,00	0,00	0,00	0,00
Total	8,00	8,00	8,00	8,00	8,00	8,00	8,00	8,00	10,00	10,00	10,00	10,00	7,00	7,00	7,00	2,00	2,00	3,00	3,00
X_{Mg}	0,05	0,05	0,05	0,05	0,30	0,30	0,28	0,30	0,32	0,32	0,32	0,32	0,35	0,28	0,25				
X_{Prp}	0,04	0,04	0,04	0,04															
X_{Alm}	0,74	0,84	0,79	0,80															
X_{Grs}	0,13	0,10	0,14	0,14															
X_{Sps}	0,08	0,02	0,03	0,02															

Sample	**NQ21c**													
Mineral	**Garnet**				**Chlorite**				**Biotite**					
Fabric	**S1**				**S1**		**S2**		**S1**					
Point	148 / 1 .	169 / 1 .	191 / 1 .	170 / 1 .	2 / 1 .	11 / 1 .	14 / 1 .	15 / 1 .	3 / 1 .	4 / 1 .	17 / 1 .	18 / 1 .	126 / 1 .	127 / 1 .
Position	Core	Rim	Core	Rim	Bt chloritization		Core	Core						
Wt %														
SiO_2	37,37	37,69	37,48	37,74	25,40	25,97	26,03	25,59	36,55	36,43	36,89	36,39	36,60	36,86
TiO_2	0,05	0,04	0,08	0,01	0,12	0,12	0,11	0,10	1,67	1,66	1,83	1,70	1,82	1,62
Cr_2O_3	0,00	0,00	0,03	0,02	0,02	0,00	0,04	0,04	0,03	0,03	0,02	0,05	0,06	0,01
Al_2O_3	20,81	20,85	20,76	20,82	22,85	22,42	22,42	21,96	19,30	19,34	18,97	18,25	19,06	18,86
Fe_2O_3	0,23	0,00	0,15	0,38	0,00	0,00	0,00	0,00	0,00	0,00	0,00	0,00	0,00	0,00
FeO	28,40	31,78	28,99	33,17	21,01	20,75	20,76	20,90	17,15	17,32	16,96	16,66	17,08	16,68
MnO	7,83	3,68	7,33	2,27	0,14	0,13	0,11	0,11	0,06	0,06	0,09	0,08	0,10	0,06
MgO	2,41	3,26	2,47	3,67	17,33	17,69	17,93	17,50	11,43	11,18	11,41	11,69	11,32	11,69
CaO	3,15	2,79	3,18	2,31	0,02	0,01	0,01	0,02	0,01	0,00	0,00	0,00	0,02	0,00
Na_2O	0,01	0,00	0,00	0,03	0,03	0,00	0,00	0,00	0,23	0,19	0,30	0,29	0,20	0,21
K_2O	0,00	0,00	0,00	0,00	0,03	0,03	0,01	0,01	8,88	8,92	8,98	8,73	9,01	8,96
Total	100,26	100,10	100,48	100,43	86,95	87,11	87,41	86,24	95,31	95,13	95,44	93,82	95,27	94,93
No. O	12,00	12,00	12,00	12,00	14,00	14,00	14,00	14,00	11,00	11,00	11,00	11,00	11,00	11,00
Si	3,00	3,02	3,01	3,01	2,64	2,70	2,69	2,69	2,82	2,82	2,84	2,85	2,83	2,85
Ti	0,00	0,00	0,01	0,00	0,01	0,01	0,01	0,01	0,10	0,10	0,11	0,10	0,11	0,09
Cr	0,00	0,00	0,00	0,00	0,00	0,00	0,00	0,00	0,00	0,00	0,00	0,00	0,00	0,00
Al	1,97	1,97	1,96	1,96	2,80	2,74	2,73	2,72	1,75	1,76	1,72	1,68	1,73	1,72
Fe^{3+}	0,01	0,00	0,01	0,02	0,00	0,00	0,00	0,00	0,00	0,00	0,00	0,00	0,00	0,00
Fe^{2+}	1,91	2,13	1,95	2,21	1,83	1,80	1,79	1,83	1,11	1,12	1,09	1,09	1,10	1,08
Mn	0,53	0,25	0,50	0,15	0,01	0,01	0,01	0,01	0,00	0,00	0,01	0,01	0,01	0,00
Mg	0,29	0,39	0,29	0,44	2,69	2,74	2,76	2,74	1,31	1,29	1,31	1,36	1,30	1,35
Ca	0,27	0,24	0,27	0,20	0,00	0,00	0,00	0,00	0,00	0,00	0,00	0,00	0,00	0,00
Na	0,00	0,00	0,00	0,01	0,01	0,00	0,00	0,00	0,03	0,03	0,04	0,04	0,03	0,03
K	0,00	0,00	0,00	0,00	0,00	0,00	0,00	0,00	0,87	0,88	0,88	0,87	0,89	0,88
Total	8,00	8,00	8,00	8,00	10,00	10,00	10,00	10,00	8,00	8,00	8,00	8,00	8,00	8,00
X_{Mg}	0,13	0,15	0,13	0,16	0,60	0,60	0,61	0,60	0,54	0,54	0,55	0,56	0,54	0,56
X_{Prp}	0,10	0,13	0,10	0,15										
X_{Alm}	0,64	0,71	0,65	0,74										
X_{Grs}	0,09	0,08	0,09	0,07										
X_{Sps}	0,18	0,08	0,17	0,05										

Sample	**NQ21c**											
Mineral	**White mica**			**Staurolite**				**Plagioclase**			**Ilmenite**	
Fabric	**S1**			**S1**	**S2**			**S1**			**S1**	
Point	5 / 1 .	6 / 1 .	13 / 1 .	1 / 1 .	10 / 1 .	124 / 1 .	125 / 1 .	7 / 1 .	128 / 1 .	129 / 1 .	8 / 1 .	9 / 1 .
Position				Core	Core	Core	Rim	Center	Center	Center		
Wt%												
SiO_2	46,81	46,53	46,31	28,04	28,25	28,62	28,24	62,44	64,41	63,39	0,06	0,06
TiO_2	0,33	0,36	0,44	0,55	0,59	0,58	0,60	0,00	0,00	0,00	53,23	54,28
Cr_2O_3	0,03	0,04	0,02	0,04	0,06	0,07	0,02	0,00	0,00	0,00	0,02	0,00
Al_2O_3	35,58	36,06	35,84	52,80	52,66	52,64	52,96	23,91	22,71	23,17	0,01	0,00
Fe_2O_3	0,00	0,00	0,00	0,00	0,00	0,00	0,00	0,00	0,00	0,00	0,00	0,00
FeO	0,85	0,87	0,67	12,31	12,17	12,62	12,42	0,01	0,04	0,02	44,71	43,86
MnO	0,00	0,00	0,03	0,24	0,20	0,24	0,21	0,00	0,00	0,00	1,36	1,18
MgO	0,78	0,59	0,52	1,74	1,89	1,84	1,74	0,00	0,00	0,00	0,22	0,22
CaO	0,01	0,00	0,00	0,01	0,01	0,00	0,01	5,10	4,12	4,58	0,04	0,00
Na_2O	1,42	1,98	1,80	0,00	0,00	0,01	0,06	8,63	9,34	8,65	0,00	0,00
K_2O	9,31	8,76	8,81	0,00	0,00	0,00	0,01	0,07	0,09	0,08	0,00	0,00
Total	95,12	95,20	94,44	95,74	95,81	96,60	96,26	100,16	100,71	99,89	99,65	99,59
No. O	11,00	11,00	11,00	23,00	23,00	23,00	23,00	8,00	8,00	8,00	3,00	3,00
Si	3,10	3,07	3,09	4,05	4,08	4,10	4,06	2,76	2,83	2,82	0,00	0,00
Ti	0,02	0,02	0,02	0,06	0,06	0,06	0,06	0,00	0,00	0,00	1,01	1,03
Cr	0,00	0,00	0,00	0,00	0,01	0,01	0,00	0,00	0,00	0,00	0,00	0,00
Al	2,78	2,81	2,82	8,99	8,96	8,89	8,97	1,25	1,18	1,21	0,00	0,00
Fe^{3+}	0,00	0,00	0,00	0,00	0,00	0,00	0,00	0,00	0,00	0,00	0,00	0,00
Fe^{2+}	0,05	0,05	0,04	1,49	1,47	1,51	1,49	0,00	0,00	0,00	0,95	0,93
Mn	0,00	0,00	0,00	0,03	0,02	0,03	0,03	0,00	0,00	0,00	0,03	0,03
Mg	0,08	0,06	0,05	0,38	0,41	0,39	0,37	0,00	0,00	0,00	0,01	0,01
Ca	0,00	0,00	0,00	0,00	0,00	0,00	0,00	0,24	0,19	0,22	0,00	0,00
Na	0,18	0,25	0,23	0,00	0,00	0,00	0,02	0,74	0,80	0,75	0,00	0,00
K	0,79	0,74	0,75	0,00	0,00	0,00	0,00	0,00	0,01	0,00	0,00	0,00
Total	7,00	7,00	7,00	15,00	15,00	15,00	15,00	5,00	5,00	5,00	2,00	2,00
X_{Mg}				0,20	0,22	0,21	0,20					
X_{An}								0,25	0,19	0,23		

Sample	**NO26**															
Mineral	**Garnet**								**Ilmenite**		**Rutile**		**Plagioclase**			
Fabric	**S1**								**S1**		**S1**		**S1**			
Point	5 / 1 .	10 / 1 .	17 / 1 .	18 / 1 .	28 / 1 .	37 / 1 .	58 / 1 .	59 / 1 .	52 / 1 .	53 / 1 .	50 / 1 .	51 / 1 .	46 / 1 .	47 / 1 .	48 / 1 .	49 / 1 .
Position	Core	Rim	Core	Core	Rim	Core	Rim	Rim					Core	Rim	Core	Rim
Wt %																
SiO_2	37,77	37,79	37,44	37,68	38,20	37,94	37,31	37,81	0,09	0,07	0,03	0,06	65,74	63,15	66,30	65,15
TiO_2	0,01	0,00	0,00	0,00	0,02	0,00	0,00	0,00	51,86	52,87	99,04	98,88	0,00	0,00	0,00	0,00
Cr_2O_3	0,01	0,03	0,00	0,01	0,03	0,02	0,02	0,04	0,02	0,03	0,15	0,11	0,00	0,00	0,00	0,00
Al_2O_3	21,32	21,30	21,14	21,27	21,14	21,26	21,05	20,85	0,00	0,00	0,02	0,04	22,17	23,54	21,34	22,09
Fe_2O_3	0,80	1,09	0,30	0,92	0,13	0,00	0,64	0,46	0,88	0,00	0,19	0,19	0,00	0,01	0,00	0,00
FeO	32,25	32,27	34,46	34,23	33,20	34,84	34,22	34,58	45,58	45,67	0,00	0,00	0,00	0,00	0,05	0,00
MnO	0,41	0,46	2,01	1,63	0,48	1,93	1,53	1,99	1,07	0,72	0,02	0,00	0,00	0,00	0,00	0,00
MgO	5,41	5,57	3,85	4,07	5,31	3,55	3,86	3,92	0,02	0,16	0,00	0,00	0,00	0,00	0,00	0,00
CaO	1,97	1,94	1,08	1,47	1,95	1,45	1,52	1,14	0,02	0,00	0,02	0,01	3,16	4,89	2,50	3,37
Na_2O	0,04	0,00	0,00	0,00	0,01	0,00	0,01	0,03	0,00	0,00	0,00	0,00	10,15	9,29	10,39	9,88
K_2O	0,05	0,02	0,01	0,01	0,00	0,01	0,00	0,01	0,00	0,00	0,00	0,00	0,11	0,10	0,10	0,11
Total	100,05	100,45	100,29	101,29	100,47	101,00	100,15	100,82	99,54	99,53	99,48	99,29	101,33	100,99	100,68	100,59
No. O	12,00	12,00	12,00	12,00	12,00	12,00	12,00	12,00	3,00	3,00	2,00	2,00	1,60	1,30	1,00	0,70
Si	2,99	2,98	3,00	2,98	3,01	3,02	2,99	3,01	0,00	0,00	0,00	0,00	2,86	2,76	2,90	2,86
Ti	0,00	0,00	0,00	0,00	0,00	0,00	0,00	0,00	0,99	1,01	1,00	1,00	0,00	0,00	0,00	0,00
Cr	0,00	0,00	0,00	0,00	0,00	0,00	0,00	0,00	0,00	0,00	0,00	0,00	0,00	0,00	0,00	0,00
Al	1,99	1,98	1,99	1,98	1,96	1,99	1,99	1,96	0,00	0,00	0,00	0,00	1,14	1,21	1,10	1,14
Fe^{3+}	0,05	0,06	0,02	0,05	0,01	0,00	0,04	0,03	0,02	0,00	0,00	0,00	0,00	0,00	0,00	0,00
Fe^{2+}	2,13	2,13	2,30	2,26	2,19	2,32	2,29	2,30	0,97	0,97	0,00	0,00	0,00	0,00	0,00	0,00
Mn	0,03	0,03	0,14	0,11	0,03	0,13	0,10	0,13	0,02	0,02	0,00	0,00	0,00	0,00	0,00	0,00
Mg	0,64	0,65	0,46	0,48	0,62	0,42	0,46	0,46	0,00	0,01	0,00	0,00	0,00	0,00	0,00	0,00
Ca	0,17	0,16	0,09	0,12	0,17	0,12	0,13	0,10	0,00	0,00	0,00	0,00	0,15	0,23	0,12	0,16
Na	0,01	0,00	0,00	0,00	0,00	0,00	0,00	0,00	0,00	0,00	0,00	0,00	0,86	0,79	0,88	0,84
K	0,01	0,00	0,00	0,00	0,00	0,00	0,00	0,00	0,00	0,00	0,00	0,00	0,01	0,01	0,01	0,01
Total	8,00	8,00	8,00	8,00	8,00	8,00	8,00	8,00	2,00	2,00	1,00	1,00	5,00	5,00	5,00	5,00
X_{Mg}	0,23	0,24	0,17	0,17	0,22	0,15	0,17	0,17				X_{An}	0,15	0,22	0,12	0,16
X_{Prp}	0,22	0,22	0,15	0,16	0,21	0,14	0,15	0,16								
X_{Alm}	0,72	0,71	0,77	0,76	0,73	0,77	0,77	0,77								
X_{Grs}	0,06	0,05	0,03	0,04	0,05	0,04	0,04	0,03								
X_{Sps}	0,01	0,01	0,05	0,04	0,01	0,04	0,03	0,04								

Sample	NO26											
Mineral	**Muscovite**				**Biotite**				**Staurolite**		**Chlorite**	
Fabric	**S1**				**S1**				**S1**		Retrograde	
Point	42 / 1 .	43 / 1 .	44 / 1 .	45 / 1 .	38 / 1 .	39 / 1 .	40 / 1 .	41 / 1 .	56 / 1 .	57 / 1 .	5 / 1 .	6 / 1 .
Position				Garnet		Matrix		Grt rim	Core	Rim		
Wt%												
SiO_2	46,65	46,00	46,28	46,50	36,57	36,85	34,60	36,93	28,71	27,98	27,02	27,29
TiO_2	1,72	0,01	0,00	0,85	1,94	2,40	1,84	2,32	0,83	0,45	0,09	0,13
Cr_2O_3	0,09	0,02	0,04	0,05	0,03	0,08	0,06	0,13	0,04	0,05	0,04	0,02
Al_2O_3	30,72	36,12	36,16	36,93	19,09	19,19	19,18	18,38	54,31	55,08	21,90	21,44
Fe_2O_3	1,14	0,00	0,00	0,00	0,00	0,00	0,00	0,00	0,00	0,00	0,00	0,00
FeO	1,52	0,80	1,32	0,74	18,16	17,41	19,42	16,19	11,69	11,46	21,65	20,58
MnO	0,00	0,00	0,00	0,02	0,02	0,03	0,03	0,02	0,07	0,10	0,09	0,04
MgO	1,83	0,40	0,49	0,44	10,72	11,22	11,06	11,96	2,05	1,32	17,39	17,94
CaO	0,00	0,09	0,06	0,00	0,03	0,00	0,02	0,02	0,00	0,00	0,03	0,17
Na_2O	0,31	0,30	0,39	1,81	0,15	0,20	0,08	0,16	0,06	0,00	0,00	0,03
K_2O	10,96	10,85	10,79	8,55	9,47	9,84	8,38	9,63	0,02	0,01	0,15	0,10
Total	94,93	94,58	95,53	95,87	96,17	97,22	94,66	95,73	97,78	96,46	88,35	87,74
No. O	11,00	11,00	11,00	11,00	11,00	11,00	11,00	11,00	23,00	23,00	14,00	14,00
Si	3,15	3,09	3,08	3,06	2,81	2,79	2,71	2,83	4,05	4,00	2,78	2,81
Ti	0,09	0,00	0,00	0,04	0,11	0,14	0,11	0,13	0,09	0,05	0,01	0,01
Cr	0,00	0,00	0,00	0,00	0,00	0,00	0,00	0,01	0,00	0,01	0,00	0,00
Al	2,45	2,86	2,83	2,86	1,73	1,71	1,77	1,66	9,02	9,28	2,65	2,60
Fe^{3+}	0,06	0,00	0,00	0,00	0,00	0,00	0,00	0,00	0,00	0,00	0,00	0,00
Fe^{2+}	0,09	0,04	0,07	0,04	1,17	1,10	1,27	1,04	1,38	1,37	1,86	1,77
Mn	0,00	0,00	0,00	0,00	0,00	0,00	0,00	0,00	0,01	0,01	0,01	0,00
Mg	0,18	0,04	0,05	0,04	1,23	1,27	1,29	1,37	0,43	0,28	2,67	2,76
Ca	0,00	0,01	0,00	0,00	0,00	0,00	0,00	0,00	0,00	0,00	0,00	0,02
Na	0,04	0,04	0,05	0,23	0,02	0,03	0,01	0,02	0,02	0,00	0,00	0,01
K	0,94	0,93	0,91	0,72	0,93	0,95	0,84	0,94	0,00	0,00	0,02	0,01
Total	7,00	7,00	7,00	7,00	8,00	8,00	8,00	8,00	15,00	15,00	10,00	10,00
X_{Mg}					0,51	0,53	0,50	0,57	0,24	0,17	0,59	0,61